

**NASA CONTRACTOR
REPORT**

NASA CR-2638



NASA CR-

C.1

0062500



**LOAN COPY: RETURN TO
AFWL TECHNICAL LIBRARY
KIRTLAND AFB, N. M.**

**AEROELASTIC ANALYSIS FOR HELICOPTER ROTOR
BLADES WITH TIME-VARIABLE, NONLINEAR
STRUCTURAL TWIST AND MULTIPLE STRUCTURAL
REDUNDANCY - MATHEMATICAL DERIVATION
AND PROGRAM USER'S MANUAL**

Richard L. Bielawa

Prepared by
UNITED TECHNOLOGIES RESEARCH CENTER
East Hartford, Conn. 06108
for Langley Research Center
and U.S. Army Air Mobility R&D Laboratory

NATIONAL AERONAUTICS AND SPACE ADMINISTRATION • WASHINGTON, D. C. • OCTOBER 1976





0061500

1. Report No. NASA CR-2638		2. Government Accession No.		3. Recipient's Catalog No.	
4. Title and Subtitle Aeroelastic Analysis for Helicopter Rotor Blades With Time-Variable, Nonlinear Structural Twist and Multiple Structural Redundancy - Mathematical Derivation and Program User's Manual				5. Report Date October 1976	
				6. Performing Organization Code R76-911209-48	
7. Author(s) Richard L. Bielawa				8. Performing Organization Report No.	
9. Performing Organization Name and Address United Technologies Research Center East Hartford, CT 06108				10. Work Unit No.	
				11. Contract or Grant No. NAS 1-10960	
12. Sponsoring Agency Name and Address National Aeronautics and Space Administration Washington, DC 20546 and U.S. Army Air Mobility R&D Laboratory Moffett Field, CA 94035				13. Type of Report and Period Covered Contractor Report	
				14. Army Project No. 1F161102AH45	
15. Supplementary Notes The contract Research effort which has led to the results in this report was financially supported by USAAMRDL-Langley Directorate. This is a final report and complements NASA CR-2637. Technical Monitor: Carl E. Swindlehurst, Jr.					
16. Abstract <p>The differential equations of motion for the lateral and torsional deformations of a non-linearly twisted rotor blade in steady flight conditions together with those additional aeroelastic features germane to composite bearingless rotors are derived. The differential equations are formulated in terms of uncoupled (zero pitch and twist) vibratory modes with exact coupling effects due to finite, time variable blade pitch and, to second order, twist. Also presented are derivations of the fully coupled inertia and aerodynamic load distributions, automatic pitch change coupling effects, structural redundancy characteristics of the composite bearingless rotor flexbeam - torque tube system in bending and torsion, and a description of the linearized equations appropriate for eigensolution analyses. Three appendixes are included presenting material appropriate to the digital computer program implementation of the analysis, program G400.</p>					
17. Key Words (Suggested by Author(s)) Rotor aeroelasticity, Computer programs, Composite structures, Nonlinear structural analysis, Non-linear blade twist, Bearingless rotors			18. Distribution Statement Unclassified - Unlimited Subject Category 39		
19. Security Classif. (of this report) Unclassified		20. Security Classif. (of this page) Unclassified		21. No. of Pages 154	22. Price* \$6.25

PREFACE

The initial development of this analysis was conducted under Corporate sponsored independent research and development funding at United Technologies Research Center. Extensive refinements to the analysis were made under sponsorship of the Langley Research Center of the National Aeronautics and Space Administration and the U. S. Army Air Mobility Research and Development Laboratory, Langley Directorate as part of Contract NAS1-10960. The purpose of this contract was to perform an investigation of a bearingless helicopter rotor concept having a composite primary structure. A companion report to the one herein is NASA CR-2637 which presents the results of graphite/epoxy fatigue tests, wind tunnel experiments, correlation studies, and a preliminary design of a full scale helicopter rotor, also obtained under this contract. The correlation studies were used to provide limited validation of the herein described analysis, and the preliminary full scale design study involved substantial use of the analysis to investigate the structural dynamics and aeroelastics of the design.

The author wishes to express his appreciation to Mr. C. E. Swindlehurst and Dr. W. F. White for their encouragement and useful comments.

TABLE OF CONTENTS

	<u>Page</u>
SUMMARY	1
INTRODUCTION	2
LIST OF SYMBOLS	6
PRINCIPAL ASSUMPTIONS	16
COORDINATE TRANSFORMATIONS DUE TO PITCH ANGLE AND TWIST	18
DERIVATION OF BASIC DYNAMIC EQUATIONS OF MOTION	24
Flatwise and Edgewise Bending Equations	24
Torsion Equation	28
Rigid Flapping and Lagging Equations	30
DYNAMIC AND AERODYNAMIC LOAD DISTRIBUTIONS	32
Dynamic Load Distributions	32
Aerodynamic Load Distributions	38
RIGID BODY FEATHERING MOTION AND BASIC PITCH-FLAT/EDGE COUPLING EFFECTS	43
Rigid Body Feathering Degree-of-Freedom	44
Inclusion of Pitch-Flat/Edge Coupling	46
AEROELASTIC SIMULATION OF BLADE TORSION WOBBLE MODE	51
Flatwise Flexibility Characteristics of Flexbeam -	
Cantilevered Torque Tube Assembly	53
Elastic Rigid Feathering Torsional Restraint	56
Dynamic Equation for Wobble Mode	58
REDUNDANT ANALYSIS OF FLEXBEAM - TORQUE TUBE ASSEMBLIES	
WITH SNUBBER CONSTRAINTS	60
Bending Stiffness Characteristics of the Torque Tube	62
Torsional Stiffness Characteristics of the Flexbeam	72
Estimation of Internal Blade Shears and Moments in Blade	
Adjacent to the Juncture	79
Mathematical Formulation of the Structural Redundancy	82
LINEARIZED FORM OF EQUATIONS	84
REFERENCES	89

TABLE OF CONTENTS (Cont'd.)

	<u>Page</u>
APPENDICES	
I. Quadrature Formulae Used in Program G400	91
II. Program G400 Input Description	94
III. Program G400 Output Description	122
FIGURES	
1	3
2	19
3	22
4	43
5	46
6	52
7	53
8	57
9	61
10	63
11	73
TABLES	
I	84
II	120

AEROELASTIC ANALYSIS FOR HELICOPTER ROTOR BLADES
WITH TIME-VARIABLE, NONLINEAR STRUCTURAL TWIST
AND MULTIPLE STRUCTURAL REDUNDANCY - MATHEMATICAL
DERIVATION AND PROGRAM USER'S MANUAL

by

Richard L. Bielawa
United Technologies Research Center

SUMMARY

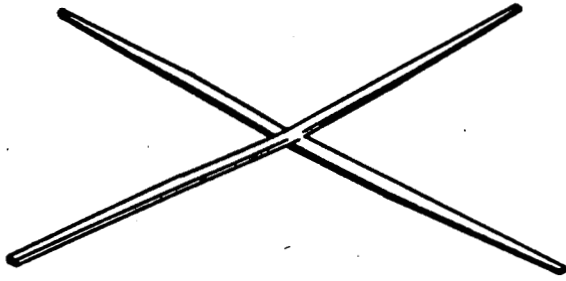
The differential equations of motion for the lateral and torsional deformations of a nonlinearly twisted rotor blade in steady flight conditions together with those additional aeroelastic features germane to composite bearingless rotors are derived. The differential equations are formulated in terms of uncoupled (zero pitch and twist) vibratory modes with exact coupling effects due to finite, time variable blade pitch and, to second order, twist. Also presented are derivations of the fully coupled inertia and aerodynamic load distributions, automatic pitch change coupling effects, structural redundancy characteristics of the composite bearingless rotor flexbeam - torque tube system in bending and torsion, and a description of the linearized equations appropriate for eigensolution analyses. Three appendices are included presenting material appropriate to the digital computer program implementation of the analysis, program G400.

INTRODUCTION

The composite bearingless rotor employs for its primary structural element a spar fashioned from radially aligned uniaxial high strength fibers (carbon, boron, etc.) in an epoxy matrix. The transverse shear modulus of such a spar is sufficiently low to produce a torsionally flexible member which when installed over a finite length (designated the flexbeam) replaces the feathering bearings normally used for blade pitch control. Figure 1 shows the schematic of a typical rotor employing such a spar. Blade pitch control is achieved by elastically twisting the inboard portion of the spar; the moment applied to the blade from the push-rod is transmitted through the aerodynamic shell or torque tube which, like the outer portion of the blade, is relatively stiff in torsion.

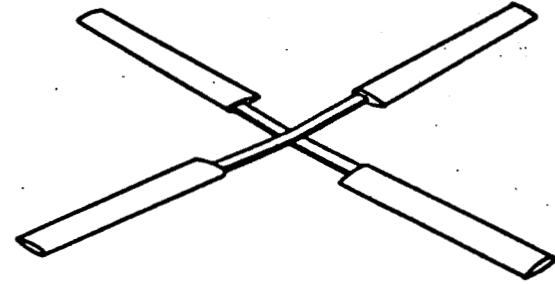
These structural features produce unique aeroelastic characteristics not readily amenable to conventional analysis: First, the primary structural member, the spar and included flexbeam is subjected to highly nonlinear and time varying structural twist which, over the flexbeam span, can approach (equivalent) total span twist angles of $+90^\circ$. Second, although the torque tube and flexbeam have contrasting specialized structural functions (torsion and bending load transmissibilities, respectively) each nonetheless exhibits significant amounts of both types of load transmissibility. Hence, the torque tube-flexbeam system comprises a doubly redundant structure: redundancy both in torsion and in bending. Third, the simple torque tube shown in Fig. 1 is that of a "cantilevered" configuration wherein the inboard end is supported both in shear and torque solely by the push-rod. Such a configuration produces not only a soft blade torsion system, but a high degree of pitch-flap coupling.

Because of these resulting unique aeroelastic characteristics, none of the various "comprehensive" (nonlinear) rotor aeroelastic analyses currently available (e.g., Refs. 1, 2, and 3) can be justifiably applied to the bearingless rotor. Most of the difficulties encountered with these analyses are due, in one form or another, to inappropriate assumptions made with regard to structural twist. Compared on this basis, the various analyses generally fall into either of two categories. In the first category, the structural twist is assumed to be linear, small, and temporally constant; such an assumption is clearly at variance with the aforementioned twist characteristics of bearingless rotors. In the second category, large nonlinear structural twists are incorporated by the use of "coupled modes" wherein the blade bending elasticity is defined by the use of the normal (vibrational) modes of an arbitrarily pretwisted blade at some nominal fixed collective angle. Unfortunately, such an approach is rigorous only in hover wherein the control angle is constant and equal to the nominal collective angle. Generally, the use of coupled modal



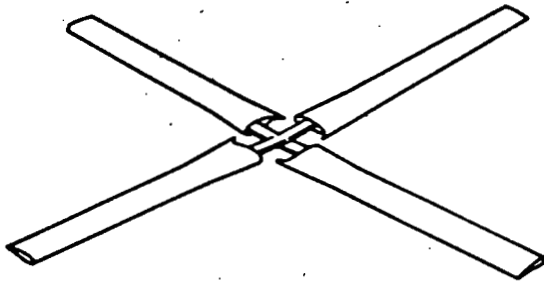
SPAR ASSEMBLY

(a)



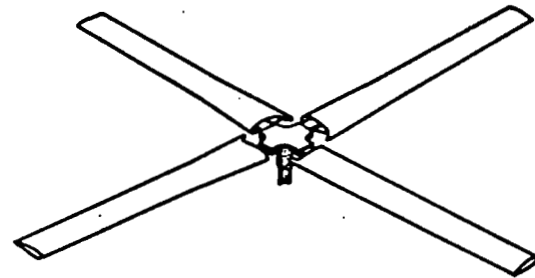
+ AIRFOIL ASSEMBLY

(b)



+ TORQUE TUBE ASSEMBLY

(c)



+ HUB ASSEMBLY

(d)

Figure 1. - Composite Bearingless Rotor

analyses for typical forward flight cases involving substantial cyclic angles leads to an obvious contradiction of the inherent assumptions upon which coupled modes are predicted. To rectify this conceptual deficiency, coupled mode analyses must incorporate, in some fashion, the mode shape and modal frequency variations over the appropriate pitch angle range as defined by the given flight case. This invariably leads either to extreme complexity and resulting computer storage and run-time requirements, or to various simplifying approximations to the variations of the mode shapes and frequencies with pitch angle. Either of these consequences, however, tend to nullify the advantages claimed for "coupled mode" analyses. In Ref. 3 is presented a consistent systematic development of such a coupled mode analyses which rigorously addresses itself to the problem arising from variable pitch angle. However, even for this exemplary analysis, the time variable (perturbational) pitch angle is assumed to be small, constant with span and, hence, inappropriate to the requirements of composite bearingless rotors. Because the use of coupled modes offered no clear advantage and because a valid, relatively simple yet practical means of incorporating nonlinear structural twist was found, a coupled modes approach was discarded in favor of one based upon more conventional uncoupled modes. Finally, in all cases the available analyses were found to be totally incapable of providing an analysis of the structural redundancy of the torque tube - flexbeam system or of a cantilever configured torque tube.

The aeroelastic analysis described herein is a multi-purpose computer program characterized by rigorous modelings of nonlinear and time varying structural twist, and of the redundant load carrying features of the bearingless rotor. Although developed in response to the requirements of composite bearingless rotors, the dynamic equations are sufficiently general for valid application to all conventional rotor systems: articulated, semiarticulated, teetering and hingeless. The computer program implementing these equations presently assumes a fixed hub, and hence, obtains solutions of the dynamic equation for only one blade. It cannot, therefore, be used for teetering rotor systems which inherently require a two-bladed implementation of these equations. The differential equations of blade beam bending (flatwise and edgewise) and torsion are solved using a Galerkin procedure wherein the normal "uncoupled mode" shapes and spanwise derivatives of the blade pitch angle and the nonlinear twist are appropriately combined to describe the "coupled" blade deflections. The general approach to the development of the aeroelastic analysis closely parallels and draws upon that used and reported in Ref. 1. Two types of solution are available: eigensolutions of various linearized equation sets for coupled frequency and/or stability analysis purposes, and time-history solutions of the complete nonlinear equations for harmonic analysis and/or transient aeroelastic response calculation purposes. The aerodynamic description includes the use of predetermined static airfoil data, constant or variable inflow (vorticity induced and/or momentum derived) and unsteady dynamic stall data.

This document presents the more salient details of this aeroelastic analysis. Specific items to be described are: 1) the principal inherent assumptions, 2) the coordinate transformation used to introduce pitch and twist effects, 3) application of the Galerkin procedure to obtain the basic modal equations, 4) descriptions of the required load distributions, 5) introduction of pitch-flat/edge coupling, 6) simulation of the "wobble mode," 7) inclusion of the redundant load carrying features of the flexbeam-torque tube assembly of the bearingless rotor, and 8) the detailed statement of the linearized equations used in the eigensolution.

These eight sections essentially present the derivation of equations of motion whose solutions can then be implemented using a variety of numerical techniques. In Appendix I is presented a brief description of the quadrature techniques employed in the existing digital computer program implementation of these equations, program G⁴00. Appendix II contains a detailed description of the input required to run this digital computer program, and Appendix III presents a comprehensive description of the computer generated output.

LIST OF SYMBOLS

a_∞	free stream sonic velocity.
A	area of blade section.
[A]	inertia matrix.
\hat{A}_{PQ}, A_{PQ}	general submatrices of partitioned inertia matrix without and with the effects of coupling due to automatic pitch change, respectively.
B	tip loss factor, used in momentum inflow equations and in approximate simulation of three-dimensional tip effects.
c	blade or section chord, as appropriate.
c_d	section drag coefficient
Δc_{d_0}	increment to section drag coefficient to account for surface roughness.
c_l	section lift coefficient.
$c_{m_{c/4}}$	section pitching moment coefficient about quarter chord.
C	compression at an arbitrary spanwise station.
C, D, H_1	integration constants from solution for flexbeam torsional element differential equation.
C_l, C_m	rolling and pitching moment coefficients, respectively, of the rotor; moments nondimensionalized by $(\rho \pi R^5 \Omega^2)$.
C_{LD}	coefficient of damping rate for blade lag damper.
C_T	thrust coefficient of the rotor; thrust nondimensionalized by $(\rho \pi R^4 \Omega^2)$.
D	plate bending stiffness.
e	x_2 coordinate of coincident flat-lag hinge or hingeless blade offset point.
e_A	chordwise position of section tension center, (+) forward from elastic axis.

LIST OF SYMBOLS (Cont'd.)

e_{ij}, f_{ij}	element of E and F matrices, respectively.
EI_y, EI_z	blade bending stiffness for flatwise and edgewise bending, respectively.
$[E], [F]$	torsional transfer matrices resulting from cascade multiplication and other algebraic manipulations.
f_α	spanwise angle of attack correction factor to account for three-dimensional tip effects.
$\{F(\psi)\}$	excitation vector in time-history solution form of nonlinear dynamic equations.
F_{PR}	push-rod load, (+) when directed in the z_5 direction.
F_{y_5}, F_{z_5}	concentrated forces applied to the blade in the y_5 and z_5 directions, respectively.
g	acceleration due to gravity.
GJ	torsional stiffness of blade section.
$[I_m]$	identity matrix of dimension m.
k_A	radius of gyration of section tension carrying area.
$k_{y_{10}}, k_{z_{10}}$	mass radii of gyration of blade section about axes through and perpendicular to the spanwise (x_5) axis and in the chordwise and thicknesswise directions, respectively.
K_{J_E}, K_{J_F}	spring rates of edgewise and flatwise retention springs, respectively, of torque tube to blade spar at flexbeam-torque tube juncture.
K_v	induced velocity gradient factor.
K_{S_E}, K_{S_F}	spring rates of torque tube principal axes (edgewise and flatwise) retention springs, respectively, of torque tube to flexbeam at snubber end of torque tube.

LIST OF SYMBOLS (Cont'd.)

$K_{S_{y5}}, K_{S_{z5}}$	spring rates of inplane and vertical retention springs, respectively, of torque tube to flexbeam at snubber end of torque tube.
$K_{\theta 1}$	spring rate of flexbeam torsion due to elastic and bifilar effects.
$K_{\theta 2}$	spring rate of effective root torsion restraint due to control system flexibility and flexbeam bending.
$K_{\theta 3}$	spring rate of root torsion restraint due to control system flexibility.
l	length of element of flexbeam over which torsion properties are assumed constant nondimensionalized by flexbeam length.
L	length of beam element over which the tension is assumed constant.
$\{L\}$	vector of shears, moments, and deflections given as linear combinations of other specified deflections.
$\{L_y\}, \{L_z\}$	subvectors of $\{L\}$, having shear, moment, and deflection components each in y- and z- directions, respectively.
m	blade mass distribution.
m_0	reference blade mass distribution, taken to be that of the 5th blade segment.
M	flatwise bending moment at an end of a beam element; also Mach number.
M_{LD}	moment due to lag damper.
M_R	blade root torsion restraint moment.
M_{x5}, M_{y5}, M_{z5}	components of blade moment about axes in the 5-coordinate system, arising from inertia, aerodynamic and/or concentrated mechanical effects.
NEM, NFM, NIM	numbers of assumed flatwise, edgewise, and torsion natural "uncoupled" primitive modes, respectively.

LIST OF SYMBOLS (Cont'd.)

NH	number of harmonics in variable inflow description.
NSEG	number of segments into which the blade is divided each having assumed spanwise constant section properties.
$P_{x_5}, P_{y_5}, P_{z_5}$	section shear load distributions in directions of axes in the 5- coordinate system.
q	general expression for a response variable deflection.
q_{TT_i}	element of Q_{TT} vector.
q_{v_k}	blade k'th edgewise modal response variable.
q_{w_i}	blade i'th flatwise modal response variable.
$q_{x_5}, q_{y_5}, q_{z_5}$	section moment load distributions about axes in the 5- coordinate system.
q_{θ_j}	blade j'th torsion modal response variable.
$[Q_{TT}]$	vector of torque tube deflection effectivity constants.
r	blade spanwise coordinate, measured from offset, e, in x_5 direction.
R	rotor radius.
$[R_E], [R_F]$	intermediate torque tube bending stiffness matrices.
s_{ij}	element of the S_0 matrix.
S	flexbeam length (span), or flatwise shear at an end of a beam element, as appropriate.
$S_{x_5}, S_{y_5}, S_{z_5}$	components of concentrated shear in directions of axes in the 5- coordinate system.
$[S_0], [S_1]$	trigonometrically resolved torque tube bending stiffness matrices.
t_{ij}	element of a T matrix.

LIST OF SYMBOLS (Cont'd.)

T	tension at an arbitrary blade spanwise station.
T_i	constants for polynomial representation of spanwise variable torque applied to flexbeam .
$[T_k]$	elastic transfer matrix at k'th semi-segment.
$[T_1], [T_3], [T_4], [T_5]$	coordinate system transformation matrices relating rotating coordinate system deflections to the inertial frame.
u_e	elastic spanwise deflection of arbitrary spanwise coordinate.
U	resultant air velocity relative to blade section, $\sqrt{(U_p^2 + U_T^2)}$.
U_p	air velocity component relative to blade section in (+) z_5 direction.
U_T	air velocity component relative to blade section in (-) y_5 direction.
U_x	air velocity component relative to blade section in (+) x_2 direction.
v_e, w_e	elastic edgewise and flatwise bending deflections, respectively, of an arbitrary spanwise coordinate.
$v_{i_0}, v_{i_{nc}}, v_{i_{ns}}$	zeroth and n'th cosine and sine components of variable induced velocities.
\tilde{v}_P, \tilde{v}_T	components of air velocities relative to blade section devoid of cosine and/or sine of total pitch angle and comprised of response variables.
\tilde{v}_y, \tilde{v}_z	components of air velocities relative to a blade section in chordwise and thicknesswise directions, respectively.
$\Delta v, \Delta w$	deflection correction terms due to first order twist effects.
V	strain energy.
$\Delta V, \Delta W$	deflection correction terms due to second order twist effects.

LIST OF SYMBOLS (Cont'd.)

x_2, y_2, z_2	components of the 2-coordinate system, defined to be affixed to the rotating hub.
x_5, y_5, z_5	components of the 5-coordinate system, defined to be rotating with the hub, but at the blade coned and lagged position.
Δx	length of blade spanwise segment over which the spanwise properties are assumed to be constant.
$\{x_1\}, \{x_5\}$	components of blade deflection in the inertial and 5-coordinate systems, respectively, as measured in the 5-coordinate system.
y_{10}, z_{10}	chordwise and thicknesswise position coordinate, respectively, of an arbitrary point within a blade section.
$\hat{y}_{10}, \hat{z}_{10}$	inplane and out-of-plane position coordinates, respectively, of an arbitrary point within a blade section.
$y_{10c/4}, y_{103c/4},$ y_{10CG}	chordwise distances of quarter chord, three quarter chord, and mass center, respectively, from the reference axis at a blade section.
$\{\Delta Y\}, \{\Delta Z\}$	subvectors of $\{\Delta\}$, having specified deflections in y and z directions, respectively.
Δz	deflection in z_5 direction of the push-rod attachment point due to any and all blade bending deflections, flapping and lead-lagging, with the push-rod disconnected.
Z	flatwise (vertical) deflection per unit force of inboard end of cantilevered torque tube, due to flexbeam bending
α_{eff}	effective blade section angle of attack approximately corrected for three-dimensional tip effects and used for evaluation of section aerodynamic coefficients.
α_{qs}	quasi-static blade section angle of attack.
α_R	rotor (hub axis) angle of attack.
β	blade flapping (or precone) angle; also used to denote tension (or compression) to elastic bending stiffness parameter for a beam element.

LIST OF SYMBOLS (Cont'd.)

γ_{vk}	deflection mode shape for the k'th edgewise normal mode.
γ_{wi}	deflection mode shape for the i'th flatwise normal mode.
γ_{θ_j}	deflection mode shape for the j'th torsion normal mode.
γ_{ORB}	deflection shape for the pseudo- (rigid body) torsion mode.
$\Gamma_{\text{BF}\theta_j}$	bifilar-twist coupling function for j'th torsion mode.
δ	blade lead angle; also used to denote perturbational quantity.
$\{\Delta\}$	vector of specified deflections.
ϵ	small number (less than unity) used to assess relative orders of magnitude for various terms.
η	flexbeam spanwise coordinate, measured from offset, nondimensionalized by S.
$\hat{\eta}_{k, k+1}$	spanwise coordinate of boundary point between k'th and k+1'th segments.
θ_B	built-in blade section twist angle; i.e., that section pitch angle resulting when the aerodynamic pitch angle at 75% span is zero deg.
θ_{BFB}	built-in twist angle of flexbeam measured when flexbeam is torsionally unloaded.
θ, θ_e	elastic torsion deflection angle.
θ_R	blade root torsion deflection angle.
$\theta_{S_X}, \dots, \theta_{M_Z}$	abbreviated torsion flexibility coefficients containing deflection dependency.
θ_T	blade tip torsion deflection angle.
$\theta_{vk}, \theta_{wi}, \theta_{\beta}, \theta_{\delta}$	automatic blade pitch change per unit deflection in k'th edgewise mode, i'th flatwise mode, flapping and lead-lagging motions, respectively.

LIST OF SYMBOLS (Cont'd.)

θ_0	blade pitch angle due to input control angle.
$\Delta\theta$	automatic pitch changes accruing from any and all blade bending deflection, flapping and lead-lagging.
θ	total local blade pitch angle.
$\theta_{S_X}, \dots, \theta_{M_1}$	flexbeam torsion flexibility coefficients.
$\Delta\theta_J$	total torsion deflection of flexbeam at junction point beyond built-in value.
$\kappa_{A_{X5}}$	blade section pitch damping effectivity factor.
λ	total inflow ratio, or section torsional characteristic constant, as appropriate.
λ_0	uniform portion of inflow.
λ_{RAM}	inflow contribution from forward flight "ram" effects.
μ	advance ratio.
ν	Poisson's ratio.
ρ	air density.
ϕ	inflow angle.
ψ	blade azimuthal (angular) position.
$\bar{\omega}$	(nondimensional) frequency used in quadrature formulae, taken to be uncoupled natural frequency of degree of freedom.
$\bar{\omega}_{w_i}, \bar{\omega}_{v_k}, \bar{\omega}_{\theta_j}$	(nondimensional) uncoupled natural frequencies of i'th flatwise bending mode, k'th edgewise bending mode and j'th torsion mode, respectively.
Ω	rotor rotational frequency.

LIST OF SYMBOLS (Cont'd.)

Subscripts

() _A	effects of aerodynamic origin.
() _B	structurally built-in parameter, or conditions of blade immediately outboard of juncture.
() _D	effects of dynamic origin.
() _e	due to elastic deformation.
() _E	in edgewise (section major principal axis) direction.
() _F	in flatwise (section minor principal axis) direction.
() _{FB}	flexbeam .
() _G	effects of gravitational origin.
() _I	conditions at inboard end.
() _J	conditions at flexbeam-torque tube juncture.
() _O	conditions at outboard end.
() _{PR}	push-rod.
() _R	conditions at the inboard end of the torsionally active portion of the blade.
() _S	conditions at snubber (inboard end of torque tube).
() _{TT}	torque tube.

Superscripts

() [—]	nondimensionalization by combinations of m_0 , R and/or Ω .
() [*]	differentiation with respect to (Ωt) .
() [']	differentiation with respect to (r/R) .

LIST OF SYMBOLS (Cont'd.)

- ()^(d) pertains to loads arising from deflections.
- ()^(PR) pertains to loads arising directly from push-rod load.
- ()⁽¹⁾, ()⁽²⁾ pertains to first and second parts of definitions of deflection correction terms, respectively.
- ()⁽⁻⁾, ()⁽⁺⁾ to be evaluated at a specified point minus or plus an infinitesimal amount.

PRINCIPAL ASSUMPTIONS

The principal assumptions used to derive the basic differential equation of motion are as follows:

1. The rotor is rotating at a constant angular velocity, has infinite hub impedance, and is in steady translational flight.
2. The blade elasticity is adequately described by the conventional (linear) beam bending and bar torsion characteristics described in Ref. 4. Although the effects of the additional section constants B_1 and B_2 described therein are usually considered to be negligible for helicopter applications, they are potentially important for accurately analyzing solid sectional, highly twisted propeller blades and/or wind turbines. To preserve consistency with the rigor applied to other aspects of structural twist and to achieve universality with such nonhelicopter rotor systems, these elastic section constants are retained in the full nonlinear formulation given in Ref. 4.
3. The elastic (torsion) axis of the undeflected blade is a straight line. However, when deflected in bending, the elastic axis defines a space curve about which the local torsion deflections must take place.
4. The blade aerodynamic and structural twist distributions are nonlinear; additionally the structural twist of the flexbeam (bearingless rotor applications only) is time variable.
5. The total (integrated) angle of structural twist is negligible beyond second order; cases of large local twist rates over short sections of span are not denied, however. See section on coordinate system for more details.
6. Radial foreshortening of blade elements due solely to elastic deflections, in the absence of precone (or flapping), and prelag (or lagging) is adequately represented by a second order function of flatwise bending.
7. The feathering axis is coincident with the elastic axis of the elastically undeformed blade.
8. The blade distributions of center of gravity, aerodynamic center and center of tension (intersection of flatwise and edgewise neutral axes) are, in general, noncoincident with the elastic axis.

9. The blade sections have finite thicknesswise mass, but the thicknesswise displacements of the section center-of-gravity away from the chordwise principal axis is negligible.
10. While assumptions regarding the smallness of various quantities and products of these quantities are not generally required for the implementation of time-history solutions of the full nonlinear equations, they are required for effecting consistent linearized approximations for the eigensolutions. For this case, coefficients of the perturbational variables, whose orders of magnitude exceed ϵ^2 are neglected. Here ϵ is an unspecified small number less than unity and where the assumed orders of magnitude of the various pertinent quantities, as measured by ϵ , are given in Table I.

COORDINATE TRANSFORMATIONS DUE TO PITCH ANGLE AND TWIST

The aeroelastic analysis is a modal type analysis which uses, as its basic description of the elastic deflections, hereafter called primitive modes, the normal vibration modes calculated assuming the blade to have zero coning, pitch angle and twist. These modes are sometimes referred to as "uncoupled" modes. Thus, the resulting aeroelastic bending responses, as ultimately coupled by coning, pitch angle, twist, aerodynamics, etc., must be interpreted as flatwise and edgewise responses rather than out-of-plane and inplane responses. The basic advantage claimed for this choice of primitive modes over those appropriate to a blade already twisted and pitched at some nominal angle, which are sometimes referred to as "coupled" modes, is the convenience of usage especially for bearingless rotor applications. A single set of uncoupled primitive modes needs to be calculated for any one rotor speed and is adequate for all subsequent twist and pitch angle combinations. The purpose of this section, therefore, is to describe the introduction of pitch angle and twist using uncoupled normal modes as the set of primitive modes.

The basic blade coordinate system used herein and referred to as the "5" coordinate system consists of the elastically undeflected blade at the flapped (or preconed), lagged (or prelagged) position. See Ref. 1 for a detailed discussion of the coordinate transformations preceding this. As shown below in Fig. 2, the x_5 -axis is out the span from the blade root or offset point, as appropriate; the y_5 -axis is parallel to the hub plane and positive forward, while the z_5 -axis is perpendicular to x_5 and y_5 and positive upward, but not generally parallel with the spin axis.

As is discussed above, the local elastic deformations (nondimensionalized by rotor radius, R) consist of finite series summations of normal bending modes in the flatwise and edgewise directions:

$$\bar{w}_e = \sum_{i=1}^{NFM} \gamma_{w_i}(\bar{r}) q_{w_i}(t) \quad (1)$$

$$\bar{v}_e = \sum_{k=1}^{NEM} \gamma_{v_k}(\bar{r}) q_{v_k}(t) \quad (2)$$

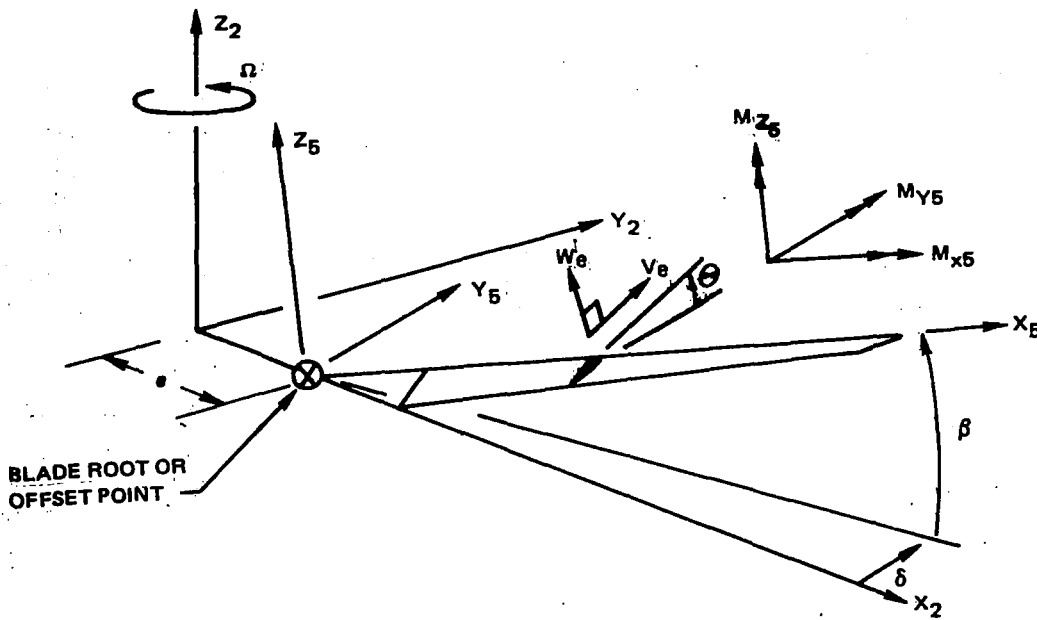


Figure 2. - Schematic of the "5" Coordinate System.

In the presence of only blade pitch angle the resulting deflections in the "5" coordinate system are simple trigonometric transformations of these flatwise and edgewise contributions. The effect of twist, however, is to require an "integrated" trigonometric transformation. This integrated effect can be achieved by means of, first, a direct trigonometric transformation not on deflection, but upon second (nondimensional) spanwise derivatives of the deflections:

$$\bar{y}_5'' = \bar{v}_e'' \cos \Theta - \bar{w}_e'' \sin \Theta \quad (3)$$

$$\bar{z}_5'' = \bar{v}_e'' \sin \Theta + \bar{w}_e'' \cos \Theta \quad (4)$$

This coordinate system transformation has the advantage that the "force" boundary conditions at the tip of the blade in the "5" coordinate system are always satisfied. Equations (3) and (4) and their first spanwise derivatives taken together with the boundary conditions imposed on γ_{w_i} and γ_{v_k} given in Eqs. (1) and (2) are sufficient for this result. Eqs. (3) and (4) can then be integrated by parts to give the fundamental deflection coordinate transformation used throughout the G400 aeroelastic analysis. This transformation becomes the usual trigonometric transformation on deflections given in Refs. 1, 4 and elsewhere in the literature, but with the addition of various deflection correction terms due to twist:

$$\bar{y}_5 = (\bar{v}_e + \Delta v - \Delta V) \cos \Theta - (\bar{w}_e - \Delta w - \Delta W) \sin \Theta + \underline{O(\Theta'^3)} \quad (5)$$

$$\bar{z}_5 = (\bar{v}_e + \Delta v - \Delta V) \sin \Theta + (\bar{w}_e - \Delta w - \Delta W) \cos \Theta + \underline{O(\Theta'^3)} \quad (6)$$

where the underlined terms are, by assumption, negligible, and where the deflection correction terms are given by the following:

first order in twist:

$$\begin{aligned} \Delta v &= \left[\int_0^{\bar{r}} \Theta' \gamma_{w_i} d\bar{r}_1 + \int_0^{\bar{r}} \int_0^{\bar{r}_1} \Theta' (\gamma'_{w_i} - \gamma'_{w_{0i}}) d\bar{r}_2 d\bar{r}_1 \right] q_{w_i} \\ &= (\Delta v_i^{(1)} + \Delta v_i^{(2)}) q_{w_i} = \Delta v_i q_{w_i} \end{aligned} \quad (7)$$

$$\begin{aligned} \Delta w &= \left[\int_0^{\bar{r}} \Theta' \gamma_{v_k} d\bar{r}_1 + \int_0^{\bar{r}} \int_0^{\bar{r}_1} \Theta' (\gamma'_{v_k} - \gamma'_{v_{0k}}) d\bar{r}_2 d\bar{r}_1 \right] q_{v_k} \\ &= (\Delta w_k^{(1)} + \Delta w_k^{(2)}) q_{v_k} = \Delta w_k q_{v_k} \end{aligned} \quad (8)$$

second order in twist:

$$\begin{aligned} \Delta v &= \left[\int_0^{\bar{r}} \Theta' \Delta w_k d\bar{r}_1 + \int_0^{\bar{r}} \int_0^{\bar{r}_1} \Theta' \Delta w_k^{(2)'} d\bar{r}_2 d\bar{r}_1 \right] q_{v_k} \\ &= (\Delta v_k^{(1)} + \Delta v_k^{(2)}) q_{v_k} = \Delta v_k q_{v_k} \end{aligned} \quad (9)$$

$$\begin{aligned} \Delta w &= \left[\int_0^{\bar{r}} \Theta' \Delta v_i d\bar{r}_1 + \int_0^{\bar{r}} \int_0^{\bar{r}_1} \Theta' \Delta v_i^{(2)'} d\bar{r}_2 d\bar{r}_1 \right] q_{w_i} \\ &= (\Delta w_i^{(1)} + \Delta w_i^{(2)}) q_{w_i} = \Delta w_i q_{w_i} \end{aligned} \quad (10)$$

It is to be noted that the total (nondimensional) twist rate, Θ' , contains the built-in twist, θ_B' , the twist due to control inputs, θ_C' , and the time dependent elastic deflection, θ_e' ($= \gamma'_{\theta_j} \cdot q_{\theta_j}$). Thus, the deflection correction terms, Δv , Δw , ΔV and ΔW , nominally contain nonlinear products of q_{θ_j} with either q_{w_i} and/or q_{v_k} . Herein, however, the products $q_{\theta_j} \cdot q_{w_i}$ and $q_{\theta_j} \cdot q_{v_k}$ are retained only in the Δv and Δw (first order) correction terms and denoted as Δv_e and Δw_e respectively; the ΔV and ΔW (second order) correction terms retain only the built-in twist rate, θ_B' , and that due to control inputs, θ_C' , in accordance with the assumed relative order-of-magnitudes given in Table I.

To complete this section, a physical interpretation of the above formulated coordinate transformation is presented by considering the following argument: Let a uniformly twisted blade possessing only flatwise flexibility be uniformly bent (in only the flatwise sense) over its span by continuously taking small bends at points outward along the span starting at the root, as shown in Fig. 3 below. Then, with each such small bend, the deflection locus of the blade tip, point P, is traced to its final deflected position, point P'. The initial part of the locus must be in a direction normal to the blade root chord since the initial flatwise bend is defined to be normal to the blade root chord. Similarly, the final part of the locus must be in a direction normal to the blade tip chord since the final flatwise bend is defined normal to the blade tip chord. Thus, the locus must define a curved path (arc PP'), as shown. In contrast, using the straight trigonometric transformation on the flatwise deflection, w_e , together with the pitch angle at the tip, θ_T , the blade tip would be predicted to be at point P'', where the flatwise deflection equals both the PP'' and the arc length PP'. The figure clearly shows that the

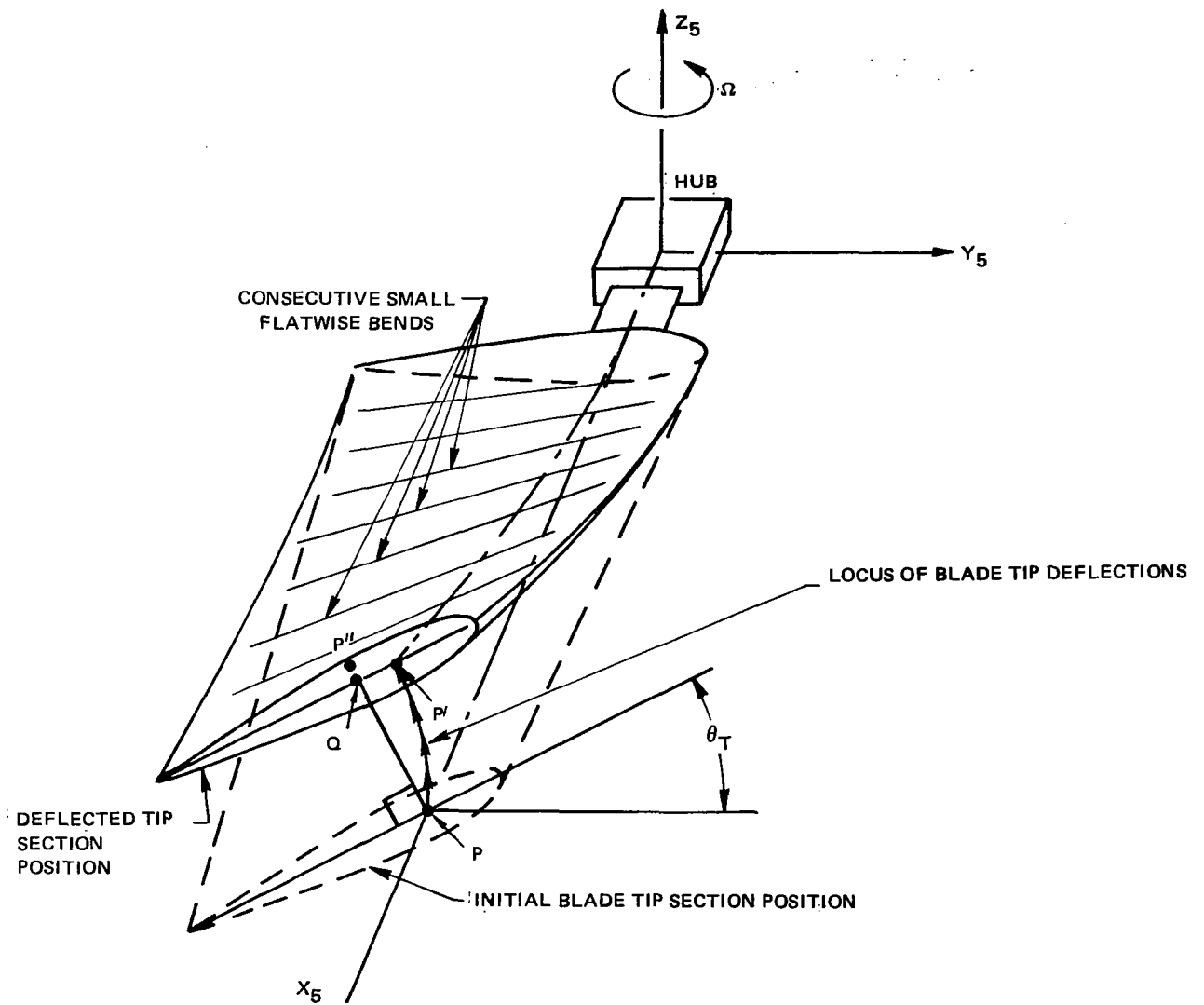


Figure 3.- Illustration of the Physical Significance of the Deflection Correction Terms Resulting from Assumed Coordinate Transformation.

straight trigonometric transformation will yield the actual deflection only if the chordwise and thicknesswise corrections, QP' and QP'' , respectively, are added to the trigonometric transformation:

$$y_5 = (QP') \cos \theta_T - (PP'' - QP'') \sin \theta_T$$

$$z_5 = (QP') \sin \theta_T + (PP'' - QP'') \cos \theta_T$$

which reduce to Eqs. (5) and (6) where PP'' is given by w_e and where QP' and QP'' are, respectively, approximated by Δv and ΔW .

Flatwise and Edgewise Bending Equations

The differential equations of blade bending are obtained by equilibrating the flatwise and edgewise moments at arbitrary span locations. Reference to Fig. 2 and the principal assumptions leads to the following moment equilibrium equations:

$$EI_y w_e'' = -M_{y_5} \cos \Theta - M_{z_5} \sin \Theta \quad (11)$$

$$EI_z v_e'' - e_A T - EB_2 \left(\theta_B' + \frac{1}{2} \theta_e' \right) \theta_e' = M_{z_5} \cos \Theta - M_{y_5} \sin \Theta \quad (12)$$

Application of the Galerkin technique requires that the equilibrium equations be in the form of loading equations; hence, Eqs. (11) and (12) must first be doubly differentiated. A method of performing this double differentiation which maintains equation compactness is given below. The first differentiation yields the following equations:

flatwise bending:

$$\left[EI_y w_e'' \right]' + \Theta \left[EI_z v_e'' - e_A T - EB_2 \left(\theta_B' + \frac{1}{2} \theta_e' \right) \theta_e' \right] = - \left[M'_{y_5} \cos \Theta + M'_{z_5} \sin \Theta \right] \quad (13)$$

edgewise bending:

$$\left[EI_z v_e'' - e_A T - EB_2 \left(\theta_B' + \frac{1}{2} \theta_e' \right) \theta_e' \right]' - \left[\Theta EI_y w_e'' \right] = \left[M'_{z_5} \cos \Theta - M'_{y_5} \sin \Theta \right] \quad (14)$$

where the derivatives of the applied moments, M'_{y_5} and M'_{z_5} are expressible as:

$$M'_{y_5} = \int_r^R p_{z_5} dr_1 - z'_5 T - q_{y_5} \quad (15)$$

$$M'_{z_5} = -\int_r^R p_{y_5} dr_1 + y'_5 T - q_{z_5} \quad (16)$$

and where the tension is given by:

$$T = \int_r^R p_{x_5} dr_1 \quad (17)$$

The applied force loading distributions, p_{y_5} and p_{z_5} , and the applied moment loading distributions q_{y_5} and q_{z_5} , all include not only the inertia and aerodynamic contributions but any loads due to mechanical loads applied by push-rods, dampers, etc. The second differentiation of the moment equilibrium equations is performed after first resolving Eqs. (13) and (14) to isolate M'_{y_5} and M'_{z_5} :

$$\begin{aligned} -M''_{y_5} = & \left\{ \left[(EI_z v''_e - e_A T - EB_2 (\theta'_B + \frac{1}{2} \theta'_e) \theta'_e)' - \Theta' EI_y w''_e \right] \sin \Theta \right. \\ & \left. + \left[(EI_y w''_e)' + \Theta' (EI_z v''_e - e_A T - EB_2 (\theta'_B + \frac{1}{2} \theta'_e) \theta'_e) \right] \cos \Theta \right\}' = (RHS)_w \end{aligned} \quad (18)$$

$$\begin{aligned} M''_{z_5} = & \left\{ \left[(EI_z v''_e - e_A T - EB_2 (\theta'_B + \frac{1}{2} \theta'_e) \theta'_e)' - \Theta' EI_y w''_e \right] \cos \Theta \right. \\ & \left. - \left[(EI_y w''_e)' + \Theta' (EI_z v''_e - e_A T - EB_2 (\theta'_B + \frac{1}{2} \theta'_e) \theta'_e) \right] \sin \Theta \right\}' = (RHS)_v \end{aligned} \quad (19)$$

Application of the Galerkin technique requires consideration of the work due to virtual displacements of the bending modes. It must be noted, however, as was shown in the preceding subsection, that in the presence of twist, flatwise and edgewise modal displacements each generate deflections in both the flatwise and edgewise directions. Hence, the proper formal application of the Galerkin technique is to integrate the inner products of loadings and virtual displacements:

$$\int_0^R \left\{ -(z_5)_{w_i} \left[M''_{y_5} + (\text{RHS})_w \right] + (y_5)_{w_i} \left[M''_{z_5} - (\text{RHS})_v \right] \right\} dr = 0 \quad (20)$$

k'th edgewise modal equation:

$$\int_0^R \left\{ -(z_5)_{v_k} \left[M''_{y_5} + (\text{RHS})_w \right] + (y_5)_{v_k} \left[M''_{z_5} - (\text{RHS})_v \right] \right\} dr = 0 \quad (21)$$

The quantities $(\text{RHS})_w$ and $(\text{RHS})_v$, as defined by Eqs. (18) and (19), involve differentiated combinations of twist and cosine and sine of the pitch angle and elastic restoring moment. Although not immediately obvious, the integrals of these (RHS) quantities with the components of deflection, as given by Eqs. (5) and (6), can be evaluated, using integration by parts, to yield the following simplified forms:

$$\int_0^R \left[(z_5)_{w_i} (\text{RHS})_w + (y_5)_{w_i} (\text{RHS})_v \right] dr = \int_0^R \gamma''_{w_i} EI_y w''_e dr \quad (22)$$

$$\int_0^R \left[(z_5)_{v_k} (\text{RHS})_w + (y_5)_{v_k} (\text{RHS})_v \right] dr = \int_0^R \gamma''_{v_k} EI_z \left[v''_e - e_A T - EB_2 \left(\theta'_B + \frac{1}{2} \theta'_e \right) \theta'_e \right] dr \quad (23)$$

The desired basic bending modal excitation equations can then be written by combining the results of Eqs. (5), (6), (15), (16), (20), (21), (22) and (23). Hereafter all quantities and equations will be written in nondimensional form (without overbars) where the nondimensionalization is accomplished using appropriate combinations of R , Ω and m_0 :

$$\begin{aligned}
& \int_0^l \left\{ -(\gamma_{w_i} - \Delta w_i)(p_{Dz_5} \cos \Theta - p_{Dy_5} \sin \Theta) - \Delta v_i(p_{Dz_5} \sin \Theta + p_{Dy_5} \cos \Theta) \right. \\
& \quad + T \left[(\gamma_{w_i}' - \Delta w_i^{(2)'}) (w_e' - \Delta w^{(2)'} - \Delta w^{(2)'}) + \Delta v_i^{(2)'} (v_e' + \Delta v^{(2)'}) \right] \\
& \quad \left. + (\gamma_{w_i}' - \Delta w_i^{(2)'}) (q_{Dy_5} \cos \Theta + q_{Dz_5} \sin \Theta) - \Delta v_i^{(2)'} (q_{Dz_5} \cos \Theta - q_{Dy_5} \sin \Theta) + \gamma_{w_i}'' EI_y w_e'' \right\} dr \\
& = \int_0^l \left\{ (\gamma_{w_i}' - \Delta w_i') (p_{Az_5} \cos \Theta - p_{Ay_5} \sin \Theta) + \Delta v_i (p_{Az_5} \sin \Theta + p_{Ay_5} \cos \Theta) - \gamma_{w_i}' q_{Ay_5} \cos \Theta \right\} dr \\
& \quad + \sum_{m=1}^M \left[(z_5(r_m))_{w_i} F_{z_{5m}} + (y_5(r_m))_{w_i} F_{y_{5m}} - (z_5'(r_m))_{w_i} M_{y_{5m}} + (y_5'(r_m))_{w_i} M_{z_{5m}} \right] \quad (24)
\end{aligned}$$

k'th edgewise bending equation:

$$\begin{aligned}
& \int_0^l \left\{ -(\gamma_{v_k} - \Delta v_k)(p_{Dz_5} \sin \Theta + p_{Dy_5} \cos \Theta) + \Delta w_k(p_{Dz_5} \cos \Theta - p_{Dy_5} \sin \Theta) \right. \\
& \quad + T \left[(\gamma_{v_k}' - \Delta v_k^{(2)'}) (v_e' + \Delta v^{(2)'}) - \Delta v_k^{(2)'} (w_e' - \Delta w^{(2)'}) \right] \\
& \quad - (\gamma_{v_k}' - \Delta v_k^{(2)'}) (q_{Dz_5} \cos \Theta - q_{Dy_5} \sin \Theta) - \Delta w_k^{(2)'} (q_{Dy_5} \cos \Theta + q_{Dz_5} \sin \Theta) \\
& \quad \left. + \gamma_{v_k}'' (EI_z v_e'' - e_A T - EB_2 (\theta_B' + \frac{1}{2} \theta_e')) \right\} dr \\
& = \int_0^l \left\{ (\gamma_{v_k} - \Delta v_k) (p_{Az_5} \sin \Theta + p_{Ay_5} \cos \Theta) - \Delta w_k (p_{Az_5} \cos \Theta - p_{Ay_5} \sin \Theta) \right\} dr \\
& \quad + \sum_{m=1}^M \left[(z_5(r_m))_{v_k} F_{z_{5m}} + (y_5(r_m))_{v_k} F_{y_{5m}} - (z_5'(r_m))_{v_k} M_{y_{5m}} + (y_5'(r_m))_{v_k} M_{z_{5m}} \right] \quad (25)
\end{aligned}$$

The subscripts A and D denote terms of aerodynamic and dynamic origin, respectively, and the finite summations over m represent the modal excitations due to a finite number of concentrated forces and moments.

Torsion Equation

In a development similar to that given above, the differential equation for torsion is obtained by first equilibrating the blade torsional moment. In Ref. 5 is derived the torsional equilibrium equation for the blade, consistent with the assumption of a space curve torsional axis:

$$\begin{aligned}
 & GJ\theta'_e + \Theta k_A^2 T + \frac{1}{2} EB_1 (\theta'^2 - \theta_B'^2) \theta' - EB_2 \theta'_B v_e'' \\
 & = \int_r^1 \left\{ [(z_{5_1} - z_5) y'_5 - (y_{5_1} - y_5) z'_5] p_{x_5}(r_1) - [(z_{5_1} - z_5) - (r_1 - r) z'_5] p_{y_5}(r_1) \right. \\
 & \quad \left. + [(y_{5_1} - y_5) - (r_1 - r) y'_5] p_{z_5}(r_1) + q_{x_5}(r_1) + y'_5 q_{y_5}(r_1) + z'_5 q_{z_5}(r_1) \right\} dr_1
 \end{aligned} \tag{26}$$

where y_{5_1} and z_{5_1} are the inplane and out-of-plane deflections evaluated at r_1 .

Differentiation of this equation yields an intermediate form of the required torsion loading equation:

$$\begin{aligned}
 & [GJ\theta'_e + \Theta k_A^2 T + \frac{1}{2} EB_1 (\theta'^2 - \theta_B'^2) \theta' - EB_2 \theta'_B v_e'']' = -q_{x_5} - y'_5 q_{y_5} - z'_5 q_{z_5} \\
 & \quad + y_5'' \int_r^1 [(z_{5_1} - z_5) p_{x_5}(r_1) - (r_1 - r) p_{z_5}(r_1) + q_{y_5}(r_1)] dr_1 \\
 & \quad - z_5'' \int_r^1 [(y_{5_1} - y_5) p_{x_5}(r_1) - (r_1 - r) p_{y_5}(r_1) - q_{z_5}(r_1)] dr_1
 \end{aligned} \tag{27}$$

Integration by parts yields a second intermediate form:

$$\begin{aligned}
 & \left[GJ\theta'_e + \Theta'k_A^2 T + \frac{1}{2}EB_1 (\theta'^2 - \theta_B'^2) \theta' - EB_2 \theta'_B v_e'' \right]' = -q_{x_5} - y'_5 q_{y_5} - z'_5 q_{z_5} \\
 & + y_5'' \int_{r_1}^1 \left[z'_{5_1} \int_{r_1}^1 p_{x_5}(r_2) dr_2 - \int_{r_1}^1 p_{z_5}(r_2) dr_2 + q_{y_5}(r_1) \right] dr_1 \\
 & - z_5'' \int_{r_1}^1 \left[y'_{5_1} \int_{r_1}^1 p_{x_5}(r_2) dr_2 - \int_{r_1}^1 p_{y_5}(r_2) dr_2 - q_{z_5}(r_1) \right] dr_1
 \end{aligned} \tag{28}$$

which, when combined with Eqs. (15), (16), and (17), with (11) and (12), and finally with (3) and (4) yields the final desired form of the loading equation:

$$\begin{aligned}
 & \left[GJ\theta'_e + \Theta'k_A^2 T + \frac{1}{2}EB_1 (\theta'^2 - \theta_B'^2) \theta' - EB_2 \theta'_B v_e'' \right]' \\
 & - \left[(EI_z - EI_y) v_e'' w_e'' - (e_A T + EB_2 (\theta'_B + \frac{1}{2} \theta'_e) \theta'_e) w_e'' \right] = -q_{x_5} - y'_5 q_{y_5} - z'_5 q_{z_5}
 \end{aligned} \tag{29}$$

Application of the Galerkin technique to this equation then follows in a straightforward manner to give the following basic form of the j'th torsion modal excitation equation:

$$\begin{aligned}
 & \int_0^1 \left\{ \gamma_{\theta_j} \left[-q_{Dx_5} - y'_5 q_{Dy_5} - z'_5 q_{Dz_5} + (EI_z - EI_y) v_e'' w_e'' - (e_A T + EB_2 (\theta'_B + \frac{1}{2} \theta'_e) \theta'_e) w_e'' \right] \right. \\
 & \left. + \gamma'_{\theta_j} \left[GJ\theta'_e + \Theta'k_A^2 T + \frac{1}{2}EB_1 (\theta'^2 - \theta_B'^2) \theta' - EB_2 \theta'_B v_e'' \right] \right\} dr \\
 & = \int_0^1 \gamma_{\theta_j} q_{Ax_5} dr + \sum_{m=1}^M \gamma_{\theta_j} (r_m) M_{x_7m}
 \end{aligned} \tag{30}$$

where, again, the summation over m represents the effect of concentrated torsion loads on the torsion modal excitation.

Rigid Flapping and Lagging Equations

The equations of motion for rigid flapping and lagging are obtained by equilibrating the moments about the articulation hinge about the y_5 and z_5 axes, respectively:

rigid flapping:

$$\int_0^l (r p_{z_5} - z_5 p_{x_5} - q_{y_5}) dr + \sum_{m=1}^M (r_m F_{z_{5m}} - M_{y_{5m}}) = 0 \quad (31)$$

rigid lagging:

$$\int_0^l (r p_{y_5} - y_5 p_{x_5} + q_{z_5}) dr + M_{LD} + \sum_{m=1}^M (r_m F_{y_{5m}} + M_{z_{5m}}) = 0 \quad (32)$$

where M_{LD} is the root moment due to the lag damper and is typically proportional to blade root angular rate:

$$M_{LD} = -C_{LD} \left[\delta^* + \dot{y}_5^*(0) \right] \quad (33)$$

with C_{LD} as the familiar linear damping rate of the damper. Note that as per Eq. (5) the (nondimensional) time derivative of elastic in-plane slope will generally contain contributions proportional to flatwise and edgewise modal deflection and to flatwise, edgewise and torsion modal rates.

The equations of motion presented above for the bending and torsion modes and for rigid flapping and lagging ((24), (25), (30), (31), and (32), respectively) are complete only in so far as the load distributions are (explicitly or implicitly) available. The following section presents implicit statements

of the loading in terms of the blade deflections, as formulated in the following section. Furthermore, these equations are basic required forms of the aeroelastic response excitation equations from which, together with appropriate expressions for the load distributions, a set of linearized equations can be expanded for eigensolutions, or a set of nonlinear equations of the form:

$$[A] \{\ddot{q}\} = \{F(\psi)\} \quad (34)$$

can be written for time-history solutions. The A matrix above consists of the coefficients of the second derivatives of the modal responses and represent terms extracted from the compact expressions for dynamic load distribution. This matrix is also discussed more fully in the following section.

DYNAMIC AND AERODYNAMIC LOAD DISTRIBUTIONS

The load distribution appearing in the above derived dynamic equations for the response variables were expressed only implicitly for two reasons: first, because it simplifies the explanation of the application of the Galerkin technique and second, because completely expanded, explicit, expressions for the loadings are tedious, cumbersome and not actually required for the more important time-history solution. Complete linearized expansions of the loadings are required, however, for a formulation of the linearized equations used in the eigensolution.

Dynamic Load Distributions

The usual approach of using D'Alembert's principle to express the inertial acceleration of the distributed blade mass as an equivalently applied dynamic load distribution is followed herein. The position vector of a point mass particle, with a chordwise and thicknesswise displacement relative to the "5" coordinate system, is written as follows:

$$\{x_5\} = \begin{pmatrix} r + u_e - y_{10}(y'_5 \cos \Theta + z'_5 \sin \Theta) - z_{10}(z'_5 \cos \Theta - y'_5 \sin \Theta) \\ y_5 + y_{10} \cos \Theta - z_{10} \sin \Theta \\ z_5 + y_{10} \sin \Theta + z_{10} \cos \Theta \end{pmatrix} \quad (35)$$

where y_{10} and z_{10} are, respectively, the (forward) chordwise and (upward) thicknesswise locations of the point mass from the reference, x_5 , axis, and where the axial deflection due to elastic flatwise bending is given by the following expression:

$$u_e = - \sum_{i,m=1}^{NFM} \frac{1}{2} \left[\int_0^r \chi'_{w_i} \chi'_{w_m} dr \right] q_{w_i} q_{w_m} \quad (36)$$

The displacement of the point mass particle relative to the inertial frame is obtained by means of four consecutive coordinate transformations and is written in the following compact form:

$$\{x_1\} = [T_1] \left[\begin{Bmatrix} e \\ 0 \\ 0 \end{Bmatrix} + [T_3][T_4]\{x_5\} \right] \quad (37)$$

where the four coordinate transformations, described in detail in Ref. 1, in consecutive order, account for rotor rotation, blade root offset, lead-lag rotation about the (articulation) hinge or offset point, and flapwise rotation also about the offset point:

$$[T_1] = \begin{bmatrix} \cos\psi & -\sin\psi & 0 \\ \sin\psi & \cos\psi & 0 \\ 0 & 0 & 1 \end{bmatrix} \quad (38a)$$

$$[T_3] = \begin{bmatrix} \cos\delta & -\sin\delta & 0 \\ \sin\delta & \cos\delta & 0 \\ 0 & 0 & 1 \end{bmatrix} \quad (38b)$$

$$[T_4] = \begin{bmatrix} \cos\beta & 0 & -\sin\beta \\ 0 & 1 & 0 \\ \sin\beta & 0 & \cos\beta \end{bmatrix} \quad (38c)$$

Upon letting:

$$[T_5] = [T_1][T_2][T_3] \quad (38d)$$

the inertial acceleration of the point blade element can be written as:

$$\{\ddot{x}_1^{**}\} = [\ddot{T}_1^{**}]\{e\} + [T_5]\{\ddot{x}_5^{**}\} + 2[\dot{T}_5^{**}]\{\dot{x}_5^{**}\} + [T_5^{**}]\{\ddot{x}_5^{**}\} \quad (39)$$

where the details of forming the indicated differentiations and matrix multiplications are omitted herein for clarity. The dynamic force load distributions are formed as follows:

$$\begin{pmatrix} S_{Dx_5} \\ S_{Dy_5} \\ S_{Dz_5} \end{pmatrix} = - \int \int_{\substack{\text{blade} \\ \text{section} \\ \text{area}}} \rho dA \{ \ddot{X}_1 \} \quad (40)$$

whose components are formed by using Eq. (39) and can be written as:

$$p_{Dx_5} = m \{ e + r(1 + 2\ddot{\delta} - \beta^2) + 2\ddot{y}_5 + u_e - \beta z_5 \} \quad (41a)$$

$$\begin{aligned} p_{Dy_5} = & -m \{ e\delta + r(\ddot{\delta} - 2\beta\dot{\beta}) + \ddot{y}_5 + 2(\ddot{u}_e - \beta\ddot{z}_5 - \dot{\beta}z_5) - (1 + 2\ddot{\delta})y_5 \\ & + y_{10CG} \left[-2(\ddot{v}'_e - \Delta\ddot{V}^{(2)'} + \Delta\ddot{V}^{(2)'}) - (1 + 2\ddot{\delta} + \ddot{\Theta}^2 + 2\beta\ddot{\Theta}) \cos\Theta - (\ddot{\Theta} + 2\dot{\beta}) \sin\Theta \right] \} \end{aligned} \quad (41b)$$

$$p_{Dz_5} = -m \{ e\beta + r(\dot{\beta} + \beta + 2\beta\dot{\delta}) + \ddot{z}_5 + 2\beta\ddot{y}_5 + y_{10CG} \left[\ddot{\Theta} \cos\Theta - (\ddot{\Theta}^2 + 2\beta\ddot{\Theta}) \sin\Theta \right] \} \quad (41c)$$

The dynamic moment load distributions are similarly formed:

$$\begin{pmatrix} q_{Dx_5} \\ q_{Dy_5} \\ q_{Dz_5} \end{pmatrix} = - \int \int_{\substack{\text{blade} \\ \text{section} \\ \text{area}}} \rho dA \begin{bmatrix} 0 & -\hat{z}_{10} & \hat{y}_{10} \\ -\hat{z}_{10} & 0 & 0 \\ \hat{y}_{10} & 0 & 0 \end{bmatrix} \{ \ddot{X}_1 \} \quad (42)$$

where the chordwise and thicknesswise integration variables resolved into the "5" coordinate system are given by:

$$\hat{y}_{10} = y_{10} \cos \Theta - z_{10} \sin \Theta \quad (43a)$$

$$\hat{z}_{10} = y_{10} \sin \Theta + z_{10} \cos \Theta \quad (43b)$$

The components of the moment load distributions can then be written as:

$$\begin{aligned} q_{D_{x_5}} = & -m \left\langle y_{10CG} \left\{ [e\beta + r(\beta^{**} + \beta + 2\beta\delta^*) + z_5^{**} + 2\beta y_5^*] \cos \Theta \right. \right. \\ & - [e\delta + r(\delta^{**} - 2\beta\beta^*) + y_5^{**} - 2(\dot{u}_e + \beta z_5^* + \beta^* z_5) - (1 + 2\delta^*) y_5] \sin \Theta \left. \right\} \\ & + k_{y_{10}}^2 \left\{ \Theta^{**} + 2\beta^* \cos^2 \Theta - (1 + 2\delta^* - \beta^2) \sin \Theta \cos \Theta \right. \\ & \left. + 2(\dot{w}_e' - \Delta W^{(2)'} - \Delta W^{(2)'}) \cos \Theta \right\} \\ & + k_{z_{10}}^2 \left\{ \Theta^{**} + 2\beta^* \sin^2 \Theta + (1 + 2\delta^* - \beta^2) \sin \Theta \cos \Theta \right. \\ & \left. + 2(\dot{v}_e' - \Delta V^{(2)'} + \Delta V^{(2)'}) \sin \Theta \right\} \left. \right\rangle \quad (44a) \end{aligned}$$

$$\begin{aligned} q_{D_{y_5}} = & -m \left\langle -y_{10CG} \left\{ e + r(1 + 2\delta^* - \beta^2) + 2y_5^* + u_e - \beta z_5 \right\} \sin \Theta \right. \\ & + k_{y_{10}}^2 \left\{ (1 + 2\delta^*) [\dot{w}_e' - \Delta W^{(2)'} - \Delta W^{(2)'} + \beta \cos \Theta] \right. \\ & \left. + 2\Theta^* [(1 + \delta^*) \cos \Theta + \beta^* \sin \Theta] \right\} \cos \Theta \\ & + k_{z_{10}}^2 \left\{ (1 + 2\delta^*) [\dot{v}_e' - \Delta V^{(2)'} + \Delta V^{(2)'} + \beta \sin \Theta] \right. \\ & \left. + 2\Theta^* [(1 + \delta^*) \sin \Theta - \beta^* \cos \Theta] \right\} \sin \Theta \left. \right\rangle \quad (44b) \end{aligned}$$

$$\begin{aligned}
q_{Dz_5} = -m \left\langle y_{10CG} \left\{ e + r(1 + 2\delta^* - \beta^2) + 2y_5^* + u_e - \beta z_5 \right\} \cos \Theta \right. \\
+ k_{y_{10}}^2 \left\{ (1 + 2\delta^*) \left[w_e' - \Delta w^{(2)'} - \Delta w^{(2)'} + \beta \cos \Theta \right] \right. \\
+ 2\Theta^* \left[(1 + \delta^*) \cos \Theta + \beta \sin \Theta \right] \left. \right\} \sin \Theta \\
- k_{z_{10}}^2 \left\{ (1 + 2\delta^*) \left[v_e' - \Delta v^{(2)'} + \Delta v^{(2)'} + \beta \sin \Theta \right] \right. \\
\left. \left. + 2\Theta^* \left[(1 + \delta^*) \sin \Theta - \beta \cos \Theta \right] \right\} \cos \Theta \right\rangle \quad (44c)
\end{aligned}$$

where y_{10CG} , $k_{y_{10}}$ and $k_{z_{10}}$ are, respectively, the chordwise mass center and the thicknesswise and chordwise mass radii of gyration.

For both the eigensolution and the time history solution, those dynamic load terms containing second time derivatives must be extracted to form the inertia coupling matrix, $[A]$, indicated in equation (34). Using the load distributions given above, the elements of this matrix can be conveniently written using the following partitioned representation of the A matrix:

$$[A] = \begin{bmatrix} A_{w_i w_m} & A_{w_i v_k} & A_{w_i \theta_j} & A_{w_i \beta} & A_{w_i \delta} \\ A_{v_k w_i} & A_{v_k v_m} & A_{v_k \theta_j} & A_{v_k \beta} & A_{v_k \delta} \\ A_{\theta_j w_i} & A_{\theta_j v_k} & A_{\theta_j \theta_m} & A_{\theta_j \beta} & A_{\theta_j \delta} \\ A_{\beta w_i} & A_{\beta v_k} & A_{\beta \theta_j} & A_{\beta \beta} & 0 \\ A_{\delta w_i} & A_{\delta v_k} & A_{\delta \theta_j} & 0 & A_{\delta \delta} \end{bmatrix} \quad (45)$$

where:

$$A_{w_i w_m} = \int_0^l m \left[(\gamma_{w_i} - \Delta w_i) (\gamma_{w_m} - \Delta w_m) + \Delta v_i \Delta v_m \right] dr \quad (46a)$$

$$A_{w_i v_k} = A_{v_k w_i} = \int_0^l m \left[(\gamma_{v_k} - \Delta v_k) \Delta v_i - (\gamma_{w_i} - \Delta w_i) \Delta w_k \right] dr \quad (46b)$$

$$A_{w_i \theta_j} = \int_0^1 m \left\{ y_{i0c} \gamma_{\theta_j} (\gamma_{w_i} - \Delta w_i) \right. \\ \left. + \sum_{m'=1}^{NEM} \left[\gamma_{\theta_j} (\Delta v_{m'} \gamma_{w_i} - \Delta v_i \gamma_{w_{m'}}) + \Delta v_i \Delta v_{E_{m'j}} \right] q_{w_{m'}} \right. \\ \left. + \sum_{k=1}^{NEM} \left[\gamma_{\theta_j} ((\gamma_{v_k} - \Delta v_k) (\gamma_{w_i} - \Delta w_i) + \Delta v_i \Delta w_k) - \Delta w_{E_{kj}} (\gamma_{w_i} - \Delta w_i) \right] q_{v_k} \right\} dr \quad (46c)$$

$$A_{w_i \beta} = A_{\beta w_i} = \int_0^1 m r \left[(\gamma_{w_i} - \Delta w_i) \cos \Theta + \Delta v_i \sin \Theta \right] dr \quad (46d)$$

$$A_{w_i \delta} = A_{\delta w_i} = \int_0^1 m r \left[\Delta v_i \cos \Theta - (\gamma_{w_i} - \Delta w_i) \sin \Theta \right] dr \quad (46e)$$

$$A_{v_k v_m} = \int_0^1 m \left[(\gamma_{v_k} - \Delta v_k) (\gamma_{v_m} - \Delta v_m) + \Delta w_k \Delta w_m \right] dr \quad (46f)$$

$$A_{v_k \theta_j} = \int_0^1 m \left\{ -y_{i0c} \gamma_{\theta_j} \Delta w_k \right. \\ \left. - \sum_{m'=1}^{NEM} \left[\gamma_{\theta_j} ((\gamma_{w_{m'}} - \Delta w_{m'}) (\gamma_{v_k} - \Delta v_k) + \Delta w_k \Delta v_{m'}) - \Delta v_{E_{m'j}} (\gamma_{v_k} - \Delta v_k) \right] q_{w_{m'}} \right. \\ \left. + \sum_{k'=1}^{NEM} \left[\gamma_{\theta_j} (\gamma_{v_k} \Delta w_{k'} - \Delta w_k \gamma_{v_{k'}}) + \Delta w_k \Delta w_{E_{k'j}} \right] q_{v_{k'}} \right\} dr \quad (46g)$$

$$A_{v_k \beta} = A_{\beta v_k} = \int_0^1 m r \left[(\gamma_{v_k} - \Delta v_k) \sin \Theta - \Delta w_k \cos \Theta \right] dr \quad (46h)$$

$$A_{v_k \delta} = A_{\delta v_k} = \int_0^1 m r \left[(\gamma_{v_k} - \Delta v_k) \cos \Theta + \Delta w_k \sin \Theta \right] dr \quad (46i)$$

$$A_{\theta_j w_i} = \int_0^l m y_{IOCG} \gamma_{\theta_j} (\gamma_{w_i} - \Delta w_i) dr \quad (46j)$$

$$A_{\theta_j v_k} = - \int_0^l m y_{IOCG} \gamma_{\theta_j} \Delta w_k dr \quad (46k)$$

$$A_{\theta_j \beta} = A_{\beta \theta_j} = \int_0^l m y_{IOCG} r \gamma_{\theta_j} \cos \Theta dr \quad (46l)$$

$$A_{\theta_j \delta} = A_{\delta \theta_j} = - \int_0^l m y_{IOCG} r \gamma_{\theta_j} \sin \Theta dr \quad (46m)$$

$$A_{\beta \beta} = A_{\delta \delta} = \int_0^l m r^2 dr \quad (46n)$$

Aerodynamic Load Distributions

The aerodynamic load distributions used in the analysis are assumed to be two dimensional and the usual strip-theory techniques as typically described in Ref. 1 are therefore employed. More specifically, at each spanwise station the two-dimensional airfoil section angle-of-attack is calculated based upon section geometric pitch angle, Θ , and inflow angle, ϕ , based upon airflow velocities at the $3/4$ chord point:

$$\alpha_{qs} = \Theta + \phi = \Theta + \tan^{-1} \left(\frac{U_P}{U_T} \right) \quad (47)$$

where:

$$\frac{U_P}{\Omega R} = \lambda \left(1 - \frac{\beta^2}{2}\right) - U_x \left[z'_5 \left(1 - \frac{\beta^2}{2}\right) + \beta \right] - \dot{z}_5^* - r \dot{\beta}^* - y_{10} \frac{3c}{4} (\dot{\Theta} + \Theta' U_x) \cos \Theta \quad (48)$$

$$\begin{aligned} \frac{U_T}{\Omega R} = e + \mu \sin(\psi + \delta) + r \left(1 - \frac{\beta^2}{2}\right) + U_x y'_5 \left(1 - \frac{\beta^2}{2}\right) \\ + \dot{y}_5^* + r \dot{\delta}^* - y_{10} \frac{3c}{4} (\dot{\Theta} + \Theta' U_x) \sin \Theta \end{aligned} \quad (49)$$

where the radial velocity component is given by:

$$\frac{U_x}{\Omega} = \mu \cos(\psi + \delta) + y_{10} \frac{3c}{4} \cos \Theta \quad (50)$$

and where the derivatives of the "5" coordinate elastic deflections are obtained from appropriate differentiation of Eqs. (5) and (6). The total rotor inflow, $\lambda(r, \psi)$, is comprised of a "ram" portion due to forward flight and a (harmonic) induced velocity portion which is assumed to be, in general, both radially and azimuthally variable:

$$\lambda(r, \psi) = \lambda_{RAM} - v_{i0}(r) - \sum_{n=1}^{NH} \left[v_{inc}(r) \cos n\psi + v_{ins}(r) \sin n\psi \right] \quad (51)$$

where:

$$\lambda_{RAM} = \frac{V_T}{\Omega R} \sin \alpha_R = \mu \tan \alpha_R \quad (52)$$

Equation (51) represents a completely general description of the harmonic rotor inflow. Regardless of how the induced velocity components are obtained, either experimentally or analytically, they are accepted by the analysis as an environmental excitation and used directly as per Eq. (48).

Two specific, optional assumptions which can be made on the induced velocity are as follows:

a. uniform inflow:

$$v_{i0}(r) = \frac{C_T}{2B^2 \sqrt{\lambda^2 + \mu^2}} \quad (53a)$$

$$v_{inc} = v_{ins} = 0; \quad n = 1, 2, \dots, NH \quad (53b)$$

b. generalized Glauert (momentum):

$$v_{i0}(r) = v_0 \text{ (uniform)} \quad (54a)$$

$$v_{i1c}(r) = r(v_{1c} + K_v v_0) \quad (54b)$$

$$v_{i1s}(r) = r v_{1s} \quad (54c)$$

$$v_{inc}(r) = v_{ins}(r) = 0; \quad n = 2, 3, \dots, NH \quad (54d)$$

where:

$$\lambda_0 = \lambda_{RAM} - v_0 \quad (54e)$$

The nonzero (zeroth and first harmonic) components of induced velocity can then be related to rotor steady thrust and hub moments using momentum considerations:

$$\frac{C_T}{B^2} = 2\sqrt{\mu^2 + \lambda_0^2} v_0 - \frac{\lambda_0}{2\sqrt{\mu^2 + \lambda_0^2}} (v_{1c}^2 + v_{1s}^2) \quad (55a)$$

$$\frac{C_m}{B^3} = -\frac{(\mu^2 + \lambda_0^2 - \lambda_0 v_0)}{2\sqrt{\mu^2 + \lambda_0^2}} v_{1c} \quad (55b)$$

$$\frac{C_d}{B^3} = -\frac{(\mu^2 + \lambda_0^2 - \lambda_0 v_0)}{2\sqrt{\mu^2 + \lambda_0^2}} v_{1s} \quad (55c)$$

The Glauert induced velocity gradient factor, K_v , in Eq. (54b) is used to account for the strong cosine component of inflow present even for zero pitching

moment. The approximation to K_v used herein is that given in Ref. 6 based upon results of Ref. 7:

$$K_v = \frac{4\mu}{3.6 |\lambda_0| + 3\mu} \quad (56)$$

The formulations given above for the local velocities together with Eq. (47) is sufficient to define a quasi-static two-dimensional angle-of-attack. Approximate three-dimensional tip effects are introduced by multiplying this quasi-static angle-of-attack by a function which is unity over most of the blade, but reduces abruptly to zero at the blade tip:

$$f_\alpha = \begin{cases} 1 & ; \quad 0 \leq r \leq 2B-1 \\ \sqrt{1 - \frac{1}{4} \left(\frac{r-2B+1}{1-B} \right)^2} & ; \quad 2B-1 < r \leq 1 \end{cases} \quad (57a)$$

where B is the conventional tip loss factor.

The effective angle-of-attack used to calculate aerodynamic coefficients is then given by:

$$\alpha_{\text{eff}} = \begin{cases} f_\alpha \alpha_{\text{qs}} & ; \quad |\alpha_{\text{qs}}| \leq \frac{\pi}{2} \\ f_\alpha \alpha_{\text{qs}} + \text{sgn}(\alpha_{\text{qs}})(1-f_\alpha)\pi & ; \quad |\alpha_{\text{qs}}| > \frac{\pi}{2} \end{cases} \quad (57b)$$

The Mach number at the airfoil section is given simply by the following expression:

$$M = \frac{U}{a_\infty} = \frac{1}{a_\infty} \sqrt{U_p^2 + U_T^2} \quad (58)$$

From the effective angle-of-attack and Mach number, the following expressions for (nondimensional) aerodynamic load distributions can be formed:

$$P_{Ay_5} = \frac{1}{2} \left(\frac{\rho R^2}{m_0} \right) c_U (c_{\ell} U_P - c_d U_T) \quad (59a)$$

$$P_{Az_5} = \frac{1}{2} \left(\frac{\rho R^2}{m_0} \right) c_U (c_{\ell} U_T + c_d U_P) \quad (59b)$$

$$q_{Ax_5} = y_{10c/4} (q_{Az_5} \cos \Theta - q_{Ay_5} \sin \Theta) + \frac{1}{2} \left(\frac{\rho R^2}{m_0} \right) c^2 U \left[U c_{m_{c/4}} - \frac{\pi}{2} c \kappa_{Ax_5}^* \right] \quad (59c)$$

where:

$$c_{\ell} = c_{\ell}(\alpha_{\text{eff}}, M) \quad (60a)$$

$$c_d = c_d(\alpha_{\text{eff}}, M) + \Delta c_{d_0} \quad (60b)$$

$$c_{m_{c/4}} = c_{m_{c/4}}(\alpha_{\text{eff}}, M) \quad (60c)$$

$$\kappa_{Ax_5} = \begin{cases} 1 - 2y_{10c/4}/c & ; \quad |\alpha_{qs}| \leq \frac{\pi}{2} \\ 2y_{10c/4}/c & ; \quad |\alpha_{qs}| > \frac{\pi}{2} \end{cases} \quad (60d)$$

$\Delta c_{d_0} \equiv$ incremental drag coefficient introduced to account for surface roughness.

The dynamic equations given in the previous subsection together with the load distributions presented above are sufficient to complete the basic aeroelastic analysis of the rotor blade. Such a basic analysis, however, omits the effects of pitch-flat/edge coupling. The following subsection includes a unified method for including such coupling.

RIGID BODY FEATHERING MOTION AND
BASIC PITCH-FLAT/EDGE COUPLING EFFECTS

The simulations of the rigid body feathering motion (if present) and the automatic blade pitch changes accruing from elastic bending deflections and/or flapping and lagging motions are both accomplished by the introduction of a torsional "pseudo"-mode. Such a mode is no more than the rigid body feathering motion of the blade as would be generated by a control input. Operationally, this "pseudo"-mode is treated in the analysis as a spanwise variable mode shape in addition to the conventional normal torsion modes used to describe the blade torsion. In general, this mode has a unit value over the blade span except, for analyses of the bearingless rotor, over the flexbeam - torque tube portion of the blade wherein the spanwise elastic torsion deflection of the flexbeam (due to a control input) is used. Reference to Fig. 4 shows the pertinent features of this pseudo-mode, especially as it is applied to bearingless rotors:

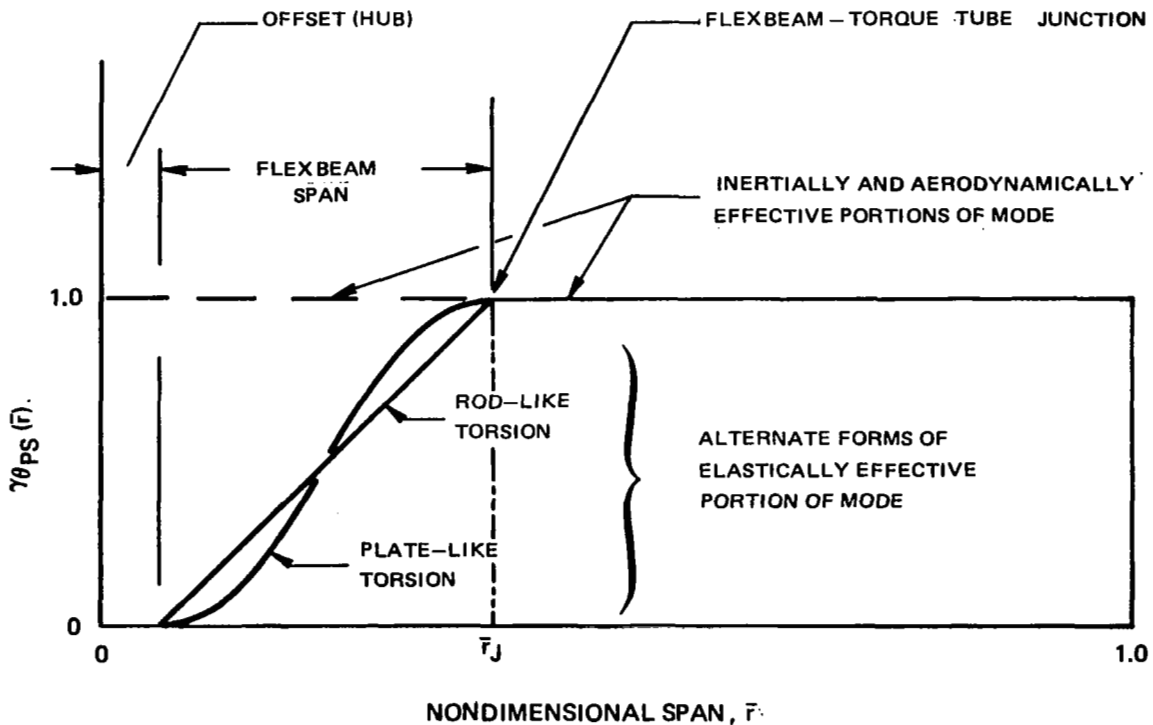


Figure 4. - Details of (Rigid Body) Torsion Pseudo Mode.

Note that the elastically effective portion of the pseudo-mode can, optionally, be taken to be a linear function typical of rod-like torsion or an ogee function more typical of plate-like torsion. Finally, it should be stressed that this pseudo-mode is not, in general, orthogonal to the blade normal modes in torsion.

For bearingless rotor applications, the pseudo-torsion mode serves the unique function of providing a convenient way of introducing time-variable structural twist (i.e., due to control inputs) into the analysis. By treating this component of twist as but an additional torsion mode proportional to control input, the following expression for total pitch angle can be written:

$$\Theta = \sum_{j=1}^{NTM} \gamma_{\theta_j} q_{\theta_j} + \gamma_{\theta_{RB}} \theta_0 + \theta_B \quad (61a)$$

Similarly, the total twist rate can be written as:

$$\Theta' = \sum_{j=1}^{NTM} \gamma'_{\theta_j} \dot{q}_{\theta_j} + \gamma'_{\theta_{RB}} \dot{\theta}_0 + \dot{\theta}_B \quad (61b)$$

By using this expression for twist rate, together with the appropriate pseudo-mode, the incremental deflection functions, Δv , Δw , ΔV and ΔW described in an above subsection, can be completely formulated.

The pseudo-torsion mode serves two additional functions common to all types of rotors: First, it provides a convenient way to include a rigid-body torsion degree-of-freedom arising from root torsion restraint (control system) flexibility and second, it enables the effects of pitch-flat/edge coupling to be systematically introduced.

Rigid-Body Feathering Degree-of-Freedom

For this purpose the total pitch angle now includes the root feathering angle, θ_R , and is expressible as:

$$\Theta = \sum_{j=1}^{NTM} \gamma_{\theta_j} q_{\theta_j} + \gamma_{\theta_{RB}} (\theta_0 + \theta_R) + \theta_B = \sum_{j=1}^{NTM+1} \gamma_{\theta_j} q_{\theta_j} + \gamma_{\theta_{RB}} \theta_0 + \theta_B \quad (62a)$$

where:

$$\gamma_{\theta_{NTM+1}} = \gamma_{\theta_{RB}} \quad (62b)$$

$$q_{\theta_{NTM+1}} = \theta_R \text{ (root torsion deflection)} \quad (62c)$$

A separate rigid-body torsion equation is written by a generalized application of the Galerkin technique wherein the torsion equation is multiplied by the pseudo-mode and integrated; this effectively calculates the torsion moment resisted by the equivalent elastic root torsion spring, K_{θ_2} :

$$\int_0^l \gamma_{\theta_{RB}} [\text{distributed torsion loading}] dr = K_{\theta_1} [\theta_0 + \theta_R + \gamma_{\theta_j}(r_j) q_{\theta_j} + \theta_B(r_j)] - \frac{(GJ)_{FB}}{S_{FB}} \theta_{B_{FB}} + K_{\theta_2} \theta_R \quad (63a)$$

where:

$$K_{\theta_1} \equiv \text{torsional stiffness of flex-beam} = \frac{[(GJ)_{FB} + Tk_{A_{FB}}^2]}{S_{FB}} \quad (63b)$$

$K_{\theta_2} \equiv$ equivalent root torsion spring due to control system flexibility, etc.

In addition to incorporating Eq. (63a) into the total set of dynamic equations, additional terms must be added to the equations for the j normal torsion modes:

$$\int_0^l \gamma_{\theta_j} [\text{distributed torsion loading}] dr = \int_0^l \gamma_{\theta_j} q_{Ax_5} dr$$

$$+ \gamma_{\theta_j}(r_j) \left\{ K_{\theta_j} [\theta_0 + \theta_R + \gamma_{\theta_m}(r_j) q_{\theta_m} + \theta_B(r_j)] - \frac{(GJ)_{FB}}{S_{FB}} \theta_{B_{FB}} \right\} \quad (64)$$

Furthermore, appropriate θ_R (and time derivative) terms must be added to the load distributions (wherever θ dependent terms appear).

Inclusion of Pitch-Flat/Edge Coupling

Automatic pitch change coupling effects can also be conveniently included in the equations of motion by use of the pseudo-torsion mode. First, however, the kinematics of the push-rod to blade attachment point must be considered. Let Δz be the upward "5" coordinate system displacement of this attachment point due to blade deflections with the push-rod momentarily disconnected. These deflections are shown in Fig. 5 for a blade section at the attachment point station:

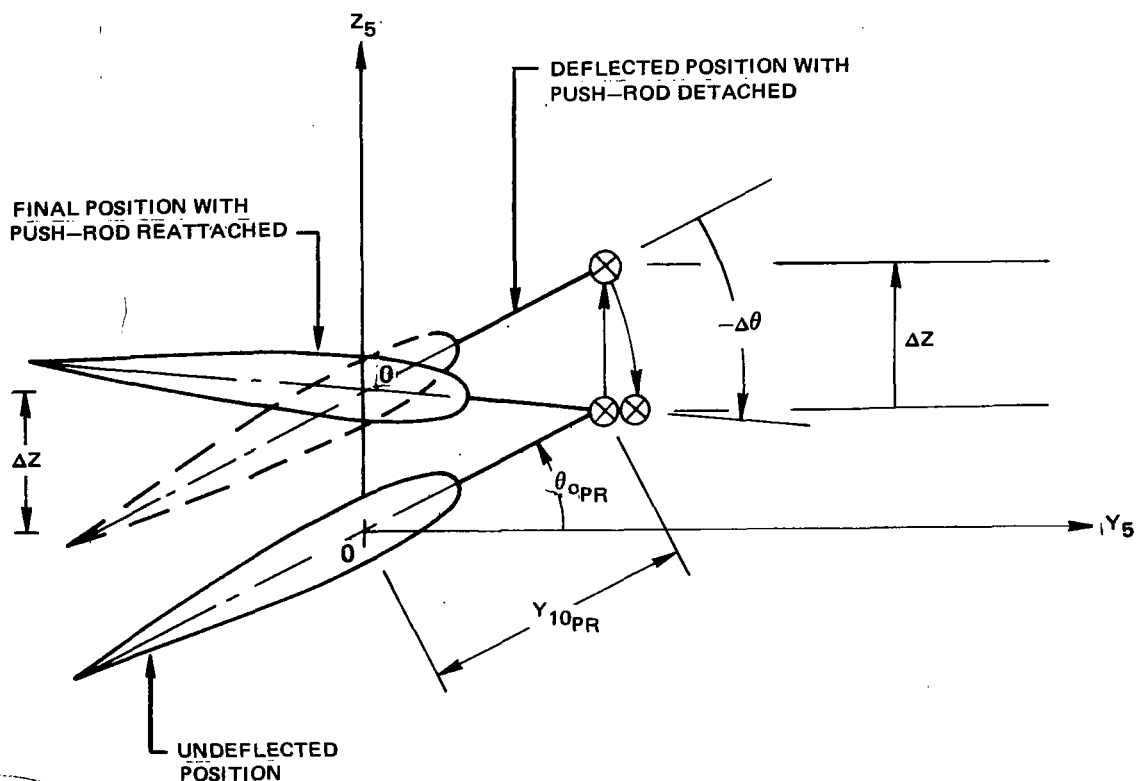


Figure 5.- Geometric Features of Automatic Pitch Change due to Blade Deflection.

When the push-rod is reattached, so that the attachment point is restored to its original z_5 position, the blade will have rotated through an incremental pitch angle ($-\Delta\theta$ as shown in the figure). Using simple trigonometry the following equation governing $\Delta\theta$ and Δz can be written:

$$\sin\theta_{O_{PR}} - \sin(\theta_{O_{PR}} + \Delta\theta) = \frac{\Delta z}{y_{IO_{PR}}} \quad (65)$$

which upon making the small angle assumption on $\Delta\theta$ becomes:

$$\Delta\theta = \frac{-\Delta z}{y_{IO_{PR}} \cos\theta_{O_{PR}}} = -\frac{\Delta z}{\hat{y}_{IO_{PR}}} \quad (66)$$

It should be noted that the Δz deflections can result, depending on rotor configuration, from flatwise bending, edgewise bending, flapping and/or lagging. Thus, $\Delta\theta$ can generally be written as:

$$\Delta\theta = \theta_{w_i} q_{w_i} + \theta_{v_k} q_{v_k} + \theta_{\beta} \beta + \theta_{\delta} \delta \quad (67)$$

and the deflection of the reference point of the blade attachment point section (point O, in Fig. 5) can similarly be written as:

$$\Delta z = -\hat{y}_{IO_{PR}} \Delta\theta = \Delta z_i q_{w_i} + \Delta z_k q_{v_k} + \Delta z_{\beta} \beta + \Delta z_{\delta} \delta \quad (68)$$

The above development can then be incorporated into a comprehensive modeling of pitch-flat/edge coupling effects by building upon the following two considerations. First, the incremental pitch angle, $\Delta\theta$, can be incorporated into the total pitch angle and twist rate, again using the pseudo-torsion mode:

$$\Theta = \sum_{j=1}^{NTM} \gamma_{\theta_j} q_{\theta_j} + \gamma_{\theta_{RB}} (\theta_0 + \Delta\theta) + \theta_B \quad (69)$$

$$\Theta' = \sum_{j=1}^{NTM} \gamma'_{\theta_j} q_{\theta_j} + \gamma'_{\theta_{RB}} (\theta_0 + \Delta\theta) + \theta'_B \quad (70)$$

Hence, the incremental pitch angle generates aerodynamic and inertia loads proportional to those which would be generated by the root deflection angle, θ_R , whose dynamics are described by Eq. (63a).

The second consideration is that in the process of equilibrating the blade in torsion and maintaining the push-rod attachment point at its level position (as indicated above in Fig. 5) a push-rod force is generated equal in magnitude to the applied torsion moments on the blade divided by the push-rod offset distance, but directed in the negative z_5 direction:

$$F_{z_{5PR}} = -M_{x_{5PR}} / \hat{y}_{IOPR} \quad (71)$$

where the torsion moment is obtained from Eq. (63a) and given by:

$$M_{x_{5PR}} = K_{\theta_2} \theta_R = \int_0^l \gamma_{\theta_{RB}} [\text{distributed torsion loading}] dr - K_{\theta_1} [\theta_0 + \Delta\theta + \gamma_{\theta_j}(r_j) + \theta_B(r_j)] + \frac{(GJ)_{FB}}{S_{FB}} \theta_{B_{FB}} \quad (72)$$

The push-rod force, $F_{z_5}^{PR}$, is then a (negative) concentrated force acting on the virtual displacement. This displacement is derived from Eq. (68) and is expressible by the following equation

$$\delta z_5 = \Delta z_i \delta q_{w_i} + \Delta z_k \delta q_{v_k} + \Delta z_\beta \delta \beta + \Delta z_\delta \delta (\delta) \quad (73)$$

Therefore, combining Eqs. (71) and (72) and using Eq. (67), the bending equations and those for flapping and lagging are modified as follows:

i'th flatwise bending, Eq. (24):

$$\int_0^l \{ (\gamma_{w_i} - \Delta w_i)(\text{inertia loads}) + \dots \} dr + \theta_{w_i} M_{x_5}^{PR} + \int_0^l \{ (\gamma_{w_i} - \Delta w_i)(\text{aerodynamic loads}) + \dots \} dr + \dots = 0 \quad (74)$$

k'th edgewise bending, Eq. (25):

$$\int_0^l \{ (\gamma_{v_k} - \Delta v_k)(\text{inertia loads}) + \dots \} dr + \theta_{v_k} M_{x_5}^{PR} + \int_0^l \{ (\gamma_{v_k} - \Delta v_k)(\text{aerodynamic loads}) + \dots \} dr + \dots = 0 \quad (75)$$

rigid flapping, Eq. (31):

$$\int_0^l (r p_{z_5} - z_5 p_{x_5} - q_{y_5}) dr + \theta_\beta M_{x_5}^{PR} + \dots = 0 \quad (76)$$

rigid lead-lagging, Eq. (32):

$$\int_0^l (r p_{y_5} - y_5 p_{x_5} + q_{z_5}) dr + \theta_\delta M_{x_5 PR} + \dots = 0 \quad (77)$$

The inertia matrix, [A], developed in an above subsection can then be modified, as a result of Eqs. (69) and (73) thru (77), to the following general forms:

$$A_{PQ} = \hat{A}_{PQ} + \theta_P \hat{A}_{\theta_N Q} + \theta_Q (\hat{A}_{P \theta_N} + \theta_P \hat{A}_{\theta_N \theta_N}) \quad (78a)$$

$$A_{P \theta_j} = \hat{A}_{P \theta_j} + \theta_P \hat{A}_{\theta_N \theta_j} \quad (78b)$$

$$A_{\theta_j Q} = \hat{A}_{\theta_j Q} + \theta_Q \hat{A}_{\theta_j \theta_N} \quad (78c)$$

where P and Q denote any of the subscripts, w_i , v_k , β or δ , and where \hat{A}_{ij} denote any of the basic inertia matrix components given in Eqs. (46a) thru (46n). This technique for the introduction of a finite push-rod force in the bending, flapping and lagging equations is appropriate only for the case wherein the root torsion retention stiffness is assumed infinite, no rigid feathering degree-of-freedom exists and the incremental pitch angle is automatic. For cases where a finite root stiffness exists the push-rod force is expressible more conveniently using deflection dependent spring forces.

The above somewhat abbreviated development is sufficient to write all the explicit terms involving automatic pitch change due to blade bending, flapping, and/or lead-lagging. For the bearingless rotor with a cantilevered torque tube however, this development must be expanded to include the finite effects of flexbeam bending. This bending gives rise to the low stiffness torsion (wobble) mode whose equations are developed in the next subsection.

AEROELASTIC SIMULATION OF BLADE TORSION WOBBLE MODE

The cantilevered torque tube configuration bearingless rotor comprises a relatively simple mechanical system. The torque tube is attached at its inboard end to the push-rod and at its outboard end to the flexbeam and outer blade portions of the blade by means of a cantilever mount (see Fig. 6).

Typically, the skin of the outer blade portion would continue inboard from the flexbeam-torque tube juncture to form the hollow torque tube. As shown in Fig. 6, this configuration is characterized by a relatively long shear load path for the push-rod loads.

Three observations can be drawn from this figure. First, because of the combination of flexbeam flexibility in both torsion and bending, the blade possesses a rigid body feathering degree-of-freedom even with infinite control system impedance. This torsion degree-of-freedom inherently involves significant vertical or flatwise motion and is referred, herein, as the "wobble" mode. Second, because flexbeam bending plays a primary role in defining the restoring moment for this mode, an analytic calculation of this flexibility is required. Third, as a result of this flexbeam bending flexibility the conventional automatic pitch change coupling described in the previous subsection is no longer completely applicable. In the present case, the effect of bending modal deflection is to develop a push-rod load which acts as an applied torque to the wobble mode, which in turn has finite impedance characteristics. Thus, for the cantilevered torque tube configuration effective pitch-flat/edge couplings may, in general, be dynamically amplified and phase lagged. The development of the equations governing the wobble mode presented herein draws upon the pseudo-torsion mode formulations of the previous subsection.

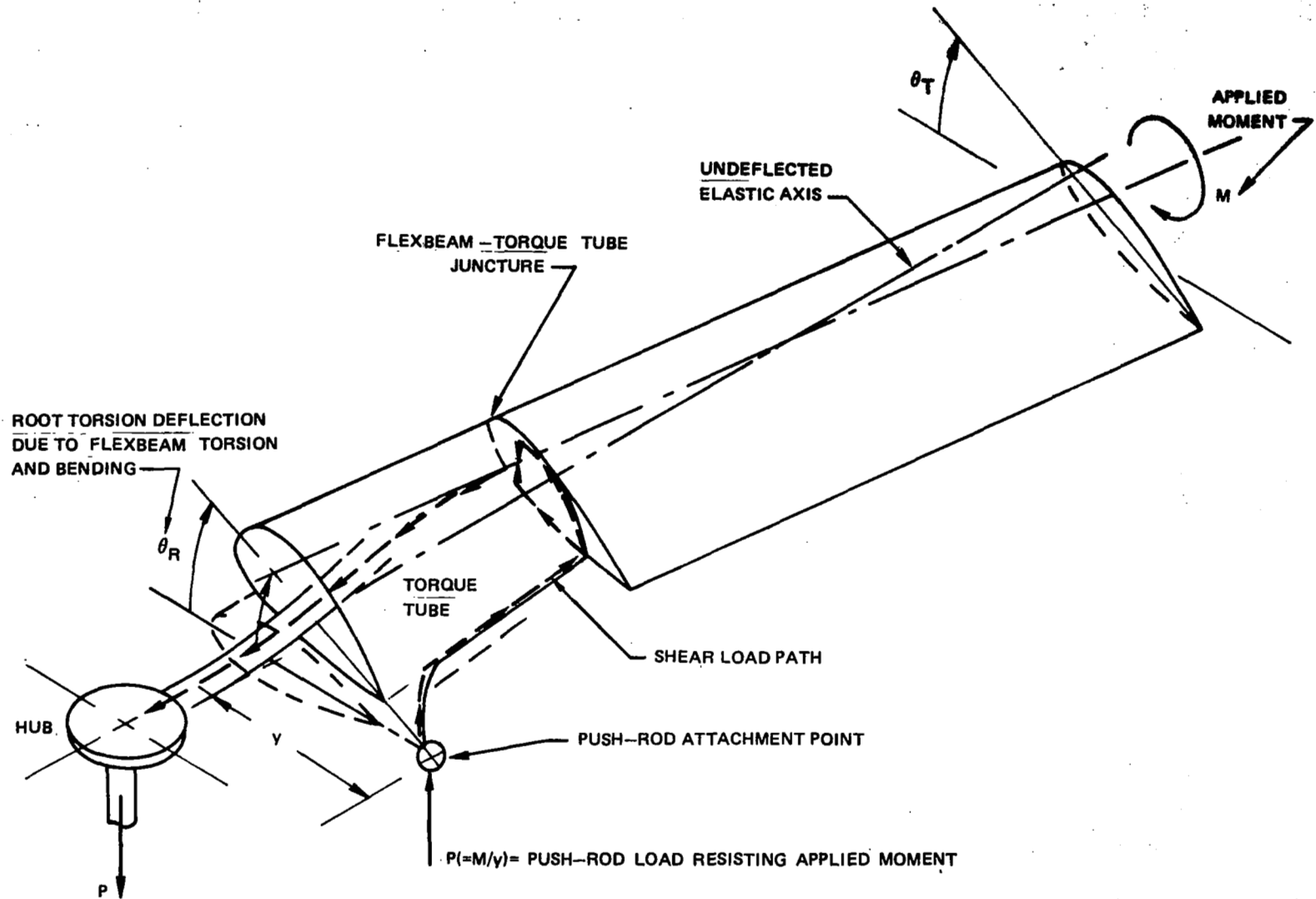


Figure 6. - Pictorial Representation of Wobble Mode and Load Path for Shears due to Push-Rod Load.

Flatwise Flexibility Characteristics of Flexbeam - Cantilevered Torque Tube Assembly

The required quantitative description of the flexbeam bending flexibility is the flatwise deflection of the inboard end of the cantilever mounted torque-tube per unit load applied at the same point. The assumptions made for this calculation are 1) that the torque tube is rigid in bending, 2) that the effects of flexbeam twist angle can be neglected, 3) that over the flexbeam span the tension is constant and equal to that due to total blade mass (i.e., the flexbeam is massless) and 4) that the junction point is at the midpoint of a blade segment. The elastic problem so formulated is solved by means of transfer matrix techniques using the distributed (lumped) mass and flatwise stiffness properties assumed for calculating the normal flatwise bending modes. Figure 7 shows the features of the mathematical model of the total blade. It is to be noted, furthermore, that all the blade segments are in a centrifugal force field.

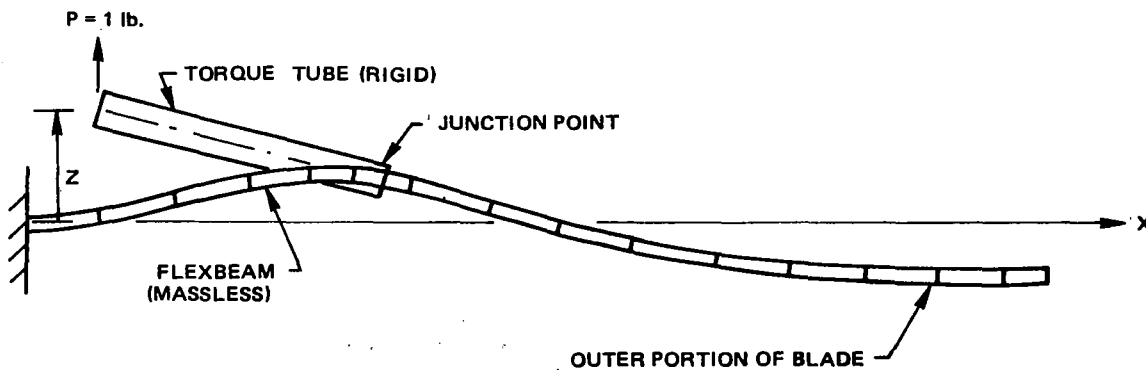


Figure 7. - Features of Mathematical Model for Calculating Flatwise Flexibility Characteristics of Inboard End of Cantilevered Torque Tube.

Since the junction point is assumed to act at the midpoint of a segment and since the centrifugal force is a strong (but known) function of span, each blade segment is further broken down into two semi-segments, each of which is then assumed to have a constant (average) tension. Then, for each semi-segment, the inboard loads and deflections, expressible as a state vector, can be related to the outboard loads and deflections by means of an appropriately calculated transfer matrix:

$$\begin{pmatrix} S \\ M \\ Z \\ Z' \end{pmatrix}_{k_I} = [T_k] \begin{pmatrix} S \\ M \\ Z \\ Z' \end{pmatrix}_{k_O} ; \quad k = 1, 2, \dots, 2(NSEG) \quad (79)$$

where:

$$[T_k] = \begin{bmatrix} 1 & 0 & 0 & 0 \\ \left[L + \left(\frac{\sinh \beta L}{\beta} - L \right) c_1 + (\cosh \beta L - 1) c_2 \right] & \left[1 + (\cosh \beta L - 1) c_1 + c_2 \beta \sinh \beta L \right] & 0 & \bar{T} \left[-\frac{\sinh \beta L}{\beta} c_1 - c_2 \cosh \beta L + c_3 \right] \\ \frac{1}{\bar{T}} \left(\frac{\sinh \beta L}{\beta} - L \right) & \frac{1}{\bar{T}} (\cosh \beta L - 1) & 1 & -\frac{\sinh \beta L}{\beta} \\ -\frac{1}{\bar{T}} (\cosh \beta L - 1) & -\frac{\beta}{\bar{T}} \sinh \beta L & 0 & \cosh \beta L \end{bmatrix} \quad (80a)$$

The various terms are evaluated at the k'th semi-segment and defined as follows:

$$\bar{T} = \text{average tension} = 1/2 (T_1 + T_0) \quad (80b)$$

$$\beta = \sqrt{\bar{T}/EI} \quad (80c)$$

$$L = 1/2 \Delta x \quad (80d)$$

$$c_1 = \frac{1}{\bar{T}} \left[T_0 + mL^2 \left(\frac{1}{2} \frac{x_I}{L} + \frac{7}{20} \right) \right] \quad (80e)$$

$$c_2 = \frac{mL^3}{\bar{T}} \left(\frac{1}{12} \frac{x_I}{L} + \frac{1}{30} \right) \quad (80f)$$

$$c_3 = \frac{mL^3}{\bar{T}} \left(\frac{1}{12} \frac{x_I}{L} + \frac{1}{20} \right) \quad (80g)$$

and where:

$$\begin{Bmatrix} S \\ M \\ Z \\ Z' \end{Bmatrix}_{k_0} = \begin{Bmatrix} S \\ M \\ Z \\ Z' \end{Bmatrix}_{(k-1)_I} \quad k=1 \text{ corresponds to the blade tip semi-segment} \quad (80h)$$

Cascade matrix multiplication, together with the introduction of the additional shear and moment at the junction point (arising from the unit load, P) and the imposition of boundary conditions (geometric at the root and loading at the tip) leads to a matrix equation of the following form:

$$\begin{Bmatrix} S \\ M \\ O \\ O \end{Bmatrix}_{\text{root}} = [T_1] \begin{Bmatrix} O \\ O \\ Z \\ Z' \end{Bmatrix}_{\text{tip}} + \{T_2\} P \quad (81)$$

This matrix equation constitutes a solvable set of four equations in four unknowns. A partial cascade multiplication of transfer matrices, T_3 , relating the junction state vector to the tip state vector, is then used to obtain the deflection and slope at the junction point:

$$\begin{Bmatrix} z_J \\ z'_J \end{Bmatrix} = \begin{bmatrix} 0 & I_2 \end{bmatrix} \begin{bmatrix} T_3 \end{bmatrix} \begin{Bmatrix} 0 \\ 0 \\ z \\ z' \end{Bmatrix}_{\text{tip}} \quad (82)$$

The final required flexibility is obtainable from these two quantities as follows:

$$Z = z_J - S_{TT} z'_J + \frac{S_{TT}^2}{K_{FJ}} \quad (83)$$

where:

S_{TT} = length of torque tube

K_{FJ} = flatwise angular spring restraining the torque-tube to the blade spar (flexbeam)

Elastic Rigid Feathering Torsional Restraint

The combined effects of flexbeam bending, flexbeam torsion and control system flexibility can be determined by examining and summing the contributions to the vertical deflection of the push-rod attachment point. As shown in Fig. 8, the attachment point is allowed to deflect sequentially due to the effects of blade bending (Δz), of flexbeam bending due to the application of the push-rod load (z_2), of flexbeam torsion (θ_R), and finally of control-system flexibility (z_3).

The final attachment point deflection is thus given by the following expressions:

$$z_3 = \Delta z - z_2 + \hat{y}_{IO_{PR}} \theta_R \quad (84)$$

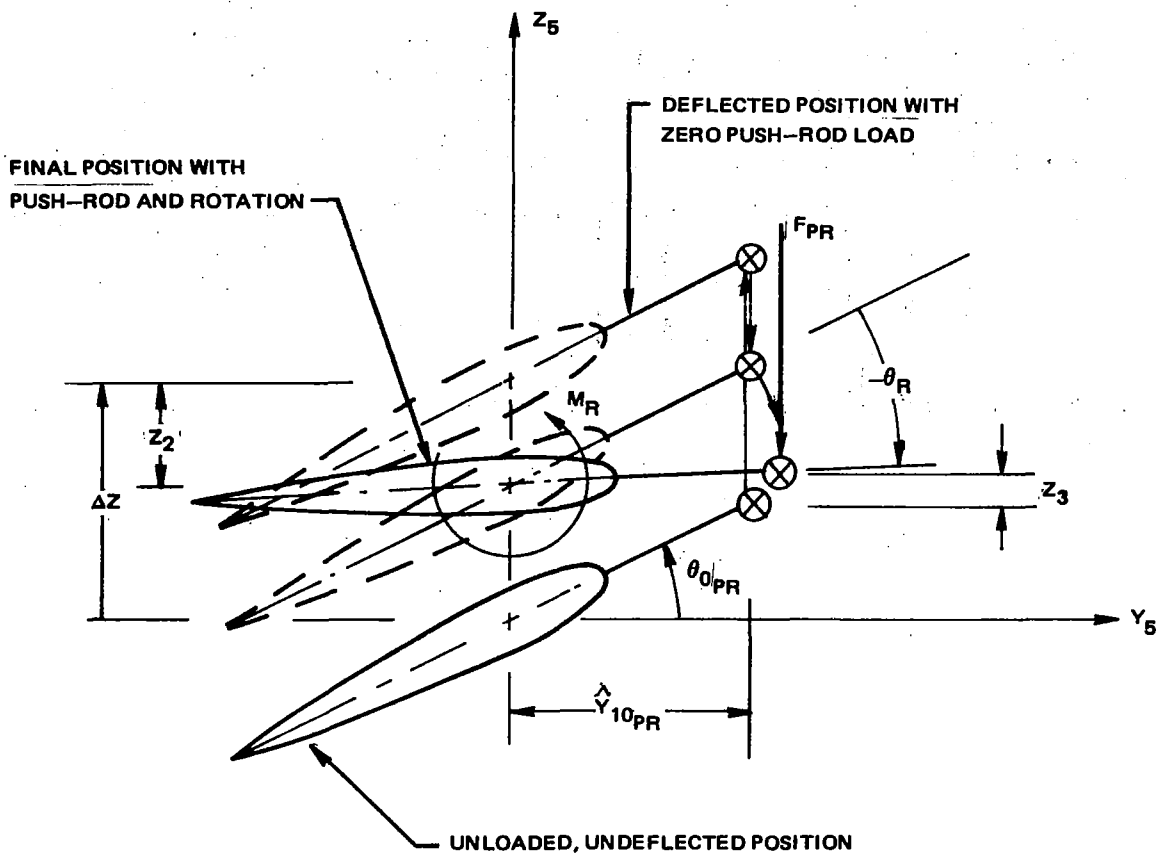


Figure 8. - Contributions to Vertical Deflection of Push-Rod Attachment Point, Cantilevered Torque Tube.

This deflection together with the actual control system stiffness, $K_{\theta 3}$, defines the push-rod load:

$$F_{PR} = \frac{K_{\theta 3}}{\hat{y}_{10PR}^2} z_3 = \frac{K_{\theta 3}}{\hat{y}_{10PR}^2} (\Delta z - z_2 + \hat{y}_{10PR} \theta_R) \quad (85)$$

where:

$K_{\theta 3}$ = actual control system stiffness.

Recognizing that the z_2 deflection is itself proportional to the push-rod load:

$$Z_2 = Z \cdot F_{PR} \quad (86)$$

enables the following expressions for the push-rod force and root moment to be written:

$$F_{PR} = \frac{K_{\theta_3} / \hat{y}_{10PR}^2}{1 + K_{\theta_3} Z / \hat{y}_{10PR}^2} (\Delta Z + \hat{y}_{10PR} \theta_R) = \frac{K_{\theta_2}}{\hat{y}_{10PR}^2} (\Delta Z + \hat{y}_{10PR} \theta_R) \quad (87a)$$

$$M_R = -\hat{y}_{10PR} F_{PR} = K_{\theta_2} (\theta_R - \Delta\theta) \quad (87b)$$

where the effective root spring, introduced in the previous subsection, K_{θ_2} , is, now given by:

$$K_{\theta_2} = \frac{K_{\theta_3}}{1 + K_{\theta_3} Z / \hat{y}_{10PR}^2} \quad (88)$$

Dynamic Equation for Wobble Mode

As was observed above in this subsection the wobble mode is essentially a rigid body feathering mode; hence, the developments of the previous subsection can be drawn upon. First, the quantity $\Delta\theta$ appearing in Eq. (87b) for this cantilevered torque tube application, must now be considered a normalization of the flatwise displacement of the attachment point rather than, as in the previous subsection, an automatic pitch change. Thus, the total pitch angle and twist do not contain the quantity $\Delta\theta$ and Eq. (61a) and (61b) become the appropriate expressions for the total pitch angle and twist, respectively. Using the root restraint moment, M_R , as defined by Eq. (I.87b) the dynamic equation for the wobble mode then becomes a modification of the rigid feathering Eq. (I.63a) given in the previous subsection:

$$\int_0^l \gamma_{\theta_{RB}} [\text{distributed torsion loading}] dr = K_{\theta_2} (\theta_R - \Delta\theta) - \frac{(GJ)_{FB}}{S_{FB}} \theta_{B_{FB}} + K_{\theta_1} [\theta_0 + \theta_R + \gamma_{\theta_j}(r_j) q_{\theta_j} + \theta_B(r_j)] \quad (89)$$

Comparison of this equation with Eq. (63a) shows a coupling of the wobble mode with blade bending through the $\Delta\theta$ term. It is reasonable to expect a similar coupling of the bending equations with rigid body torsion through a similar term. Indeed, the push-rod force, given by Eq. (87a) can be directly incorporated in the flatwise and edgewise bending equations to give the expected symmetrical elastic coupling:

$$\int_0^l \{(\gamma_{w_i} - \Delta W_i)(\text{inertia loads}) + \dots\} dr + \theta_{w_i} K_{\theta_2} (\theta_R - \Delta\theta) + \int_0^l \{(\gamma_{w_i} - \Delta W_i)(\text{aerodynamic loads}) + \dots\} dr + \dots = 0 \quad (90)$$

$$\int_0^l \{(\gamma_{v_k} - \Delta V_k)(\text{inertia loads}) + \dots\} dr + \theta_{v_k} K_{\theta_2} (\theta_R - \Delta\theta) + \int_0^l \{(\gamma_{v_k} - \Delta V_k)(\text{aerodynamic loads}) + \dots\} dr + \dots = 0 \quad (91)$$

The development of this subsection has been directed to a type of bearingless rotor configuration which is characterized by a torque tube which is relatively stiff in bending. This high degree of torque tube bending stiffness is generally required because of the inherently long load path for the push-rod shear loads. In the next subsection an alternate type of torque tube is considered wherein the torque tube bending stiffness is not generally high. This characteristic leads to a degree of bending redundancy in the flexbeam (torque tube elastic system) and an appropriate analysis technique is required.

REDUNDANT ANALYSIS OF FLEXBEAM - TORQUE TUBE ASSEMBLIES WITH SNUBBER RESTRAINTS

Basically, bearingless rotor systems are characterized by an inboard spanwise section comprised of two highly specialized and contrasting structural elements (see Fig. 9). The first is the innermost portion of the blade spar and is referred to as the flexbeam. Its function is to provide the inboard bending stiffness appropriate to hingeless rotor blades, while at the same time being very soft in torsion to allow the outer portion of the blade to be feathered. The second structural element is typically a cylindrically formed shell relatively stiff in torsion which encloses the flexbeam and is referred to as the torque tube. The structural functions of the torque tube are to provide the blade torsion system with sufficient general torsion stiffness inboard of the junction and to transmit those torques to the flexbeam which are needed to produce the input control angles. The inboard end of the flexbeam is attached directly to the hub whereas the inboard end of the torque tube attaches to the control push-rod and to the flexbeam. More precisely, the inboard end of the torque tube is restrained in torsion by the push-rod and control system, and in shear by means of an (effective) pinned point (elastomeric snubber or equivalent) attached to the flexbeam. The cantilevered torque tube described in an earlier section is restrained both in torque and shear by means of the push-rod. The redundant analysis of this latter configuration requires a much more extensive development than is presented herein for pinned or snubbed configurations. Because of the current viability of the snubbed configuration, and to a lesser extent, the additional complications of analyzing the cantilevered configuration, the present development is restricted to only pinned or snubbed configurations. The two structural elements are attached (both to each other and to the remaining outer portion of the blade) at their common outboard end point, referred to alternatively as the junction or juncture.

For typical bearingless rotor configurations the torque tube and outer blade portion skin would be integrally formed (for practical fabrication reasons). Hence, while the torque tube would nominally experience zero bending moments at its inboard end (due to the effective pinned joint), it would necessarily support bending loads at its outboard end. Equilibrating the internal loads at the junction point arising from the load transmissibilities of the flexbeam, torque tube and outer blade portions of the blade defines a doubly redundant analysis. Over the flexbeam torque tube portion of the blade, dual load paths are defined in both bending and torsion, and an appropriate solution must consequently require that the elastic deflections of the junction point, both in bending and torsion of the three structural elements, are consistent. The remaining portions of this section develop the detailed mathematical formulation and solution to this redundant analysis problem. For conceptual clarification the primary bending flexibility system is considered to be the flexbeam

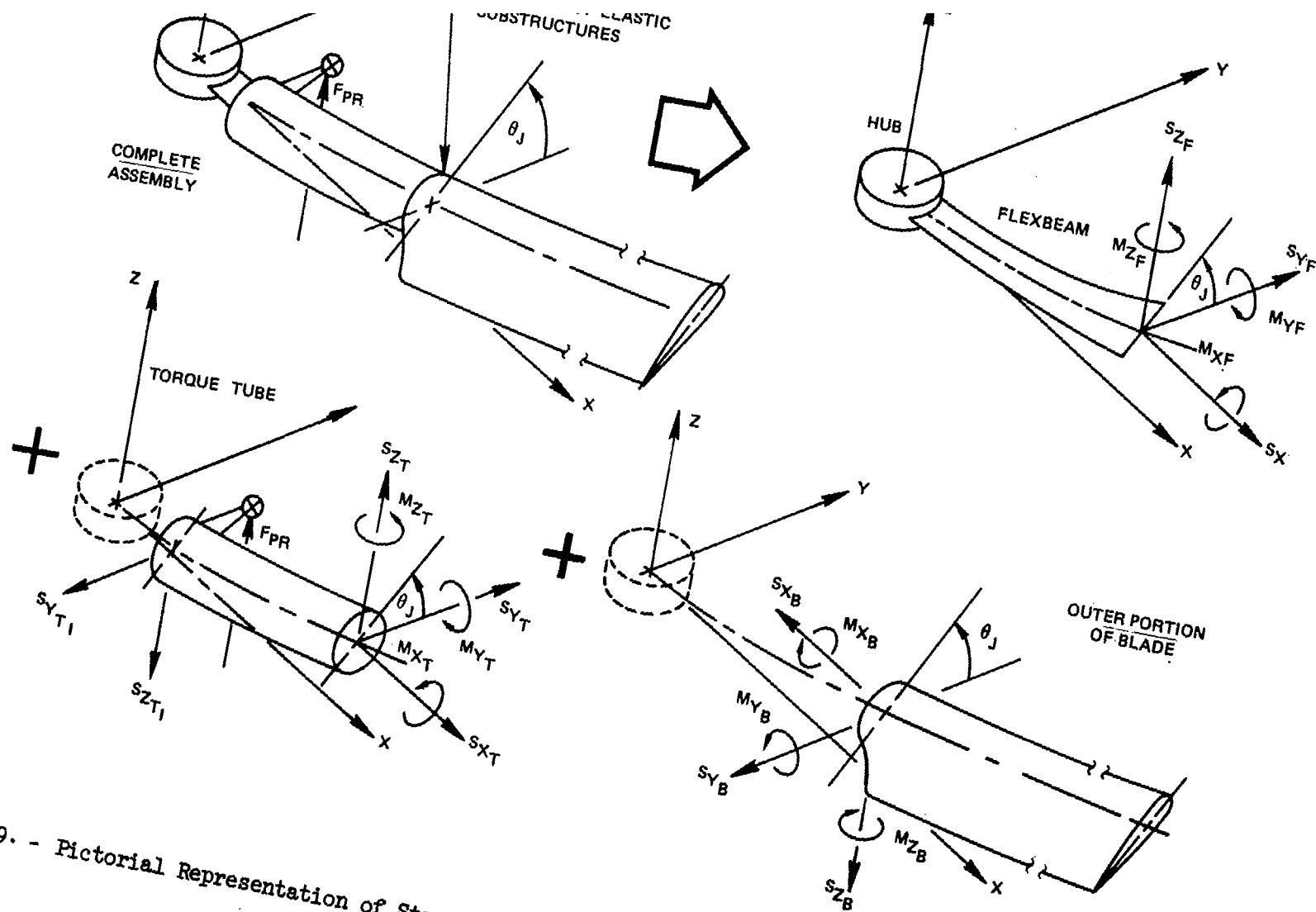


Figure 9. - Pictorial Representation of Structural Redundancy Features of Composite Bearingless Rotor.

whereas the primary torsion system is considered to be the torque tube. The subsections to follow include: first, a development of the bending stiffness characteristics of the torque tube; second, a development of the torsional stiffness characteristics of the flexbeam arising from nonlinear loadings; third, a method for estimating the internal loads immediately outboard of the junction; and finally, a mathematical synthesis of these elements to effect the complete solution to the redundant analysis.

Bending Stiffness Characteristics of the Torque Tube

The appropriate elastic bending description of the torque tube is a stiffness matrix expressing the inboard shears, the outboard shears and the outboard moments as linear combinations of the relative deflections of the ends of the torque tube. To this end the following specific assumptions are made:

1. The torque tube is a beam whose section properties have generally nonuniform spanwise variation.
2. The torque tube has negligible twist but is inclined by the pitch angle of the junction point. Hence, flatwise and edgewise stiffnesses generally couple the in-plane and out-of-plane bending characteristics.
3. The spanwise in-plane and out-of-plane load distributions over the torque-tube span act directly upon the flexbeam; i.e., the torque tube is transparent to these loadings.
4. The radial loadings due to torque tube mass (centrifugal forces) contribute to the stiffening of the torque tube in bending.
5. In addition to having distributed bending stiffnesses, the torque tube is elastically restrained at its outboard end with finite angular springs (defined in torque tube flatwise and edgewise orientations) and at the inboard end with finite lineal shear springs (defined alternatively either in torque tube flatwise and edgewise, or in hub out-of-plane and in-plane orientations).
6. The torque tube is supported radially either at its inboard end (torque tube in tension) or at its outboard end (torque tube in compression).

Assuming the torque tube to be a beam allows a transfer matrix solution similar to that employed in the previous section for calculating the flatwise flexibility of the flexbeam. Analysis of a beam segment with constant properties forms the basis for evaluating each component transfer matrix and follows from a consideration of such a beam segment shown below in Fig. 10.

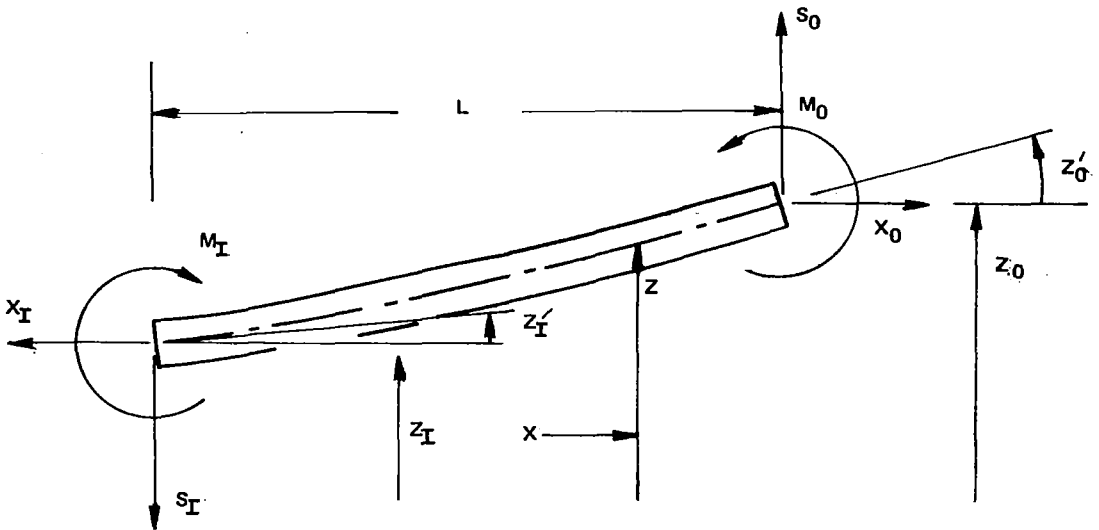


Figure 10. - Loads and Deflections of a Beam Element with Constant Section Properties.

Use of the standard beam theory requires the bending equilibrium equation for the k'th element to be written as:

$$(EI)_k z'' - \bar{T}_k z = (L_k - x) S_{0k} + M_{0k} - \bar{T}_k z_{0k} \quad (92)$$

where the average tension is:

$$\bar{T}_k = \frac{1}{2} (X_{I_k} + X_{O_k}) \quad (93)$$

As shown in Fig. 10, \bar{T}_k represents the average tension over the beam element. Note that for torque tubes in compression \bar{T}_k would be a negative number. The boundary conditions appropriate to Eq. (92) are:

$$\left. \begin{aligned} z &= z_{I_k}, & z' &= z'_{I_k} & \text{at } x &= 0 \\ z &= z_{O_k}, & z' &= z'_{O_k} & \text{at } x &= L_k \end{aligned} \right\} \quad (94)$$

For torque tube elements in tension the above formulation duplicates that given in the previous section and the resulting transfer matrix, as given by Eqs. (80a,b,c, and d) is applicable to this case. For the case of a torque tube in compression, the quantity, β , is then defined as:

$$\beta = \sqrt{-T/EI} = \sqrt{C/EI} \quad (95)$$

and the resulting component transfer matrix is given as:

$$[T_k] = \begin{bmatrix} 1 & 0 & 0 & 0 \\ \left[L + \left(L - \frac{\sin \beta L}{\beta} \right) d_1 + \left(1 - \frac{\cos \beta L}{\beta} \right) d_2 \right] & \left[1 + (1 - \cos \beta L) d_1 + \beta \sin \beta L d_2 \right] & 0 & \bar{c} \left[-\frac{\sin \beta L}{\beta} d_1 - d_2 \cos \beta L + d_3 \right] \\ \frac{1}{\bar{c}} \left(L - \frac{\sin \beta L}{\beta} \right) & \frac{1}{\bar{c}} (1 - \cos \beta L) & 1 & -\frac{\sin \beta L}{\beta} \\ \frac{-1}{\bar{c}} (1 - \cos \beta L) & \frac{-\beta}{\bar{c}} \sin \beta L & 0 & \cos \beta L \end{bmatrix}_k \quad (96a)$$

$$d_1 = \frac{1}{\bar{c}} \left[-C_0 + \bar{m}L^2 \left(\frac{x_I}{2L} + \frac{7}{20} \right) \right] \quad (96b)$$

$$d_2 = \frac{mL^3}{\bar{c}} \left(\frac{x_I}{12L} + \frac{1}{30} \right) \quad (96c)$$

$$d_3 = \frac{mL^3}{\bar{c}} \left(\frac{x_I}{12L} + \frac{1}{20} \right) \quad (96d)$$

As in the previous section, the total (uncoupled) stiffness matrices, for both flatwise and edgewise bending, are obtained by a cascade multiplication of the component transfer matrices as indicated below:

$$[T] = \prod_1^K [T_k] \quad (97)$$

The uncoupled edgewise and flatwise stiffness matrices are defined in the "6" coordinate system and are denoted as:

$$\begin{Bmatrix} S y_6 \\ M z_6 \\ y_6 \\ y'_6 \end{Bmatrix}_s = [T_E] \begin{Bmatrix} S y_6 \\ M z_6 \\ y_6 \\ y'_6 \end{Bmatrix}_J \quad (98a)$$

$$\begin{Bmatrix} S z_6 \\ -M y_6 \\ z_6 \\ z'_6 \end{Bmatrix}_s = [T_F] \begin{Bmatrix} S z_6 \\ -M y_6 \\ z_6 \\ z'_6 \end{Bmatrix}_J \quad (98b)$$

where the subscripts (S) and (J) denote, respectively, the snubber and juncture ends of the torque tube. Eqs. (98a and b) must then be coupled by the effects of juncture moment springs, snubber shear springs and torque tube pitch angle, θ_J . The juncture moment retention springs are defined by the following simple relationships:

$$(M_{z_6})_J = -(y'_{6J_{TT}} - y'_{6J_{FB}}) \cdot K_{JE} \quad (99a)$$

$$(M_{y_6})_J = (z'_{6J_{TT}} - z'_{6J_{FB}}) \cdot K_{JF} \quad (99b)$$

Similarly, for inboard snubber shear springs aligned in the torque tube flatwise and edgewise directions ("6" coordinate system), the following relationships hold:

$$(S_{y_6})_s = (y_{6s_{TT}} - y_{6s_{FB}}) \cdot K_{sE} \quad (100a)$$

$$(S_{z_6})_s = (z_{6s_{TT}} - z_{6s_{FB}}) \cdot K_{sF} \quad (100b)$$

Noting that M_{y_6s} and M_{z_6s} are both zero (snubber transmits shear only), Eqs. (99a and b and 100a and b) can then be combined with the definition for the uncoupled stiffness matrices (98a and b) to give the following matrix equations.

$$\begin{bmatrix} 1 & -t_{11} & -t_{12} + t_{14} K_{JE}^{-1} & 0 \\ 0 & -t_{21} & -t_{22} + t_{24} K_{JE}^{-1} & 0 \\ K_{sE}^{-1} & -t_{31} & -t_{32} + t_{34} K_{JE}^{-1} & 0 \\ 0 & -t_{41} & -t_{42} + t_{44} K_{JE}^{-1} & 1 \end{bmatrix}_E \begin{Bmatrix} S_{y_{6s}} \\ S_{y_{6J}} \\ M_{z_{6J}} \\ y'_{6s} \end{Bmatrix}_{TT} = \begin{bmatrix} 0 & t_{13} & t_{14} \\ 0 & t_{23} & t_{24} \\ -1 & t_{33} & t_{34} \\ 0 & t_{43} & t_{44} \end{bmatrix}_E \begin{Bmatrix} y_{6s} \\ y_{6J} \\ y'_{6J} \end{Bmatrix}_{FB} \quad (101a)$$

$$\begin{bmatrix} 1 & -t_{11} & -t_{12} + t_{14} K_{JF}^{-1} & 0 \\ 0 & -t_{21} & -t_{22} + t_{24} K_{JF}^{-1} & 0 \\ K_{sF}^{-1} & -t_{31} & -t_{32} + t_{34} K_{JF}^{-1} & 0 \\ 0 & -t_{41} & -t_{42} + t_{44} K_{JF}^{-1} & 1 \end{bmatrix}_F \begin{Bmatrix} S_{z_{6s}} \\ S_{z_{6J}} \\ -M_{y_{6J}} \\ z'_{6s} \end{Bmatrix}_{TT} = \begin{bmatrix} 0 & t_{13} & t_{14} \\ 0 & t_{23} & t_{24} \\ -1 & t_{33} & t_{34} \\ 0 & t_{43} & t_{44} \end{bmatrix}_F \begin{Bmatrix} z_{6s} \\ z_{6J} \\ z'_{6J} \end{Bmatrix}_{FB} \quad (101b)$$

In both of these matrix equations the respective premultiplicative matrices on the left hand sides can be inverted to give modified stiffness matrices denoted in the following abbreviated form:

$$\begin{Bmatrix} S_{y_{6s}} \\ S_{y_{6J}} \\ M_{z_{6J}} \\ y'_{6s} \end{Bmatrix}_{TT} = [R_E] \begin{Bmatrix} y_{6s} \\ y_{6J} \\ y'_{6J} \end{Bmatrix}_{FB} \quad (102a)$$

$$\begin{Bmatrix} Sz_{6s} \\ Sz_{6j} \\ -My_{6j} \\ z'_{6s} \end{Bmatrix}_{TT} = [R_F] \begin{Bmatrix} z_{6s} \\ z_{6j} \\ z'_{6j} \end{Bmatrix}_{FB} \quad (102b)$$

These equations can be represented even more compactly using the following notation:

$$\begin{Bmatrix} Ly_6 \\ Lz_6 \end{Bmatrix}_{TT} = \begin{bmatrix} R_E & | & 0 \\ 0 & | & R_F \end{bmatrix} \begin{Bmatrix} \Delta Y_6 \\ \Delta Z_6 \end{Bmatrix}_{FB} \quad (103)$$

Because both edgewise and flatwise transfer matrices were derived "uncoupled" (i.e., each assumes zero deflection for the other), the loads given by Eq. (103) are properly interpreted to lie in the planes defined by the torque tube sections at the snubber and at the juncture. These planes are oriented by rotations about the y_5 and z_5 (or y_6 and z_6) axes by amounts determined by the blade slopes at the snubber and juncture points. For what follows, the subscript "7" is given to the moments so defined by the torque tube stiffness matrix with the understanding that they lie in the plane defined by the torque tube section at the juncture.

Transformation to the "5" coordinate system using trigonometric resolutions (rotations through the angle, θ_J) on the elastic load vectors, Ly_6 and Lz_6 , and the deflection vectors ΔY_6 and ΔZ_6 then yield the following coupled form:

$$\begin{Bmatrix} Ly_5 \\ Lz_5 \end{Bmatrix}_{TT} = \begin{bmatrix} R_E \cos^2 \theta_J + R_F \sin^2 \theta_J & | & (R_E - R_F) \sin \theta_J \cos \theta_J \\ (R_E - R_F) \sin \theta_J \cos \theta_J & | & R_E \sin^2 \theta_J + R_F \cos^2 \theta_J \end{bmatrix} \begin{Bmatrix} \Delta Y_5 \\ \Delta Z_5 \end{Bmatrix}_{FB} \quad (104)$$

or, in abbreviated notation:

$$\{L_5\}_{TT}^{(d)} = [S_0] \{\Delta_5\}_{FB} \quad (105)$$

where the (d) superscript denotes loads due to the $(\Delta_5)_{FB}$ deflections.

$$\{L_5\}_{TT}^{(d)} \equiv \begin{Bmatrix} S_{y_{5s}} \\ S_{y_{5j}} \\ M_{z_{7j}} \\ y'_{5s} \\ S_{z_{5s}} \\ S_{z_{5j}} \\ -M_{y_{7j}} \\ z'_{5s} \end{Bmatrix}^{(d)} = [S_1] \begin{Bmatrix} y_{5s} \\ y_{5j} \\ y'_{5j} \\ z_{5s} \\ z_{5j} \\ z'_{5j} \end{Bmatrix}_{FB} = [S_1] \{\Delta_5\}_{FB} \quad (108)$$

where the subscript (FB) on the right-hand side indicates deflections of the flexbeam at points where the torque tube and/or torque tube retention springs are attached. Note that the torque tube inboard slopes are included in the load vector first to indicate that they, like the loads, result from the specified deflections on the RHS of this equation, and second, to show where in the analysis these quantities are formed when needed for pitch-flat/edge coupling calculations. In practice, these quantities, once formed are partitioned out and handled separately. In subsequent development they will be omitted from the load vector, for clarity.

The total internal loads acting at the ends of the torque tube consist of those elastically produced by the deflections, given by the above equation, and those loads arising from blade root torques and the resulting push-rod loads. The torque tube and loads due to push-rod loads are already implicitly included in the flatwise and edgewise bending excitation equations by reason of the particular method for including pitch-flat/edge coupling discussed in an above section. These loads, however, must be explicitly evaluated to implement the torsional redundancy portion of the redundant analysis. The remaining portion of this subsection discusses those derivations needed to calculate the pitch-flat/edge coupling when a flexible torque tube is employed, how Eq. (108) for elastic flexibility is used to account for the bending redundancy portion of the redundant analysis, and how the torque tube loads due to push-rod force can be estimated.

As was described in an above section and shown in Fig. 6, pitch-flat/edge coupling effects are calculated from the geometry of the pitch-horn and from knowledge of the unconstrained vertical deflection of the attachment

point, Δz , for unit deflections of the various modes. With the above analytical description of torque tube bending flexibility this can be readily accomplished. The Δz deflections per modal deflection for this case can be obtained from the last row of Eq. (108) for $(z'_{5s})_{TT}$ and from $(z_{5s})_{TT}$ which is either equal to $(z_{5s})_{FB}$ or, if the snubber spring rates are finite, calculable from the linear relationships given by Eqs. (100b) through (105) and (106b) through (108) using routine algebraic manipulations. After these manipulations are performed, $(z_{5s})_{TT}$ and $(z'_{5s})_{TT}$ and, by linear combination, Δz , can be expressed as a linear combination of the flexbeam deflections due to unit modal deflections:

$$\Delta z = (z_{5s})_{TT} + (r_{PR} - r_s)(z'_{5s})_{TT} = [Q_{TT}] \begin{Bmatrix} y_{5s} \\ y_{5j} \\ y'_{5j} \\ z_{5s} \\ z_{5j} \\ z'_{5j} \end{Bmatrix} \quad (109)$$

per unit modal deflection

The above equation for Δz is then used with the derivation in Section V to obtain the values of modal pitch-flat/edge coupling.

The bending redundancy portion of the redundant analysis is accomplished by treating the snubber and juncture loads defined by Eq. (108) as concentrated loads for direct inclusion in Eqs. (24) and (25) as is provided for in these response equations. Due to the linear character of Eq. (108), the bending redundancy can be included in the eigensolution as well as the time-history solution.

Calculation of the external torque tube and loads resisting the push-rod force is accomplished by equivalencing the virtual work due to the push-rod load with that due to the equilibrating torque tube and loads. To this end Eqs. (109) can be used in the following manner:

$$\begin{aligned} \delta V &= F_{PR} \cdot \delta \Delta z = F_{PR} [Q_{TT}] \cdot \delta \{\Delta_5\}_{FB} \\ &= - \left[-S_{y_{5s}}, S_{y_{5j}}, M_{z_{5j}}, -S_{z_{5s}}, S_{z_{5j}}, -M_{y_{5j}} \right] \cdot \delta \{\Delta_5\}_{FB} \end{aligned} \quad (110)$$

Therefore, since the component virtual displacements are independent, the external end loads needed to equilibrate the push-rod force, F_{PR} , are given by the following:

$$\{L_5\}_{TT}^{(PR)} = \begin{Bmatrix} q_{TT1} \\ -q_{TT2} \\ -q_{TT3} \\ q_{TT4} \\ -q_{TT5} \\ q_{TT6} \end{Bmatrix} F_{PR} \quad (111)$$

which, when combined with Eq. (108), yields the total internal loads at the ends of the torque tube:

$$\{L_5\}_{TT} = \{L_5\}_{TT}^{(d)} + \{L_5\}_{TT}^{(PR)} = [S_1] \begin{Bmatrix} y_{5s} \\ y_{5j} \\ y'_{5j} \\ z_{5s} \\ z_{5j} \\ z'_{5j} \end{Bmatrix}_{FB} + \begin{Bmatrix} -q_{TT1} \\ q_{TT2} \\ q_{TT3} \\ -q_{TT4} \\ q_{TT5} \\ -q_{TT6} \end{Bmatrix} F_{PR} \quad (112)$$

In addition to the loads given by the above equation, the radial shear at the juncture, $S_{x_{5j}}$, is given by the following:

$$(S_{x_{5j}})_{TT} = \begin{cases} 0 & ; \text{ torque tube in tension} \\ -\int_0^{r_j} (p_{x_5})_{TT} dr; & \text{ torque tube in compression} \end{cases} \quad (113)$$

Note that the axial torsion moment at the outboard end, $(M_{x_{7j}})_{TT}$, includes the effect of the flexbeam resisting moment and, hence, must be solved for using the redundant analysis. The following subsection formulates the analysis stiffness matrices required to define the detailed torsional stiffness of the flexbeam.

Torsional Stiffness Characteristics of the Flexbeam

Calculation of an appropriate stiffness matrix statement for the flexibility of the flexbeam requires that two special characteristics of the flexbeam be accounted for: First, the composite material flexbeam is a plate-like beam whose cross section has a typical aspect ratio of order of magnitude 10; furthermore although the flexbeam is relatively soft in torsion (low GJ), it retains a relatively high bending modulus (high EI). Hence, it is reasonable to expect that the appropriate differential equation governing the torsional elastic characteristics should contain the torsional stiffening effects due to plate bending. Second, the B_1 and B_2 constants were retained in the general development of the blade torsion equation (Eq. 30) principally for applicability to non-helicopter rotor applications (i.e. propellers and wind turbines). However, the effect of these constants on the total stiffnesses of composite bearingless (helicopter) rotor flexbeams is considered to be negligible. Indeed, assuming a large section aspect ratio ($\frac{c}{t} \geq 10$), the ratio of twist squared stiffening to St. Venant (GJ) stiffening can be approximated by the following torsion stiffness ratio:

$$\frac{(EB\theta'^2)}{(GJ)} \approx \frac{2}{135} \left(\frac{E}{G}\right) \left(\frac{c}{t}\right)^2 \left(\frac{c}{L} \Delta\theta\right)^2$$

For comparable section and planform aspect ratios (c/t and L/c , respectively) and even for an (E/G) ratio of 25, typical of unidirectional carbon-epoxy sections, the above torsion stiffness ratio reduces to approximately $0.4\Delta\theta^2$. The total flexbeam twist angle, $\Delta\theta$, then must be in excess of 25 degrees to achieve a torsion stiffness ratio of 0.1, which is considered justifiably small for present purposes. Third, because of the length of the flexbeam and the nature of the bending loads and deflections at its outboard end (resulting from torque tube and outer blade generated internal loads), the torsion moment over the flexbeam span is generally variable and contains components due to all six concentrated loads at the juncture. These three considerations thereby define the following differential equation for a torsional element with constant section properties:

$$-\frac{DC^3}{12R^3} \theta''' + \frac{1}{R} (GJ + Tk_A^2) \theta' = M_{x_9}(r) \quad (114)$$

wherein boundary conditions on θ and θ' must be specified at the inner and outer ends of each torsion element. At the ends of the total length flexbeam (inboard end ($k = 1$), and the juncture end ($k = K$)), the appropriate boundary conditions are:

$$\begin{aligned} \theta(0) = \theta'(0) = \theta'(r_j) &= 0 \\ \theta(r_j) &= \theta_j - \theta_{BFB} \equiv \Delta\theta_j \end{aligned} \tag{115}$$

Before solving Eq. (114) let us first examine the structure of the right-hand side. Figure 11 below shows the origins of the spanwise variable internal torque which accrue from combinations of loading and deflection at the out-board (juncture) end of the flexbeam .

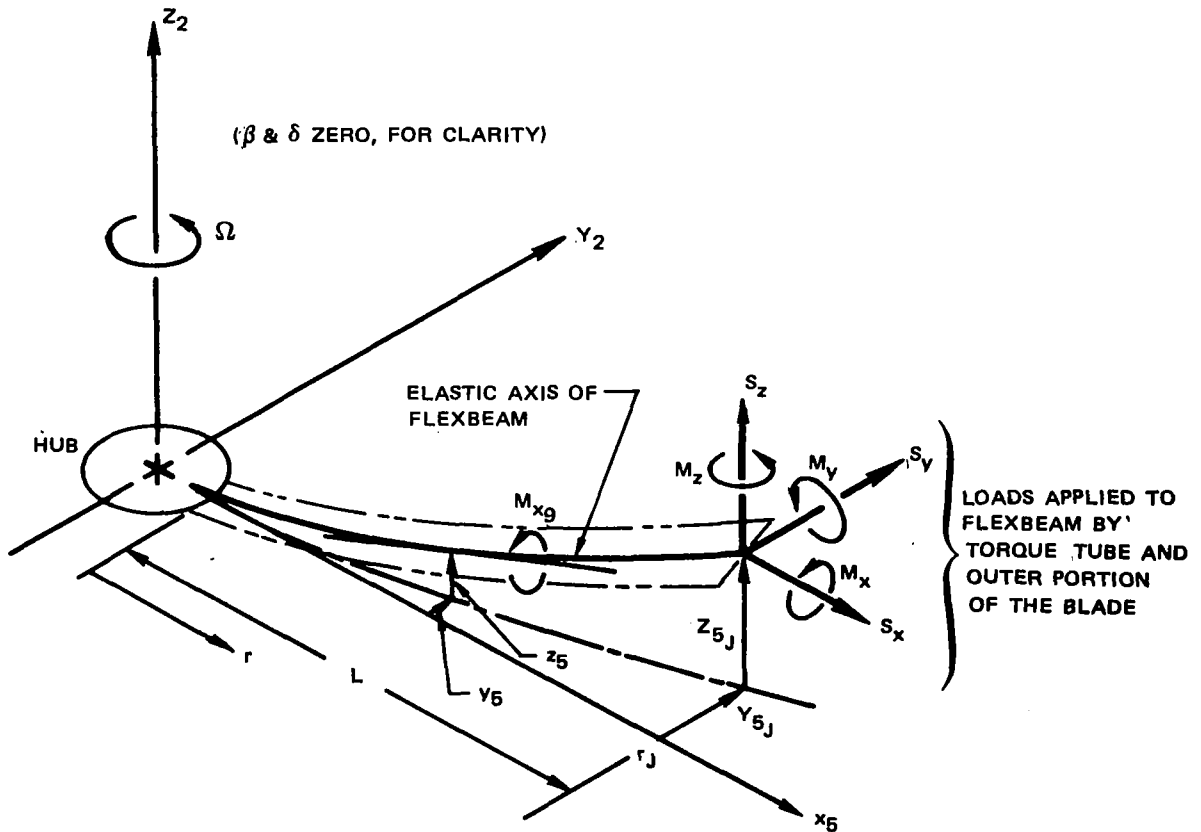


Figure 11. Pictorial View of Flexbeam Showing Deflections and Applied Loads Producing Spanwise Variable Torsion Moment.

Eq. (27) can be readily adapted to the present case wherein the loads are concentrated at a point; the following expression for the spanwise variable torsion moment, M_{x_9} , can then be written as:

$$\begin{aligned}
 M_{x_9}(r) = & \left[(z_{5j} - z_5) y'_5 - (y_{5j} - \bar{y}_5) z'_5 \right] S_{x_5} - \left[z_{5j} - z_5 - (S-r) z'_5 \right] S_{y_5} \\
 & + \left[y_{5j} - y_5 - (S-r) y'_5 \right] S_{z_5} + y'_5 M_{y_5} + z'_5 M_{z_5} + M_{x_5}
 \end{aligned} \tag{116}$$

Since the span of the flexbeam is short relative to the total blade span, the in-plane and out-of-plane deflections, y_5 and z_5 , respectively, can be approximated by polynomials defined by the deflections and slopes at the juncture. With the definition of a flexbeam spanwise variable:

$$\eta = r/S \tag{117}$$

the deflection (and corresponding slope) in either of the two directions can be expressed by the following general expressions:

$$(y_5 \text{ or } z_5) = f = (3f_j - \bar{3}f'_j)\eta^2 - (2f_j - \bar{3}f'_j)\eta^3 \tag{118a}$$

$$(y'_5 \text{ or } z'_5) = f' = \frac{1}{L} \left[(6f_j - 2\bar{3}f'_j)\eta - (6f_j - 3\bar{3}f'_j)\eta^2 \right] \tag{118b}$$

where:

$$\bar{3} = S/R \tag{118c}$$

By using Eqs. (118a and b), Eq. (116) can be expressed as a polynomial in the flexbeam spanwise variable, η :

$$\begin{aligned}
 M_{x_9}(\eta) = & (2\eta - 3\eta^2 + \eta^4)S_{x_5}(y_{5J}z'_{5J} - z_{5J}y'_{5J}) + (1 - 6\eta + 9\eta^2 - 4\eta^3)(S_{z_5}y_{5J} - S_{y_5}z_{5J}) \\
 & + 2\bar{S}(\eta - 2\eta^2 + \eta^3)(S_{z_5}y'_{5J} - S_{y_5}z'_{5J}) + \frac{6}{S}(\eta - \eta^2)(M_{y_5}y_{5J} + M_{z_5}z_{5J}) \\
 & - (2\eta - 3\eta^2)(M_{y_5}y'_{5J} + M_{z_5}z'_{5J}) + M_{x_5}
 \end{aligned} \tag{119}$$

Thus, the right-hand side of Eq. (114) is seen to be a polynomial of fourth degree in the spanwise variable η . Since the flexbeam, like the torque tube, will have section properties variable with span, a transfer matrix solution using span segments must be employed. For any constant section spanwise segment the appropriate general solution to Eq. (114) becomes:

$$\theta = Ce^{\lambda\eta} + De^{-\lambda\eta} + \sum_{i=0}^5 H_i \eta^i \tag{120}$$

where C, D and H_i are constants to be determined from the boundary conditions and from the polynomial coefficients of Eq. (119), and where the section characteristic constant, λ , is given by:

$$\lambda = \frac{2S}{C} \sqrt{\frac{3}{DC} (GJ + Tk_A^2)} \tag{121}$$

Since all the boundary conditions given by (115) can be used only after all the component transfer matrices are cascaded, one of the H_i constants, H_0 specifically, must be treated as a state variable (like θ and θ') and varied by each component transfer matrix. Eq. (120) can then be used to form an intermediate (partial) transfer matrix equation:

$$\begin{Bmatrix} \theta \\ \theta' \\ H_0 \end{Bmatrix}_k = \begin{bmatrix} \cosh \lambda \ell & -\frac{1}{\lambda} \sinh \lambda \ell & (1 - \cosh \lambda \ell) \\ -\lambda \sinh \lambda \ell & \cosh \lambda \ell & \lambda \sinh \lambda \ell \\ 0 & 0 & 1 \end{bmatrix} \begin{Bmatrix} \theta_{k+1} \\ \theta'_{k+1} \\ H_{0k} \end{Bmatrix} + \sum_{i=1}^5 H_{ik} \begin{Bmatrix} \eta_I^i - \eta_0^i \cosh \lambda \ell + i \eta_0^{i-1} \frac{\sinh \lambda \ell}{\lambda} \\ i \eta_I^{i-1} + \eta_0^i \lambda \sinh \lambda \ell - i \eta_0^{i-1} \cosh \lambda \ell \\ 0 \end{Bmatrix} \quad (122)$$

where, for each k'th segment, the constants H_{ik} ($i = 1, 2, \dots, 5$) are completely determined by the section properties and the polynomial coefficients of Eq. (119). The length of the k'th spanwise segment, ℓ_k , is conveniently taken to be the blade break-up segment length, Δx_k , divided by \bar{S} . More specifically, using the following notations:

$$A_k = \left(\frac{DC^3}{12\ell} \right)_k \quad B_k = \frac{1}{\ell_k} (GJ + Tk_A^2)_k$$

$$M_{x_9}(\eta) = \sum_{i=0}^4 T_i \eta^i \quad (123)$$

the explicit expressions for H_{ik} can be written as:

$$H_{1k} = \frac{1}{B_k} \left[T_0 + 2 \left(\frac{A}{B} \right)_k T_2 + 24 \left(\frac{A}{B} \right)_k T_4 \right] \quad (124a)$$

$$H_{2k} = \frac{1}{B_k} \left[\frac{1}{2} T_1 + 3 \left(\frac{A}{B} \right)_k T_3 \right] \quad (124b)$$

$$H_{3k} = \frac{1}{B_k} \left[\frac{1}{3} T_2 + 4 \left(\frac{A}{B} \right)_k T_4 \right] \quad (124c)$$

$$H_{4k} = \frac{1}{4B_k} T_3, \quad H_{5k} = \frac{1}{5B_k} T_4 \quad (124d \& e)$$

Equation (122) is deemed a partial transfer matrix because it does not yet include the transfer of the H_0 constant from one segment to the next; one additional relationship is thus required to complete the transfer matrix formulation. For this purpose, Eq. (114) can be integrated across an inter-segment junction point, ($\eta = \hat{\eta}_{k,k+1}$):

$$\left[-A\theta'' + B\theta \right]_{\eta=\hat{\eta}_{k,k+1}^{(-)}} - \left[-A\theta'' + B\theta \right]_{\eta=\hat{\eta}_{k,k+1}^{(+)}} = \int_{\hat{\eta}_{k,k+1}^{(-)}}^{\hat{\eta}_{k,k+1}^{(+)}} M_{x_9}(\eta) d\eta = 0 \quad (125)$$

Since the torsion moment is a smooth continuous function over the entire span the integral in the above equation must equal zero. Therefore the quantity $(-A\theta''+B\theta)$ must be continuous across the inter-segment junction point. This relationship results in the following additional required equation:

$$\begin{aligned} \left[-A\theta'' + B\theta \right]_{\eta=\hat{\eta}_{k,k+1}^{(-)}} &= B_k H_{0k} + \sum_{i=1}^5 H_{ik} \left[B_k \hat{\eta}_{k,k+1}^i - A_k i(i-1) \hat{\eta}_{k,k+1}^{i-2} \right] \\ &= B_{k+1} H_{0,k+1} + \sum_{i=1}^5 H_{i,k+1} \left[B_{k+1} \hat{\eta}_{k,k+1}^i - A_{k+1} i(i-1) \hat{\eta}_{k,k+1}^{i-2} \right] \end{aligned} \quad (126)$$

Combining Eqs. (122) and (126) yields the following final expression for the complete transfer matrix equation:

$$\begin{aligned} \begin{Bmatrix} \theta \\ \theta' \\ H_0 \end{Bmatrix}_k &= \begin{bmatrix} \cosh(\lambda\ell)_k & -\frac{1}{\lambda_k} \sinh(\lambda\ell)_k & \frac{B_{k+1}}{B_k} [1 - \cosh(\lambda\ell)_k] \\ -\lambda_k \sinh(\lambda\ell)_k & \cosh(\lambda\ell)_k & \frac{B_{k+1}}{B_k} \lambda_k \sinh(\lambda\ell)_k \\ 0 & 0 & B_{k+1} / B_k \end{bmatrix} \begin{Bmatrix} \theta \\ \theta' \\ H_0 \end{Bmatrix}_{k+1} \\ &+ \sum_{i=1}^5 H_{ik} \begin{Bmatrix} \eta_I^i - \eta_0^i \cosh \lambda\ell + \frac{(i)}{\lambda} \eta_0^{i-1} \sinh \lambda\ell \\ (i) \eta_I^{i-1} + \eta_0^i \lambda \sinh \lambda\ell - (i) \eta_0^{i-1} \cosh \lambda\ell \\ 0 \end{Bmatrix}_k \\ &+ \sum_{i=1}^5 \left[H_{ik} \left(-\eta_{0k}^i + \frac{A_k}{B_k} (i)(i-1) \eta_{0k}^{i-2} \right) + H_{i,k+1} \left(\frac{B_{k+1}}{B_k} \eta_{0k}^i - \frac{A_{k+1}}{B_k} (i)(i-1) \eta_{0k}^{i-2} \right) \right] \begin{Bmatrix} 1 - \cosh \lambda\ell \\ \lambda \sinh \lambda\ell \\ 1 \end{Bmatrix}_k \end{aligned} \quad (127)$$

Note that the H_{1k} constants, ($i = 1, 2, \dots, 5$) in the above equation are completely determined by Eqs. (12⁴a through e). This transfer matrix equation for the k 'th segment can then be suitably cascaded to yield a final matrix equation, relating the state variables at the flexbeam root to those at the juncture:

$$\begin{Bmatrix} \theta \\ \theta' \\ H_0 \end{Bmatrix}_1 = [E] \begin{Bmatrix} \theta \\ \theta' \\ H_0 \end{Bmatrix}_k + [F] \begin{Bmatrix} T_0 \\ T_1 \\ T_2 \\ T_3 \\ T_4 \end{Bmatrix} \quad (128)$$

The E and F matrices appearing in this equation are the result of appropriate cascading and, hence, are not sufficiently simple to express explicitly herein. They are calculable, however, in a straightforward manner using routine matrix algebra.

Application of the boundary conditions, Eq. (115) together with the elimination of $(H_0)_1$ and $(H_0)_k$ from the above equation set results in the following expression for the elastic torsion deflection of the flexbeam at the juncture:

$$\Delta\theta_J = \frac{1}{(e_{11}e_{23} - e_{21}e_{13})} \sum_{i=0}^4 T_i (f_{2,i+1}e_{13} - f_{1,i+1}e_{23}) \quad (129a)$$

where e_{ij} and f_{ik} are the elements of the E and F matrices, respectively, and where from Eq. (119):

$$\begin{Bmatrix} T_0 \\ T_1 \\ T_2 \\ T_3 \\ T_4 \end{Bmatrix} = \begin{bmatrix} 0 & 1 & 0 & 0 & 0 & 1 \\ 2 & -6 & 2\bar{5} & 6/\bar{5} & -2 & 0 \\ -3 & 9 & -4\bar{5} & -6/\bar{5} & 3 & 0 \\ 0 & -4 & 2\bar{5} & 0 & 0 & 0 \\ 1 & 0 & 0 & 0 & 0 & 0 \end{bmatrix} \begin{Bmatrix} S_{x_5} (y_{5J} z'_{5J} - z_{5J} y'_{5J}) \\ S_{z_5} y_{5J} - S_{y_5} z_{5J} \\ S_{z_5} y'_{5J} - S_{y_5} z'_{5J} \\ M_{y_5} y_{5J} + M_{z_5} z_{5J} \\ M_{y_5} y'_{5J} + M_{z_5} z'_{5J} \\ M_{x_5} \end{Bmatrix} \quad (129b)$$

FB

Equations (129a and b) can be combined using the following compact notation:

$$\begin{aligned} \Delta\theta_J = & \theta_{S_x} S_{x_5} (y_{5J} z'_{5J} - z_{5J} y'_{5J})_{FB} \\ & + \theta_{S_0} (S_{z_5} y_{5J} - S_{y_5} z_{5J})_{FB} + \theta_{S_1} (S_{z_5} y'_{5J} - S_{y_5} z'_{5J})_{FB} \\ & + \theta_{M_0} (M_{y_5} y_{5J} + M_{z_5} z_{5J})_{FB} + \theta_{M_1} (M_{y_5} y'_{5J} + M_{z_5} z'_{5J})_{FB} \\ & + \theta_{M_x} M_{x_5 FB} \end{aligned} \quad (130a)$$

or alternatively:

$$\begin{aligned} \Delta\theta_J = & \theta_{S_x} S_{x_5 FB} + \theta_{M_x} M_{x_5 FB} + \theta_{S_y} S_{y_5 FB} \\ & + \theta_{S_z} S_{z_5 FB} + \theta_{M_y} M_{y_5 FB} + \theta_{M_z} M_{z_5 FB} \end{aligned} \quad (130b)$$

where the various stiffness coefficients in Eq. (130b) are deflection dependent.

Thus, the elastic torsion deflection, $\Delta\theta_J$, is seen to result not only from the usual radially oriented feathering torque, M_{x_5} , but from various nonlinear combinations of loads and deflection. The following subsection presents those calculations needed to estimate the internal loads just outboard of the juncture which must be equilibrated with the torque tube and flexbeam loads at the juncture.

Estimation of Internal Blade Shears and Moments in Blade Adjacent to the Juncture

Two basic methods exist for estimating the instantaneous internal loads in the outer portion of the blade: mode deflection and force-integration. A comprehensive discussion of these two methods and their accuracy characteristics is contained in Ref. 8 and will be omitted herein. Briefly, the former is relatively simple to implement but requires smooth spanwise load distributions for accurate estimates with a small number of modal variables; the latter is, *prima facie*, a more complicated method to implement but estimates the loads with superior accuracy. The latter method (force integration) was chosen because, for most practical helicopter applications, it is significantly more accurate, and because the disadvantage by reason of complexity is mollified by certain available features implicit in the general analysis solution.

Because the torsional redundance portion of the redundant analysis itself entails significant nonlinearities, the redundant analysis effects are most meaningfully included only in the total nonlinear formulation wherein the equations are solved by numerical integration to obtain time-histories. Examination of the various differential equations formulated for the aeroelastic responses, Eqs. (24), (25), (30), (31), and (32) reveals that the inertia and aerodynamic load distributions are used explicitly. That is, with the exception of the double (nondimensional) time derivatives of the response variables, which are extracted to form the inertia matrix, all load distributions such as Eqs. (41) and (44) are calculated and used directly in the spanwise integrations required for the various response excitations. Thus, the major necessary complexity inherent in force-integration, that of having to calculate explicitly the load distributions, is for the most part already satisfied. The remaining requirement for implementation is to approximate the doubly differentiated responses (vibratory accelerations, \ddot{q}) and include them in the load distributions.

The general time-history solution, as indicated by Eq. (26), implies that at any one time step when the excitations are being calculated, the acceleration is not yet known: The (RHS) of Eq. (26), which nominally excludes all \ddot{q} 's, is first evaluated to calculate the \ddot{q} 's given on the (LHS) of this equation. Thus, to implement the force-integration calculation, approximations to the \ddot{q} 's implicitly appearing in the (RHS) must be made. Fortunately, the force-integration method is generally "forgiving" of such approximations since loads due to vibratory acceleration usually act as dynamic corrections to the "pseudo-static" loads. A discussion and formulation of the extrapolation formula required to approximate these accelerations is contained in Appendix I; briefly, for any response with an inherent natural frequency, $\bar{\omega}$, the acceleration can be approximated as:

$$\ddot{q}_k \approx 2 \cos(\bar{\omega} \Delta \psi) \ddot{q}_{k-1} - \ddot{q}_{k-2} \quad (131)$$

where $\Delta \psi$ is the integration step size. With this approximation formula, Eqs. (41a, b, and c) and (44a, b, and c) can be evaluated and the following expressions for the internal concentrated blade loads outboard and adjacent to the juncture can then be calculated. In these expressions, unless otherwise indicated, the load distributions are understood to contain both inertia and aerodynamic contributions:

$$S_{x_5B} = \int_{r_J}^1 \rho_{Dx_5} dr \quad (132a)$$

$$S_{y_5B} = \int_{r_J}^1 \rho_{y_5} dr \quad (132b)$$

$$S_{z_5B} = \int_{r_J}^1 \rho_{z_5} dr \quad (132c)$$

$$M_{x_5B} = \int_{r_J}^1 [q_{x_5} + \rho_{z_5}(y_5 - y_{5J}) - \rho_{y_5}(z_5 - z_{5J})] dr \quad (132d)$$

$$M_{y_5B} = \int_{r_J}^1 [q_{Dy_5} - \rho_{z_5}(r - r_J) + \rho_{Dx_5}(z_5 - z_{5J})] dr \quad (132e)$$

$$M_{z_5B} = \int_{r_J}^1 [q_{Dz_5} + \rho_{y_5}(r - r_J) - \rho_{Dx_5}(y_5 - y_{5J})] dr \quad (132f)$$

Additionally, the push-rod force, F_{PR} , appearing in Eq. (112) must similarly be approximated. Upon using the principal (linear) component of the flexbeam torsional stiffness, the push-rod force can be approximated by:

$$F_{PR} = \frac{1}{y_{IO_{PR}}} \left\{ \frac{1}{S_{FB}} \left[(GJ)_{\text{equ.}} \Delta \Theta_J + T k_A^2 \Theta_J \right]_{FB} \right. \\ \left. - \int_{r_R}^1 [q_{x_5} + y'_{5R} q_{y_5} + z'_{5R} q_{z_5} + \rho_{z_5}(y_5 - y_{5R} - y'_{5R}(r - r_R)) \right. \\ \left. - \rho_{y_5}(z_5 - z_{5R} - z'_{5R}(r - r_R))] dr \right\} \quad (133)$$

where the subscript (R) denotes conditions at the root of the torsionally active portion of the blade. The above approximations together with the results of the two preceding subsections are sufficient to explicitly formulate the details of the redundant analysis solution which is accomplished in the following subsection.

Mathematical Formulation of the Structural Redundancy

The results of the previous subsections can be brought together to form a solution for all internal loads in the vicinity of the juncture. From the deflections of the juncture and inboard torque tube attachment point (snubber) all concentrated juncture loads in the torque tube except torsion moment are evaluated by means of Eqs. (112) and (113). All loads outboard of the juncture are known from interaction of the spanwise loadings and are calculable using Eqs. (132a through f). Consequently, by equilibrating the internal juncture loads and imposing the consistency constraint on the elastic torsion deflection of flexbeam, the flexbeam and thence, torque tube torsion moments are determined. First, however, some attention must be paid to the internal bending moments in the torque tube at the juncture. These moments as calculated using Eq. (112) are oriented in the torque tube section plane at the juncture and must be rotated back to the "5" coordinate system using the following coordinate transformation pair:

$$\begin{Bmatrix} M_{x_7} \\ M_{y_7} \\ M_{z_7} \end{Bmatrix} = \begin{bmatrix} 1 & y'_{5J} & z'_{5J} \\ -y'_{5J} & 1 & 0 \\ -z'_{5J} & 0 & 1 \end{bmatrix} \begin{Bmatrix} M_{x_5} \\ M_{y_5} \\ M_{z_5} \end{Bmatrix} \quad (134a)$$

$$\begin{Bmatrix} M_{x_5} \\ M_{y_5} \\ M_{z_5} \end{Bmatrix} = \begin{bmatrix} 1 & -y'_{5J} & -z'_{5J} \\ y'_{5J} & 1 & 0 \\ z'_{5J} & 0 & 1 \end{bmatrix} \begin{Bmatrix} M_{x_7} \\ M_{y_7} \\ M_{z_7} \end{Bmatrix} \quad (134b)$$

The primary purpose of this redundant analysis is to obtain the incremental torsion moment exerted by the flexbeam to the torque tube, ΔM_{x_7} , which is given by:

$$\Delta M_{x_7_{TT}} = -M_{x_7_{FB}} = -(M_{x_5_{FB}} + y'_{5J} M_{y_5_{FB}} + z'_{5J} M_{z_5_{FB}}) \quad (135)$$

But the flexbeam loads are related to the outer blade and torque tube loads by the equilibration of loads:

$$\begin{Bmatrix} S \\ M \end{Bmatrix}_{FB} = \begin{Bmatrix} S \\ M \end{Bmatrix}_B - \begin{Bmatrix} S \\ M \end{Bmatrix}_{TT} \quad (136)$$

Use of the coordinate transformation, Eq. (134a), on the outer blade moments Eqs. (132d through f), the torque tube loads, Eqs. (112 and 113) and the equilibration of loads given by Eq. (136) sufficiently determines all loads in the "7" coordinate system except M_{x7FB} , which can be determined, however, from the torsion stiffness equation of the flexbeam. Upon inclusion of the effects of flexbeam built-in twist, θ_{BFB} , this equation can be rewritten as:

$$\begin{aligned} \Delta\theta_J = \theta_J - \theta_{BFB} = & \theta_{s_x} S_{x5FB} + \theta_{s_y} S_{y5FB} + \theta_{s_z} S_{z5FB} \\ & + \theta_{M_x} \left[M_{x7FB} - y'_{5J} M_{y7FB} - z'_{5J} M_{z7FB} - \theta_{BFB} \left(\frac{TK_A^2}{S} \right)_{FB} \right] \\ & + \theta_{M_y} (y'_{5J} M_{x7FB} + M_{y7FB}) + \theta_{M_z} (z'_{5J} M_{x7FB} + M_{z7FB}) \end{aligned} \quad (137)$$

and solving for M_{x7FB} yields the final required result:

$$\begin{aligned} \Delta M_{x7TT} = -M_{x7FB} = & (\theta_{M_x} + y'_{5J} \theta_{M_y} + z'_{5J} \theta_{M_z})^{-1} \left[-\Delta\theta_J - \theta_{M_x} \theta_{BFB} \left(\frac{TK_A^2}{S} \right)_{FB} \right. \\ & + \theta_{s_x} S_{x5FB} + \theta_{s_y} S_{y5FB} + \theta_{s_z} S_{z5FB} \\ & \left. + (\theta_{M_y} - y'_{5J} \theta_{M_x}) M_{y7FB} + (\theta_{M_z} - z'_{5J} \theta_{M_x}) M_{z7FB} \right] \end{aligned} \quad (138)$$

This incremental moment is then included as a concentrated torsion moment to the torsion response, Eq. (30) as is therein provided, to complete the redundant analysis.

The section to follow develops the equations needed for aeroelastic eigen-solutions using a fixed azimuth approach. While the linearized equations derived do contain the bending redundancy, they omit the (essentially nonlinear) torsion redundancy described in this subsection.

LINEARIZED FORM OF EQUATIONS

For time-history solutions of the complete nonlinear equations the complete explicit expansions of the inertial and aerodynamic load distributions are not required. In fact, the implicit descriptions of these load distributions (Eqs. (41), (44), and (59)) actually facilitate the formulation of these equations and eliminate the requirement for assessing orders of magnitude in order to achieve tractability through simplification. On the other hand, the unique and desirable features of eigensolutions (i.e., relatively short computation time for solution, identification of all coupled mode frequency and damping characteristics and the availability of established analysis techniques for assessing the behavior of linear systems) are sufficiently attractive to warrant equation linearization using explicit expansions of these loadings. The purpose of this subsection, therefore, is to present the main results of this linearization. The relative orders of magnitude of the various dynamic and elastic quantities are presented in Table I; from this tabulation the various coefficients in the

TABLE I

Assumed Relative Orders of Magnitude of Quantities Appearing in Aeroelastic Dynamic Equations.

ϵ^0	$\epsilon^{1/2}$	ϵ	$\epsilon^{3/2}$	ϵ^2
\bar{r}	θ^*, θ^{**}	v_e, w_e	$\Delta v_B, \Delta w_B$	$\Delta v_e, \Delta w_e$
$\cos \theta$	$\sin \theta, \theta'_B$	$\beta^*, \beta^{**}, \delta^*, \delta^{**}$	\bar{k}_{Y10}^{-2}	$\Delta V, \Delta W$
$\gamma_{w_i}, \gamma_{v_k}, \gamma_{\theta_j}$	β, δ	q, q^*, q^{**}		u_e, \bar{u}_e
$\Delta v_{e_{ij}}, \Delta w_{e_{kj}}$	$\Delta v_{B_j}, \Delta w_{B_k}$	$\Delta v_{e_j}, \Delta w_{e_k}$		
$u_{e_{im}}$	v_e'', w_e''	$\Delta V_k, \Delta W_i$		
\bar{T}	$\bar{E}I_z$	$\bar{E}I_y$		
		\bar{Y}_{10CG}, \bar{e}		
		$\bar{k}_A^{-2}, \bar{k}_{Z10}^{-2}$		

resulting expanded equations of motion were evaluated and retained only if they did not exceed ϵ^2 . As a result, some terms so retained remain nonlinear, but are generally of a quadratic form (i.e., $q_a \cdot q_b^*$, $\beta \cdot \beta^*$, $q_a \cdot q_b$, etc.). However, these terms can be locally linearized about predeflected positions. The expanded equations presented in Table I are consistently expanded to ϵ^2 in the coefficients and have the quadratic nonlinear dynamic and elastic terms segregated for clarity.

Reasonable explicit expansions and linearizations of the aerodynamic load distributions, contained only implicitly in the above equations, can be achieved within the context of various optional simplifying assumptions. The aerodynamic linearization actually developed for the analysis parallels the aerodynamic description given in an above subsection so that the total linearization achieved should represent a true "local linearization" of the total nonlinear equations at any point in time.

Using Eq. (I.59) as a starting point the following terms are seen to contain all the independent response variables whose perturbations must be made:

$$U_p = \tilde{v}_p - \tilde{v}_y \sin \Theta - \tilde{v}_z \cos \Theta \quad (139a)$$

$$U_T = \tilde{v}_T + \tilde{v}_y \cos \Theta - \tilde{v}_z \sin \Theta \quad (139b)$$

$$\alpha_{qs} = \theta_0 + \theta_e + \Delta \theta + \tan^{-1} \left(\frac{U_p}{U_T} \right) \quad (139c)$$

$$M = \frac{\Omega R}{\alpha_{\infty}} \sqrt{U_p^2 + U_T^2} \quad (139d)$$

where:

$$\tilde{v}_p = \lambda \left(1 - \frac{\beta^2}{2} \right) - \beta U_x - r \beta^* \quad (140a)$$

$$\tilde{v}_T = e + r \left(1 - \frac{\beta^2}{2} + \delta \right) + \mu \left[\left(1 - \frac{\delta^2}{2} \right) \sin \psi + \delta \cos \psi \right] \quad (140b)$$

$$\begin{aligned} \tilde{v}_y = & (\gamma_{v_k} - \Delta v_k) \dot{q}_{v_k}^* + \Delta v_i \dot{q}_{w_i}^* + \Delta v_{e_{ij}} q_{w_i} \dot{q}_{\theta_j}^* \\ & - \dot{\Theta} [(\gamma_{w_i} - \Delta w_i) q_{w_i} - \Delta w_k q_{v_k}] + U_x [(\gamma'_{v_k} - \Delta v_k^{(2)'}) q_{v_k} + \Delta v_i^{(2)'} q_{w_i}] \end{aligned} \quad (140c)$$

$$\begin{aligned} \tilde{v}_z = & (\gamma_{w_i} - \Delta w_i) \dot{q}_{w_i}^* - \Delta w_k \dot{q}_{v_k}^* - \Delta w_{e_{kj}} q_{v_k} \dot{q}_{\theta_j}^* \\ & + \dot{\Theta} [(\gamma_{v_k} - \Delta v_k) q_{v_k} + \Delta v_i q_{w_i} + y_{10} \frac{3c}{4}] + U_x [(\gamma'_{w_i} - \Delta w_i^{(2)'}) q_{w_i} - \Delta w_k^{(2)'} q_{v_k} + \dot{\Theta} y_{10} \frac{3c}{4}] \end{aligned} \quad (140d)$$

and where U_x is given by Eq. (50).

Assuming that the partial derivatives of the airfoil aerodynamic coefficients, c_ℓ , c_d , and $c_{mc}/4$, with respect to angle-of-attack and Mach number are available, the following expressions can be written for perturbational aerodynamic load distributions:

$$\begin{aligned} \delta p_{A_{y_5}} = & \frac{1}{2} \frac{\rho R^2}{m_0} c \left\{ \frac{U_P}{U} [C_\ell U_P - C_d U_T] \right. \\ & + U \left[C_\ell + U_P \frac{1}{U^2} \left(\frac{\partial C_\ell}{\partial \alpha} U_T + \frac{\partial C_\ell}{\partial M} M U_P \right) - \frac{U_T}{U^2} \left(\frac{\partial C_d}{\partial \alpha} U_T + \frac{\partial C_d}{\partial M} M U_P \right) \right] \left. \right\} \delta U_P \\ & + \left\{ \frac{U_T}{U} [C_\ell U_P - C_d U_T] + U \left[\frac{U_P}{U^2} \left(-\frac{\partial C_\ell}{\partial \alpha} U_P + \frac{\partial C_\ell}{\partial M} M U_T \right) \right. \right. \\ & \left. \left. - C_d - \frac{U_T}{U^2} \left(-\frac{\partial C_d}{\partial \alpha} U_P + \frac{\partial C_d}{\partial M} M U_T \right) \right] \right\} \delta U_T \\ & + U \left[U_P \frac{\partial C_\ell}{\partial \alpha} - U_T \frac{\partial C_d}{\partial \alpha} \right] \delta \Theta \left. \right\} \end{aligned} \quad (141)$$

$$\begin{aligned}
\delta p_{Az_5} = & \frac{1}{2} \frac{\rho R^2}{m_0} c \left\{ \left\{ \frac{U_P}{U} [C_L U_T + C_D U_P] \right. \right. \\
& + U \left[\frac{U_T}{U^2} \left(\frac{\partial C_L}{\partial \alpha} U_T + \frac{\partial C_L}{\partial M} M U_P \right) + C_D + \frac{U_P}{U^2} \left(\frac{\partial C_D}{\partial \alpha} U_T + \frac{\partial C_D}{\partial M} M U_P \right) \right] \left. \right\} \delta U_P \\
& + \left\{ \frac{U_T}{U} [C_L U_T + C_D U_P] + U \left[C_L + \frac{U_T}{U^2} \left(-\frac{\partial C_L}{\partial \alpha} U_P + \frac{\partial C_L}{\partial M} M U_T \right) \right. \right. \\
& \left. \left. + \frac{U_P}{U^2} \left(-\frac{\partial C_D}{\partial \alpha} U_P + \frac{\partial C_D}{\partial M} M U_T \right) \right] \right\} \delta U_T \\
& + U \left(U_T \frac{\partial C_L}{\partial \alpha} + U_P \frac{\partial C_D}{\partial \alpha} \right) \delta \Theta \left. \right\} \quad (142)
\end{aligned}$$

$$\begin{aligned}
\delta q_{Ax_5} = & \frac{1}{2} \frac{\rho R^2}{m_0} c^2 \left\{ \left[-\kappa_{Ax_5}^* \frac{U_P}{U} + 2C_m U_P + \frac{\partial C_m}{\partial \alpha} U_T + \frac{\partial C_m}{\partial M} M U_P \right] \delta U_P \right. \\
& + \left[-\kappa_{Ax_5}^* \frac{U_T}{U} + 2C_m U_T - \frac{\partial C_m}{\partial \alpha} U_P + \frac{\partial C_m}{\partial M} M U_T \right] \delta U_T \\
& \left. - \kappa_{Ax_5} U \delta \Theta + \gamma_{10c/4} \delta [\cos \Theta p_{Az_5} - \sin \Theta p_{Ay_5}] \right\} \quad (143)
\end{aligned}$$

where:

$$\delta U_P = \delta \tilde{v}_P - (\tilde{v}_y \cos \Theta - \tilde{v}_z \sin \Theta) \delta \Theta - \sin \Theta \delta \tilde{v}_y - \cos \Theta \delta \tilde{v}_z \quad (144a)$$

$$\delta U_T = \delta \tilde{v}_T - (\tilde{v}_y \sin \Theta + \tilde{v}_z \cos \Theta) \delta \Theta + \cos \Theta \delta \tilde{v}_y - \sin \Theta \delta \tilde{v}_z \quad (144b)$$

and where $\delta \tilde{v}_p$, $\delta \tilde{v}_T$, $\delta \tilde{v}_y$, and $\delta \tilde{v}_z$ are obtained from appropriate differentiations of Eqs. (140) and (62b) or (69).

Further explicit expansions of the perturbational airload distributions beyond this point would rapidly become overly tedious, and voluminous and would, thus, not serve much additional purpose. The above development together with appropriate straightforward perturbations of the component air velocities are sufficient to form the desired perturbational airloads. The perturbational inertia loads are obtained in a similar manner using Eqs. (41a, b and c) and Eqs. (44a, b and c).

REFERENCES

1. Arcidiacono, P. J.: Prediction of Rotor Instability at High Forward Speeds. Vol. I, Differential Equations of Motion for a Flexible Helicopter Rotor Blade in Steady Flight Including Chordwise Mass Unbalance Effects. USAAVLABS Technical Report 68-18A, February 1969.
2. Davis, J. M.; Bennett, R. L.; and Blankenship, B. L.: Rotorcraft Flight Simulation with Aeroelastic Rotor and Improved Aerodynamic Representation. USAAMRDL Technical Report 74-10A, June 1974.
3. Sopher, R.: Derivation of Equations of Motion for Multi-Blade Rotors Employing Coupled Modes and Including High Twist Capability. (Sikorsky Aircraft SER-50912; NASA Contract NAS2-6463.) NASA CR-137810, 1975.
4. Houbolt, J. C.; and Brooks, G. W.: Differential Equation of Motion for Combined Flapwise Bending, Chordwise Bending, and Torsion of Twisted Non-uniform Rotor Blades. NACA Report 1346, 1958.
5. Bielawa, R. L.: A Second Order Nonlinear Theory of the Aeroelastic Properties of Helicopter Rotor Blades in Forward Flight. Ph.D. thesis, Massachusetts Institute of Technology, June 1965.
6. Payne, P. R.: Helicopter Dynamics and Aerodynamics. Pitman and Sons, pp. 40-45, London, 1959.
7. Castles, W., Jr.; and DeLeeuw, T. H.: The Normal Component of the Induced Velocity in the Vicinity of a Lifting Rotor and Some Examples of its Application. NACA TR-1184.
8. Bisplinghoff, R. L.; Ashley, H.; and Halfman, R. L.: Aeroelasticity. Addison-Wesley Publishing Co., Inc. 1955, pp. 646-650.
9. Arcidiacono, P. J.; Carta, F. O.; Cassellini, L. M.; and Elman, H. L.: Investigation of Helicopter Control Loads Induced by Stall Flutter. USAAVLABS Technical Report 70-2, 1970.
10. Bielawa, R. L.: Synthesized Unsteady Airfoil Data with Applications to Stall Flutter Calculations. American Helicopter Society, 31st Annual National Forum Proceedings, No. 935, May 1975.

REFERENCES (Cont'd)

11. Heyson, H. H.: Linearized Theory of Wind Tunnel Jet Boundary Corrections and Ground Effect for VTOL-STOL Aircraft. NASA TR-RL24, 1962.
12. Landgrebe, A. J.; and Egolf, T. A.: UARL Prescribed Wake Rotor Inflow Program (Single Rotor Version), NASA CR-137899, 1975.
13. Bielawa, R. L.: Dynamic Analysis of Multi-Degree-of-Freedom Systems Using Phasing Matrices. American Helicopter/NASA Specialists Meeting on Rotorcraft Dynamics Proceedings No. 4, Moffett Field, California, February 1974.
14. Nikolsky, A. A.: Helicopter Analysis. John Wiley and Sons, Inc., New York, 1951, pp. 92-93.
15. Kuczinsky, W. A.: Inflight Rotor Stability Monitor. NASA Symposium on Flutter Testing Techniques, NASA Flight Research Center, Edwards AFB, California, October 1975.
16. Hall, W. E.: Application of Floquet Theory to the Analysis of Rotary Wing VTOL Stability. SUDDAR No. 400, Stanford University Center for Systems Research. (NASA Contract NAS-25143), 1970.

APPENDIX I

QUADRATURE FORMULAE USED IN PROGRAM G400

The time-history solution of the fully nonlinear set of dynamic equations of motion, Eq. (26), requires an appropriate set of numerical integration, extrapolation and differentiation formulae. Numerical integration in (nondi-
 mensional) time is required for the basic solution of the nonlinear equation set in a conventional step-by-step fashion. Furthermore, when various of the elastic modal response variables are characterized by large natural frequencies ($\geq 12P$), numerically stable integrations would require prohibitively small integration step sizes. For such cases it becomes reasonable to assume that the inertia (\ddot{q}) term is negligible compared with the elastic ($\bar{\omega}^2 q$) term. This assumption permits eliminating the double integration of the inertia term and substituting a "quasi-static" solution which involves an appropriate extrapolation of the response variable. Finally, whereas Eq. (26) implies that the right-hand side is a function devoid of explicit linear terms in q (the highest derivatives of q), various explicit or implicit nonlinear terms in these derivatives may still exist. Two particular sources of nonlinear double time derivative dependency are the estimation of dynamic loads for use in the redundant analysis, and the calculation of the second time derivative of angle of attack as required for the unsteady airloads formulation (see Refs. 9 and 10 for a detailed description of this formulation). Because of such nonlinearity, the usual time-history algorithm of solving for \ddot{q} at a given time using knowledge of the lower derivatives at that same instant is disrupted. Hence, approximation to \ddot{q} , based upon a reasonable extrapolation of past values, is required for evaluation of these nonlinear terms on the right hand side of Eq. (26). The following subsections describe the numerical algorithms used to satisfy these three solution requirements.

Numerical Integration

Double integration of the response variable accelerations, \ddot{q} , to obtain \dot{q} and q at the next time step is accomplished using a variant of the Adams method (without correctors). In this variant the accelerations are locally assumed to be simple harmonics of their respective characteristic frequencies in order to integrate over each subsequent time step. Denoting this frequency as an "integration" frequency, $\bar{\omega}$, the following algorithms result:

$$\ddot{q}_{k+1} = \ddot{q}_k + \left(\frac{\cos \bar{\omega} \Delta \psi - \cos 2\bar{\omega} \Delta \psi}{\bar{\omega} \sin \bar{\omega} \Delta \psi} \right) \ddot{q}_k - \left(\frac{1 - \cos \bar{\omega} \Delta \psi}{\bar{\omega} \sin \bar{\omega} \Delta \psi} \right) \ddot{q}_{k-1} \quad (I.1)$$

$$q_{k+1} = q_k + \left(\frac{1 - \cos \bar{\omega} \Delta \psi}{\bar{\omega} \sin \bar{\omega} \Delta \psi} \right) (\ddot{q}_k + \ddot{q}_{k+1}) \quad (\text{I.2})$$

where $\Delta \psi$ is the integration step size. For each elastic (modal) degree of freedom the integration frequency is taken to be its inputted uncoupled natural frequency. The usual pendular frequencies of a rotating, hinged, rigid beam are taken as the integration frequencies of the flapping and lead-lag degrees of freedom.

Quasi-Static Solution

The static solution on any one of the response variables, q_s , is achieved by manipulating the simultaneous equation solution of Eq. (34)

$$\ddot{q}_{s_k} = f_s(q_k, \ddot{q}_k, \psi_k) \quad (\text{I.3})$$

into the following approximate form:

$$\hat{q}_{s_k} = \frac{1}{\bar{\omega}^2} f_s(q_k, \ddot{q}_k, \psi_k) + q_{s_k} \quad (\text{I.4})$$

where, in general \hat{q}_{s_k} and q_{s_k} are not equal. The newly formed quantity, \hat{q}_{s_k} , is used only to effect an extrapolation to the subsequent time step:

$$\ddot{q}_{k+1} = \frac{1}{2\Delta\psi} (\hat{q}_k - \hat{q}_{k-2}) \quad (\text{I.5})$$

$$q_{k+1} = \frac{1}{3} (4\hat{q}_k + \hat{q}_{k-1} - 2\hat{q}_{k-2}) \quad (\text{I.6})$$

The results of Eqs. (I.5) and (I.6) are then used in exactly the same way as those of Eqs. (I.1) and (I.2) to evaluate the right-hand (excitation) side of the equations of motion, Eq. (26). Furthermore, it should be stressed that these equations give valid approximations only for, and should be limited to, those cases where the integration frequency is large.

Extrapolation of q^{**}

As with the numerical integration scheme presented in an above subsection, extrapolation of q^{**} is achieved by assuming the accelerations to be locally simple harmonic. The resulting extrapolation formula becomes:

$$q_k^{**} \approx 2(\cos \bar{\omega} \Delta \psi) q_{k-1}^{**} - q_{k-2}^{**} \quad (I.7)$$

APPENDIX II

PROGRAM G400 INPUT DESCRIPTION

The required input to the program consists of the following major punched card data blocks in order of loading:

- I. Airfoil Data
- II. Inertia, Elastic, Geometric and other Operational Data
(in Loader Format)
- III. Blade Mode Shape Data
- IV. Harmonics of Variable Inflow

Details for preparing the data for each of these blocks are given in the sections which follow. An additional section of this appendix provides information for facilitating program operation and improving its efficiency.

I. Airfoil Data

This data block consists of tables of two-dimensional lift, drag and pitching moment coefficients each versus angle of attack for various Mach numbers. Additionally, if unsteady aerodynamics are used, the static stall angles and linear coefficient slopes for both lift and pitching moment are included in this table. Provision is made for inputting and using only one set of aerodynamic coefficients; hence, it is assumed that the same airfoil section is used over the entire blade span. Provision is also made in the program for optionally using an analytic representation of the NACA 0012 airfoil; if this option is invoked it is not necessary to provide any airfoil data to the program. For usage of the analytic NACA 0012 airfoil option, however, the required input for this block of data must be a single card with blank or zeroed columns 1 and 2. For the general case, however, the airfoil data are loaded in three subblocks (corresponding to c_l , c_d , and $c_{mC/4}$ data) using the following general format; note that the required punch format is indicated by the FORTRAN format information in parenthesis:

card #1:

NZ

TITLE(optional)

(I2,A78)

card #2:

J N M A(1) CL(1) A(2) CL(2) ...A(4) CL(4)

(I2,10F7.0)

cards #2+

A(5) CL(5) ...

(F9.0,9F7.0)

...A(N) CL(N) ALSTAL DCLDAQ

(F9.0,9F7.0)

where: NZ is the number of Mach numbers for which groups of c_l data are to be read in; TITLE is any (optional) identifying information. J is the number of data entries to be inputted into each such group. N is the number of angle-of-attack $-c_l$ abscissa-ordinate pairs to be inputted; N is restricted to a maximum of 34 without, and 33 with the use of unsteady aerodynamics. M is the Mach number appropriate to the data group. A(i) are the N angle-of-attack abscissae in degrees and CL(i) are the N lift coefficient ordinates. ALSTAL and DCLDAQ are, respectively, the static stall angle, in degrees, and the lift curve slope at zero angle-of-attack, in per degree; these items are needed only if the unsteady airloads option is invoked.

Cards 2 and 2+ are repeated for each successively higher Mach number. A maximum of 12 Mach numbers is allowed and the lowest and highest Mach numbers need not define the total working range as the search technique uses the boundary data for Mach numbers beyond the inputted range. Thus, repeated data for zero and supersonic Mach numbers are not needed. The lowest Mach number inputted must contain an angle-of-attack range of from -180° to 180° or from 0° to 180° depending on whether or not unsymmetric airfoil data is being inputted; all higher Mach number data need extend only from -30° to 30° or from 0° to 30° in a similar manner.

The general format described above is repeated for the c_d and $c_{m_c/4}$ subblocks in that order. The static stall angles and aerodynamic coefficient curve slopes at zero angle-of-attack are deleted for the c_d subblock.

II. Inertia, Elastic, Geometric and Other Operational Data

This data block includes those items used to define the more detailed dynamic features and/or those which are most likely to vary from case to case. The format for these data is as follows:

$NN \ L \ DATA(L) \ DATA(L+1) \dots DATA(L+4) \qquad (I2, I4, 5F12.0)$
--

where: NN is the card word count, i.e., the number of data items on the card to be inputted, columns 1 and 2; NN must not exceed 5. L is the location or identifying number of the first data item on the card columns 3 - 6 right adjusted. DATA(L+i) represents the various data items on the card, columns 7-18, 19-30, 31-42, 43-54, and 55-66, in floating point format. The locations or identifying numbers for the various data and control items are listed below along with definitions and other pertinent comments; note that data locations not assigned data are implied to be intentionally left blank and/or not inputted:

<u>Location</u>	<u>Item</u>	<u>Description</u>
1	ΩR	Rotor tip speed, ft/sec.
2	R	Rotor radius, ft.
3	ρ	Air density, lb-sec ² /ft ⁴ .
4	a_∞	Speed of sound, ft/sec.
5	b	Number of blades.
6	\bar{e}	Nondimensional offset distance of start of deformable and/or deflectable portion of rotor blade, e/R .
7	B	Tip loss, used to define equivalent momentum area and three-dimensionality corrections to computed two-dimensional airloads near the blade tip.

<u>Location</u>	<u>Item</u>	<u>Description</u>
8	NSEG	Number of blade segments used to define spanwise variable arrays.
9	$\Delta\psi$	Azimuth increment used in the numerical integration of the dynamic equations, deg. (See section on general information for efficient program usage.)
10	N_F	Number of "flap trials", i.e., maximum number of rotor revolutions for which the blade time-history will be computed in an attempt to obtain convergence to periodicity. If a transient response is desired for only a portion of one rotor revolution the program will compute a time-history solution for any nonzero fractional N_F value inputted. An identically zero value will cause the time-history solution to be by-passed entirely.
11	ϵ_F	Flapping tolerance to within which the aeroelastic/dynamic responses must repeat on successive revolutions in order for the motion to be considered converged to periodicity. The tolerance applied to lead-lag motion is equal to $5\epsilon_F$.
12	A_{1s}	Longitudinal cyclic pitch, coefficient of minus $\cos\psi$ term in Fourier expansion of blade control pitch angle, deg.
13	B_{1s}	Lateral cyclic pitch, coefficient of minus $\sin\psi$ term in Fourier expansion of blade control pitch angle, deg.
14	$\theta_{.75R}$	Blade collective pitch angle as defined at the 75% radius, deg.
15	λ	Mean rotor inflow ratio.
16	V	Forward flight velocity, kts.
17	σ	Rotor solidity (= $bc/\pi R$).

<u>Location</u>	<u>Item</u>	<u>Description</u>
18	Δc_{d_0}	Increment added to all values of c_d obtained from tabulated airfoil data or from the analytic NACA 0012 data. Airfoil data generally correspond to smooth wind tunnel models and Δc_{d_0} is often used to adjust for the higher drag of production blades; a commonly used value of Δc_{d_0} is 0.002.
19	(Control)	Make greater than zero (1.) for first case or when new <u>blade modal data</u> are to be inputted. Program automatically sets this control number to (-1.) after each loading of modal data.
20	$N_{\text{cut-out}}$	Number of blade segments, starting at inboard end and defining the cut-out region, for which the lift and moment coefficients are set to zero.
21	$(c_d)_{\text{cut-out}}$	The drag coefficient used on the first $N_{\text{cut-out}}$ segments.
22	θ_1	Built-in linear blade twist angle; i.e., difference between tip and root built-in angles, positive when tip angle is greater (L.E. up) than root angle, deg.
23	$\Delta \psi_{\text{print}}$	Azimuth increment used to present printed output of various pertinent aerodynamic, dynamic and elastic load distributions as well as aeroelastic responses and stresses, deg. This input quantity should be an integral multiple of location 9, deg.
24	θ_β	"Direct" value of pitch-flap coupling ($= \Delta \theta / \Delta \beta$). A nonzero value will suppress a calculation of this quantity from the inputted pitch-horn/push-rod geometry.
25	θ_δ	Pitch-lag coupling ($= \Delta \theta / \Delta \delta$).

<u>Location</u>	<u>Item</u>	<u>Description</u>
26	C_{LD}	Viscous lag damper coefficient, ft-lb-sec.
27	c	Blade chord if chord is constant, otherwise omit, ft.
28	NFM	Number of flatwise bending modes to be used (4 max).
29	NEM	Number of edgewise bending modes to be used (3 max).
30	NTM	Number of elastic torsion modes to be used (3 max) (note that the total number of dynamic degrees-of-freedom is limited to 10. Thus, if the articulation degrees-of-freedom, β and/or δ , are used, or if the rigid feathering d.o.f. is invoked, NFM, NEM and NTM will be automatically changed to keep the total degrees-of-freedom to no more than 10.).
31-34	$\bar{\omega}_{wi}$	Flatwise modal frequencies, nondimensional with respect to Ω , in ascending modal order.
37-39	$\bar{\omega}_{vk}$	Edgewise modal frequencies, nondimensional with respect to Ω , in ascending modal order.
40-42	$\bar{\omega}_{\theta j}$	Torsion modal frequencies, nondimensional with respect to Ω , in ascending modal order.
43	A_{2s}	Second harmonic cyclic pitch coefficient of minus $\cos 2\psi$ in Fourier expansion of blade control pitch, deg.
44	B_{2s}	Second harmonic cyclic pitch coefficient of minus $\sin 2\psi$ in Fourier expansion of blade control pitch, deg.

<u>Location</u>	<u>Item</u>	<u>Description</u>
45	g	Acceleration due to gravity, ft/sec ² ; a negative value implies inverted flight.
46	(Control)	Make nonzero (1.) if airfoil data for a <u>nonsymmetric airfoil</u> are to be used.
47	(Control)	Make nonzero (1.) if the total (<u>transient</u>) <u>time-history</u> is to be outputted; i.e., responses calculated before convergence to periodicity is obtained.
48	(Control)	Make nonzero (1.) if the <u>modal responses</u> and <u>hub shears and moments</u> are to be (negative) <u>Fourier analyzed</u> after periodicity has been obtained.
49	(GJ) _{root}	Torsional rigidity at the blade root, lb/ft ² .
50	K _θ _{root}	Torsional spring connecting root of blade to fixed structure to represent control system flexibility, ft-lb/rad. A non-zero value will automatically introduce the rigid-body feathering degree-of-freedom as an addition "torsion mode". Note that this "mode" will inherently couple with the NIM normal elastic torsion modes at frequencies both below and above the inputted torsion frequencies (locations 40-42); hence, a smaller integration interval will generally be required.
51	(Control)	Make nonzero (1.) to simplify the numerical <u>spanwise integration techniques</u> from the nominal trapezoidal rule to rectangular (Eulerian) form. Rectangular integration is effected by setting the quadrature numbers used for spanwise integration equal to the inputted segment lengths (loc. (100-114)). Usage of this option is recommended for blade

<u>Location</u>	<u>Item</u>	<u>Description</u>
		configurations with significant discontinuities in spanwise properties (e.g., counterweights, tip weight, step twists, etc.).
52	(Control)	Make nonzero (1.) to output modal <u>integration constants</u> used in the eigensolution and, to a limited extent, in the time-history solution.
53	(Control)	Make nonzero (1.) to <u>load prepunched (vorticity) induced velocity distributions</u> .
54	(Control)	Make nonzero (1.) to <u>use the induced velocities</u> loaded as per location 53.
55	α_s	Shaft angle of attack, deg. This input item serves a dual role: when variable inflow is used (either vorticity induced or Glauert momentum) α_s is used to define λ_{ram} . Also, when a major iteration is to be performed (nonzero location 60) and when trims on propulsive force are deactivated (zero location 59) the program will trim to this inputted shaft angle.
56	L_{req}	Requested value of lift to be used in major iteration, lb.
57	PF_{req}	Requested value of propulsive force to be used in major iteration, lb.
58	ϵ_{Lift}	Tolerance on lift for major iteration, lb. A zero value deactivates trimming on lift.
59	ϵ_{PF}	Tolerance on propulsive force for major iteration, lb. A zero value deactivates trimming on propulsive force. The automatic trim calculation (major iteration)

<u>Location</u>	<u>Item</u>	<u>Description</u>
		must trim either to a required propulsive force or to a required shaft angle of attack; therefore a deactivation of trim to propulsive force automatically directs the trim calculation to trim to requested shaft angle, location 55.
60	N_{MI}	Maximum number of major iterations to be made in an attempt to achieve trim. A zero value will deactivate the major iteration; a negative value will activate a stall avoidance calculation if, when attempting to trim, the rotor becomes stalled. (See section on general information for efficient program usage.)
61	β_B	Built-in precone angle, deg. An identically zero value denotes a rotor blade articulated in flapping; similarly, a finite nonzero value signifies a blade nonarticulated in flapping.
62	PM_{req}	Requested value of pitching moment for major iteration, lb-ft (positive nose up).
63	ϵ_{PM}	Tolerance on pitching moment for major iteration, lb-ft. A zero value deactivates trimming on pitching moment.
64	RM_{req}	Requested value of rolling moment for major iteration, lb-ft (positive port side up).
65	ϵ_{RM}	Tolerance on rolling moment for major iteration lb-ft. A zero value deactivates trimming on rolling moment.
67	β	Initial condition on articulated flapping angle, rad.
68	β^*	Initial condition on (nondimensional) articulated flap angle rate.

<u>Location</u>	<u>Item</u>	<u>Description</u>
69	δ	Initial condition on articulated lead-lag angle, rad. (positive forward).
70	δ^*	Initial condition on (nondimensional) articulated lead-lag rate.
72	δ_B	Built-in prelead angle, deg. An identically zero value denotes a rotor blade articulated in lead-lag; similarly a finite nonzero value signifies a blade nonarticulated in lead-lag.
73	(Control)	Make nonzero (1.) to harmonically analyze and output <u>harmonics of flatwise stresses</u> .
74	(Control)	Make nonzero (1.) to harmonically analyze and output <u>harmonics of edgewise stresses</u> .
75	(Control)	Make nonzero (1.) to harmonically analyze and output <u>harmonics of torsional stresses</u> .
76	(Control)	Make nonzero (1.) to bypass the <u>eigen-solution</u> .
77	ψ	Initial condition on rotor azimuth, deg. This value, like all inputted initial conditions, is likewise used to define the loadings on the blade about which linear perturbations are to be taken in the eigensolution.
78	(FCR)	Factor in momentum inflow equations to account for dual (coaxial) rotor operation:

$$\lambda = \lambda_{\text{ram}} - \frac{C_T}{(\text{FCR})B^2\sqrt{\mu^2 + \lambda^2}}$$

Note that C_T in the above equation is

<u>Location</u>	<u>Item</u>	<u>Description</u>
		the usual thrust coefficient as defined for a single rotor. An identically zero value of (FCR) defaults to a value of 2.; a value between 1. and 2. will denote a coaxial rotor operating somewhere between hover and high speed forward flight.
79	(Control)	Generalized <u>Glauert</u> (momentum derived) <u>variable inflow</u> option. A zero value deactivates usage. A value of 1. causes the inputted induced velocity components to be used, as inputted; a value of 2. causes the inputted values to be used initially, and then varied in trim calculations in place of control angles; a value of 3. causes the control and shaft angles to be fixed and the induced velocity components to be varied only to satisfy momentum equations in any requested major iteration. If the value is 1., the induced velocity components will be varied to satisfy momentum considerations in addition to the usual trim calculation.
80-82	$\bar{v}_0, \bar{v}_{1c}, \bar{v}_{1s}$	Initial conditions on the "momentum" induced velocity components comprising a <u>Glauert-like variable inflow</u> description. Note that the "vorticity" variable inflow (controlled by locations 53 and 54) and the momentum variable inflow can be used separately or simultaneously.
83	SR	Sample rate for Transient Spectral Stability Analysis (TSSA). (See Appendix III for a discussion of this technique.) Every (SR)'th point in a transient time-history is saved for use in a TSSA. A zero value bypasses the TSSA.

<u>Location</u>	<u>Item</u>	<u>Description</u>
84-86	(Control)	Channel selection for each of three available for the TSSA. The channels available are: 1-4, flatwise bending modal responses; 5-7, edgewise bending modal responses; 8-10 torsion modal responses; 11, articulated rotor flapping; 12, articulated rotor lagging; 13, 14, and 15, blade tip vertical, in-plane and torsion deflections, respectively.
87	ω_L	Lower bound of frequency band chosen for TSSA nondimensional with respect to Ω .
88	ω_U	Upper bound of frequency band chosen for TSSA nondimensional with respect to Ω .
89	(Control)	Initial estimate of <u>percentage of total transient data</u> used in each time displaced data sample block in TSSA.
90	(Control)	Number of <u>transient (time displaced) Fourier coefficient calculations</u> made to establish modal damping in TSSA; maximum value is 200.
91	N_{FREQ}	Number of desired resonant frequencies to be extracted from frequency band defined by locations 87 and 88.
92	(Control)	Resonant frequency identification criterion. Make (0., 1.) to identify resonant frequencies using criterion of (maximum Fourier Transform amplitudes, maximum F.T. amplitudes + deletion of "image" frequencies). Note that image frequencies result from the Floquet-like response characteristics of rotors in forward flight.
94	ζ_{vse}	Critical (viscous) damping ratio used to approximate structural damping in edgewise bending modes.

<u>Location</u>	<u>Item</u>	<u>Description</u>
97	$\theta_{1\text{equ}}$	Linear equivalent blade (nonlinear) twist angle defined similar to location 22, deg. A nonzero value for $\theta_{1\text{equ}}$ is required to use the inputted nonlinear twist arrays and is used to calculate that portion of the aerodynamic inflow velocity at the 3/4 chord position, U_p , accruing from radial flow and twist.
98	(Control)	Make nonzero (1.) for <u>stress calculations</u> using the mode deflection method. Zero value defaults to force integration method.
99	(Control)	Location used to <u>end a case</u> or series of cases. Make (+1.) to end the Loader Format data block for the case defined by the Loader data and load additional cases at the conclusion of that case. Make (-1.) to end the Loader data and read no further cases. In both instances the word count, LL, (see beginning of this section above) should be (-1). <u>Note: this entry must appear singly on an input card, and that card must be the last card for the case.</u>
100-114	Δx	Nondimensional blade segment lengths, in order from root to tip, maximum of 15 values, starting from the offset location. Accuracy is generally improved if the last segment is small (≤ 0.03).
115-129	M_1	Mass of each blade segment, lb-sec ² /ft.
130-144	θ_{Ba}	Aerodynamic built-in nonlinear twist angle distribution, deg. Since collective angle is defined at the 75% span location, θ_{Ba} should have a zero value at 75% span. Should the structural twist angle distribution differ from θ_{Ba} , their appropriate data must be

<u>Location</u>	<u>Item</u>	<u>Description</u>
		loaded into locations 690-704; otherwise, θ_{B_a} will be used for both aerodynamic and structural applications. Nonlinear twist distributions will be used only if a nonzero value is inputted into location 97, θ_{1_equ} .
145-159	c	Blade chord at center of each blade segment (use for nonconstant chord blades only), root to tip, ft.
160-174	K_F	Constants relating (nondimensional) flatwise second derivative to flatwise stress ($= Ec/R$) _F , evaluated at center of each segment, root to tip, psi.
175-189	K_E	Constants relating (nondimensional) second derivative to edgewise stress ($= Ec/R$) _E , root to tip, psi.
190-204	τ/M	Constants relating torsional moment to torsional stress, root to tip, in ⁻³ .
205-219	K_{z10}	Chordwise mass radii of gyration of blade segments about elastic (reference) axis, root to tip, nondimensional with respect to R.
220-234	K_{y10}	Thicknesswise mass radii of gyration of blade segments about axis perpendicular to chord line and through the reference axis, root to tip, nondimensional with respect to R.
235-249	\bar{k}_A	Area radii of gyration about elastic axis, root to tip, nondimensional with respect to R.
250-264	$\bar{y}_{10c}/4$	Distances from elastic axis forward to airfoil quarter chord position, root to tip, nondimensional with respect to R.

<u>Location</u>	<u>Item</u>	<u>Description</u>
265-279	\bar{y}_{10CG}	Distance from elastic axis forward to airfoil section mass centers, root to tip, nondimensional with respect to R.
280-283	q_{wi}	Initial conditions on i'th flatwise bending mode deflections.
286-289	* q_{wi}	Initial conditions on i'th flatwise bending mode (nondimensional) rates.
292-294	q_{vk}	Initial conditions on k'th edgewise bending mode deflections.
295-297	* q_{vk}	Initial conditions on k'th edgewise bending mode (nondimensional) rates.
298-300	$q_{\theta j}$	Initial conditions on j'th torsion mode deflections.
301-303	* $q_{\theta j}$	Initial conditions on j'th torsion mode (nondimensional) rates.
600-614	$(I/c)_F$	Section moduli for flatwise bending, root to tip, in ³ . Note that the products of $(I/c)_F$ and K_F (locations 160-174) must equal the bending stiffness distribution, EI/R.
615-629	$(I/c)_E$	Section moduli for edgewise bending, root to tip, in ³ . See remarks above for flatwise bending section moduli.
630-639	(Control)	Stress selection number for each of (at maximum) 10 channels whose time-history data strings are saved and used for automatic plotting. Value is determined by formula: $J \times 100 + N$, where $J = (0,1,2,3)$ as stress is (flatwise, edgewise, torsion, flexbeam torsion) and $N =$ segment number. (Input locations provided, but option inoperative.)

<u>Location</u>	<u>Item</u>	<u>Description</u>
640-649	STRSCALE	Vertical axis scaling for the automatic plotting of each stress channel selected in locations 630-639, psi x 10 ³ /in. (Input locations provided, but option inoperative.)
660-674	EB ₁	Torsional stiffness (to be multiplied by twist rate squared), as defined in reference 4, lb-ft ⁴ .
675-689	EB ₂	Torsion to edgewise elastic coupling stiffness (to be multiplied by twist rate), as defined in reference 4, lb-ft ³ .
690-704	θ_{BS}	Structural built-in nonlinear twist angle distribution, root to tip if different from aerodynamic twist, deg. See remarks above for aerodynamic built-in twist, location 130-144.
705-719	$\Delta\theta_B$	Built-in (structural) twist angle change per segment length distribution, root to tip, deg. Note that this item is a direct statement of the built-in twist rate distribution, θ'_B ; if all values of this distribution are inputted as zero, the twist rate distribution is computed internally using numerical methods from the inputted twist angle distributions, locations 130-144 or 690-704, as appropriate.
720-734	\bar{e}_A	Distances from reference (elastic) axis forward to edgewise bending neutral axis, root to tip, nondimensional with respect to R.
735-744	D _{FB}	Flexbeam plate bending stiffness distribution, lb-ft. Note that all items in locations 735 through 824 are required only for a redundant analysis of the torque-tube (flexbeam span of bearingless rotor (CBR) configurations) (see location 991).

<u>Location</u>	<u>Item</u>	<u>Description</u>
745-754	GJ_{FB}	Flexbeam torsion (St. Venant) stiffness distribution, lb-ft ² .
755-764	C_{FB}	Flexbeam section width (chord) distribution, ft.
765-774	$(EI_y)_{TT}$	Torque tube flatwise bending stiffness distribution, lb-ft ² .
775-784	$(EI_z)_{TT}$	Torque tube edgewise bending stiffness distribution, lb. ft ² .
785-794	M_{TT_i}	Mass of each torque tube segment whose span is defined by location 100-109, lb-sec ² /ft.
795-804	$(\bar{y}_{10CG})_{TT}$	Distances from reference axis forward to torque tube mass centers whose masses are given in locations 785-794, nondimensional with respect to R. (Input locations provided, but quantity is not used.)
805-814	$(I/c)_{F_{TT}}$	Section moduli for torque tube flatwise bending, in ³ . (Input locations provided, but quantity not used.)
815-824	$(I/c)_{E_{TT}}$	Section moduli for torque tube edgewise bending, in ³ . (Input locations provided but quantity not used.)
957	h	Height of positively thrusting rotor from ground or wind tunnel floor for purposes of evaluating Heyson corrections to rotor angle of attack (see Ref. 11), ft.
958	H_{WT}	Height of wind tunnel test section for purposes of evaluating Heyson corrections, ft. Note that zero values for the wind tunnel test section dimensions implies that ground effect corrections, rather than wind tunnel wall corrections, are to be made.

<u>Location</u>	<u>Item</u>	<u>Description</u>
959	W_{WT}	Width of wind tunnel test section for purposes of evaluating Heyson corrections, ft.
975	CASE	Case number.
976	θ_{BPR}	Built-in elevation angle of push-rod attachment point, measurable when $\theta_{.75} = 0$, deg.
977	NDEL3I	Segment number of inboard attachment point of pitch input structural members (Pitch horn, feathering cuff or torque tube) to blade spar.
978	NDEL3O	Segment number of outboard attachment point of pitch input structural member to blade spar. Note that if this structural element is attached to the blade spar at a single point (cantilevered configuration) NDEL3I and NDEL3O must both be inputted with the same appropriate value. For bearingless rotor (CBR) applications NDEL3O serves the additional function of defining the outer limit of the flexbeam; this limit is taken as the inner boundary of the NDEL3O'th segment.
979	r_{PR}	Radial location (blade station) of push-rod to pitch input structural member attachment point, in.
980	y_{10PR}	Location forward of feathering axis of push-rod to pitch input structural member attachment point, in. Note that input items 977-980 together with the inputted modal data provide the geometric data from which pitch-flap, pitch-flat and pitch-edge coupling are calculated. These calculations are bypassed if either of locations 978 or 980 are inputted identically zero.

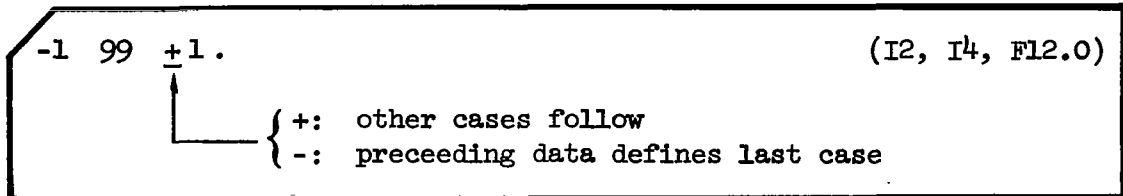
<u>Location</u>	<u>Item</u>	<u>Description</u>
981	$N_{O_{FB}}$	Segment number of innermost end of the feathering flexure; defaults to 1.
982	$\theta_{B_{FB}}$	Built-in twist angle of the flexbeam, positive leading edge up at outboard end of flexbeam, deg. Note that $\theta_{B_{FB}}$ is defined relative to the inputted twist angle distribution, which in turn is defined for zero collective angle.
983	\overline{GJ}_{FB}	Average torsional stiffness of the flexbeam lb-ft ² .
984	$k_{T_{FB}}$	Equivalent or critical torsion stress coefficient for flexbeam; i.e., stress per unit average torsion strain as defined by total flexbeam twist, in-psi.
985	(Control)	Make nonzero (1.) to include the " <u>wobble</u> " mode for cantilever torque tube configured bearingless rotors.
986	(Control)	When finite snubber stiffnesses are inputted (locations 987 and 988) the stiffnesses are assumed to be aligned (vertically and horizontally, torque tube flatwise and edgewise) as location 986 is (0., 1.)
987	$K_{S_{z5}} (K_{S_F})$	Snubber vertical (torque tube flatwise) spring rate, lb/ft.
988	$K_{S_{y5}} (K_{S_E})$	Snubber horizontal (torque tube edgewise) spring rate, lb/ft.
989	(Control)	When the torque tube flexbeam redundant analysis is invoked (location 991) the <u>torque tube</u> is assumed to be in (<u>tension, compression</u>) as location (989) is (0., 1.).

<u>Location</u>	<u>Item</u>	<u>Description</u>
990	N_{OTT}	Segment number of innermost end of torque tube; defaults to 1.
991	(Control)	Make nonzero (1.) to <u>activate the redundant analysis</u> option. When the redundant analysis is activated, the flexbeam and torque tube stiffness and mass inputs, locations (735) through (794), must be appropriately nonzero.
992	(Control)	Used to weigh the effectiveness of non-linear <u>ΔEI bending excitation of torsion</u> over the flexbeam span; the effectiveness is taken to be (100%, 0%, 100% (x) pseudo-torsion mode shape as location (992) is (0., 1., 2.)).
993	Λ_{FB}	Flexbeam aspect ratio parameter ($= \frac{S}{C} \sqrt{1.5(1-\nu)}$) to determine plate-like deflection for torsion "pseudo-mode". A zero value gives a rod-like deflection shape.
994	K_{WOB}	Spring rate of rotational spring connecting outboard end of torque tube to the blade spar about chordwise axis, ft-lb/rad. A zero value implies zero stiffness for pinned-pinned torque tube configurations and infinite stiffness for snubbed configurations.
995	K_{VOB}	Spring rate of rotational spring connecting the outboard end of the torque tube to the blade spar about an axis perpendicular to the chord line, ft-lb/rad (see above).
996	(Control)	<u>Analytic (static) airfoil option.</u> Make nonzero (1.) to use the built-in analytic approximation to the static NACA 0012 airfoil data.

<u>Location</u>	<u>Item</u>	<u>Description</u>
997	(Control)	<u>Unsteady airfoil data option.</u> Make nonzero ($\geq 1.$) to use the synthesized unsteady airfoil data technique described in reference 10. This can be used with either the explicitly inputted airfoil data or the built-in analytic NACA 0012 static airfoil data. For nonzero values greater than unity, the "cutoff Mach number" (Mach number above which the unsteady data is disregarded in favor of quasi-static data) is taken to be the inputted value minus one (1.) rather than the built-in default value of 0.6. However, only nonstandard cutoff Mach numbers between 0.1 and 0.95 are accepted.
998	$\Delta \psi_{F389}$	Azimuth increment used to generate punched card output to be used as input data to UTRC program F389 for computing variable inflow. This option is bypassed with a (0.) input value. A description of the format of these output punched cards is contained in reference 12.
999	K_{plot}	Scale for automatic plots of various time-history data strings, see locations 84-86 and 630-639. (Input location provided, but option is inoperative.) This option is currently inoperative but would be bypassed with a (0.) input value, when operational.
1000	(Control)	Make nonzero (1.) to activate usage of the <u>tabulated time-histories</u> of incremental control angles.
1001	$N_{\Delta \theta .75}$	Number of abscissa-ordinate point pairs used to define time-history of $\Delta \theta_{.75}(t)$; calculation of this time-history is bypassed with a (0.) value.

<u>Location</u>	<u>Item</u>	<u>Description</u>
1002-1050	$\Delta\theta_{.75}$	Table of $\Delta\theta_{.75}$ abscissa-ordinate pairs; $U(\Delta\theta_{.75}) = \text{deg.}; U(t) = \text{sec.}$
1051	$N_{\Delta A_{1s}}$	Number of abscissa-ordinate point pairs used to define time-history of $\Delta A_{1s}(t)$; zero value bypasses calculation.
1052-1100	ΔA_{1s}	Table of ΔA_{1s} abscissa-ordinate point pairs; $U(A_{1s}) = \text{deg.}; U(t) = \text{sec.}$
1101	$N_{\Delta B_{1s}}$	Number of abscissa-ordinate point pairs used to define time-history of $\Delta B_{1s}(t)$; zero value bypasses calculation.
1102-1150	ΔB_{1s}	Table of ΔB_{1s} abscissa-ordinate point pairs; $U(B_{1s}) = \text{deg.}; U(t) = \text{sec.}$

Last Card for Block II (Loader) Data:

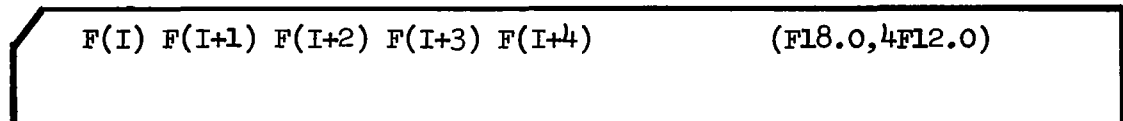


III. Blade Mode Shape Data

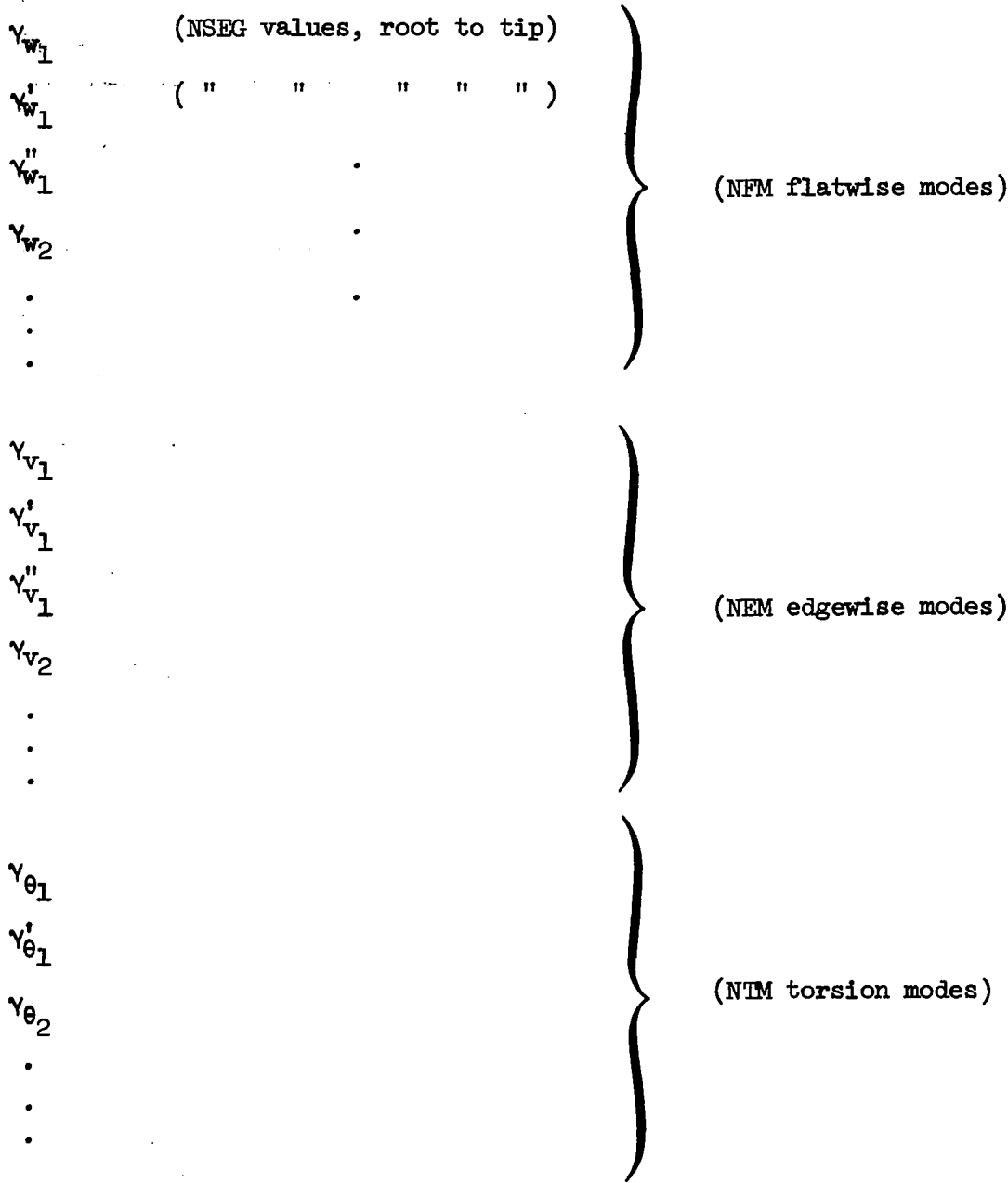
Included in this data are the radial distributions of the blade (uncoupled) flatwise, edgewise and torsion normal mode shapes and their derivatives. These quantities must generally be provided from an external source such as United Technologies Corporation program E159 or an equivalent, in the following punched card format:



subsequent cards:



where: NFM, NEM, and NTM are, respectively, the numbers of flatwise bending, edgewise bending and torsion normal modes whose mode shapes and derivatives are to be inputted. NSEG is the number of blade spanwise stations for which the inputted modal data are defined. $F(i)$ are each of the below listed modal functions (defined at the i 'th spanwise stations) and I must be either 1, 6 or 11 reflecting the requirement of five entries per card until NSEG entries are made for each F function inputted. The modal functions must be loaded in the following order:



IV. Variable Harmonic Inflow

If location 53 of the Loader block of operational data is nonzero, the following block of variable harmonic inflow is loaded in:

card #1:

NHARML	(I3)
--------	------

card #2:

XLAMO(I)	(F14.0)
----------	---------

card #3:

XLAMC(I,1) XLAMC(I,2) ...	(5F14.0)
---------------------------	----------

card #3 + (NHARML/5):

XLAMS(I,1) XLAMS(I,2) ...	(5F14.6)
---------------------------	----------

Subsequent cards repeat the pattern wherein I, the spanwise station index, varies from 1 to NSEG. NHARML is the number of harmonics of inflow to be loaded, and XLAMO(i), XLAMC(i,n) and XLAMS(i,n) are, respectively, the zeroth, n'th cosine and n'th sine components of harmonic inflow at the i'th radial station, wherein a positive Fourier series is assumed. The inflow is defined positive up and has the units of ft/sec.

V. Multiple Case Runs

The above described data set-up defines the correct ordering of required data blocks for a general case. When multiple cases are run the second and subsequent cases utilize most of the data inputted for the first case. The following rules apply to the running of multiple cases:

1. Airfoil data is loaded only for the first case; all subsequent cases within the run use the same tabular data, if analytic data is not used.

2. Only those items within the operational (Loader) data which are to be changed from case to case need be inputted.
3. Item 99 of the operational data controls the running of subsequent cases; a (+1.) value causes a subsequent case to be loaded whereas a (-1.) value terminates the computer run after the current case.
4. Unless otherwise specified (by a +1. value for operational data item 19) the inputted modal array data block is used for all cases within the run and, hence, no subsequent input of this data need be made.
5. Similarly, unless otherwise specified (by a +1. value for operational data item 53) the inputted harmonic variable inflow data block is used for all cases within the run and, hence, no subsequent input of this data need be made.
6. Operational data items 19 and 53 discussed above are both automatically set to zero at the conclusion of the data input for every case.
7. Terminal conditions on the blade azimuth angle, item 77, and on the degrees-of-freedom, items 67-70, and 280-303, for any case are carried over as initial conditions on these quantities for the subsequent case. Thus, for some applications, e.g., investigations of unstable responses, it would be appropriate to reinitialize these items on the subsequent cases.

General Information to Facilitate Operation of Program
And Improve Efficiency

Aside from considerations of the actual aeroelastic parameters describing the blade configuration, which are covered in the above sections, additional attention should be paid to the mechanics of obtaining efficient numerical solutions of the dynamic equations. In this regard, there arise two basic areas of concern wherein this section should be of assistance. The first of these areas is the proper selection of parameters for efficient temporal numerical integration of the dynamic equations (flapping or minor iterations) and the second is the proper selection of parameters for effecting a satisfactory rotor trim (major iteration). The following subsections provide information for making proper parameter selection in each of these areas.

Temporal Numerical Integration - As is discussed in Appendix I temporal integration of the higher differentiated response variables to obtain the lower ones is achieved in the G400 program using a variant of the Adams integration algorithm (see equations I.1 and I.2). The selected algorithm is

defined by means of the azimuthal integration step size, $\Delta\psi$, and the integration frequency, $\bar{\omega}$.

The integration step size should be an integral divisor of 360; a proper choice depends on the maximum coupled frequency inherent in the various aeroelastic responses. A reasonable upper limit for $\Delta\psi$ is 45 divided by the maximum such frequency in per rev. Values of $\Delta\psi$ greater than this upper limit will compromise the integration accuracy and, for sufficiently large values, will cause the computed responses to develop "numerical" instabilities. As a corollary, a check on any response which is predicted to be unstable by the analysis, is to rerun the case with a reduced integration step size to test for the possibility of the unstable response being merely a numerical instability.

For each response degree-of-freedom a different integration frequency, $\bar{\omega}$, is used in the integration algorithm; this frequency is, for each of the elastic modes, the respective inputted natural frequencies (locations 31-34, 37-39, and 40-42). The usual pendular frequencies of a rotating, hinged, rigid beam are taken as the integration frequencies of the flapping and lead-lag degrees-of-freedom. In addition to defining modal stiffnesses and integration frequencies, the inputted frequencies serve yet another purpose. As noted above, the proper value of integration step size, $\Delta\psi$, varies inversely with the maximum modal frequency. Thus, run times (caused by reduced step size) will significantly increase as any one modal frequency increases. Since any degree-of-freedom exhibiting a large natural frequency tends to respond quasi-statically, i.e., as if the acceleration (q) term were negligible, a reasonable approximation to the response calculation is to avoid the numerical integration of the q term entirely and treat the response quasi-statically. This option can be invoked for any such high-frequency mode by inputting the appropriate frequency negatively; a negative sign will not affect the proper usage of the frequency in the calculation of the dynamic equations. Note that this optional response calculation can be invoked singly or in combination for any of the elastic modal responses, (negative values in any of locations 31-34 and 37-42).

Hub Force and Moment Trim - Operation of the trim or major iteration feature of the program is controlled by input locations 55 thru 60, 62 thru 65 and, for some applications, 79. The main control for the major iteration is location 60, the number of major iterations, N_{MI} . A zero value causes the major iteration feature to be completely deactivated. On the basis of past usage, a reasonable range for this input appears to be from 5 to 10, depending on the tightness of the convergence tolerances selected and the "goodness" of the initial guesses on the control parameters. Convergence of the major iteration is adversely affected by any lack of convergence of the responses

to periodicity within each trim iteration and by incursion of the rotor into a significantly stalled flight regime. Note that a negative value of N_{MI} will activate a stall avoidance calculation wherein the controls will be perturbed to reachieve unstalled flight rather than to achieve the prescribed trim condition. Should a major iteration fail to converge within any one run the last used control angles and initial conditions on response variables are generally available in output punched card form and/or partially in the output printed records of each major iteration (see Appendix III) for use in subsequent major iterations.

The trim iteration is operationally flexible as to what hub loads it will drive to requested values. Generally, the various requested hub loads, lift, propulsive force, pitching and rolling moment are activated in turn by specifying nonzero values for each of their respective tolerances. More specifically, the following table describes the optional combinations of hub loads and rotor shaft angle available with the G400 trim capability:

TABLE II

SUMMARY OF OPTIONAL BASIC TRIM COMBINATIONS

Option	Lift	Prop. Force	Pitch. Momt.	Roll Momt.	$\theta_{.75R}$	A_{1s}	B_{1s}	α_s
1	S	U	U	U	V	F	F	S,(V)
2	S	S	U	U	V	F	F	V
3	U	U	S	S	F	V	V	S,(V)
4	S	U	S	S	V	V	V	S,(V)
5	S	S	S	S	V	V	V	V
6	U	U	S	U	F	V	F	S,(V)
7	S	U	S	U	V	V	F	S,(V)
8	S	S	S	U	V	V	F	V

where: F: Control parameter kept fixed
V: Control parameter varied
S: Trim parameter specified and trimmed to
U: Trim parameter unspecified and ignored

Note that for each option available, the individual trim parameter is activated by inputting a positive, nonzero value for the respective parameter tolerance. For each option the trim calculation trims either to the specified propulsive force or the inputted shaft angle, α_s (location 55) as the propulsive force tolerance, ϵ_{PF} , is finite or zero, respectively. A reasonable choice of tolerance values for the hub force and moment loads can be obtained from considerations of the helicopters inertia properties and acceptable deviations of the load factor from unity, and of the pitching and rolling accelerations from zero.

The trim calculation can be also used in conjunction with the Glauert variable inflow. Location 79 controls the usage of this simplified form of variable inflow. A variety of trim calculation operations are achieved when this control location is nonzero. If this control option is 1., the Glauert variable inflow induced velocity components \bar{v}_0 , \bar{v}_{1c} , and \bar{v}_{1s} (locations 80-82) would be varied in addition to those parameters shown in Table II to effect momentum balances in thrust, pitching moment, and rolling moment as well as the specified trim. If the control option is 2., only the velocity components would be varied (instead of the control angles, $\theta_{.75R}$, A_{1s} , and B_{1s}), but in an analogous manner. If the control option is 3., the trim calculation would again only vary the velocity components, but to achieve momentum balance only, with no specified trim.

APPENDIX III

PROGRAM G400 OUTPUT DESCRIPTION

The complete printed output generated by the G400 program can be classified into the following five major categories:

- I. Listing of Input Data
- II. Parameters Calculated from the Input Data
- III. Results of Solution Part I - Eigensolutions
- IV. Results of Solution Part II - Time-History Solution
- V. Results of Solution Part III - Transient Spectral Stability Analysis

This appendix will describe the pertinent output pages associated with each of these categories. It should be noted that while output will always be generated for the first two categories, output for the remaining categories depends upon the optional utilization of solution parts I, II, and/or III. The subsections which follow describe, in turn, the details of each of these five categories.

Listing of Input Data

Output in this category includes a listing of the static airfoil data (if any is inputted), a descriptive listing of the "inertia, elastic, geometric and other operational" (Loader Format) data, and a listing of the harmonic variable inflow: blocks I, II, and IV, respectively, of the input data described in Appendix II. If static airfoil data is inputted, then a listing of this data will be outputted for c_l , c_d and $c_{m_c}/4$, each with the format shown in Sample Page 1. where each column represents data at one Mach number. Within each column the first line gives the number of angle-of-attack/aerodynamic coefficient pairs defining the functionality; the second line is the Mach number, and the ensuing line pairs are the angle-of-attack/aerodynamic coefficient pairs, where the angles-of-attack are in degrees. This output closely follows the input format described in Appendix II.

A description of the Loader Format data output is omitted herein since this output merely duplicates the description already given in even greater detail in Appendix II. In Sample Page 2 is shown the listings of the inputted harmonic variable inflow, both by harmonic components and by azimuthal variation for each of the (maximum of) fifteen blade segments. As with the input format, the inflow is defined positive up, has the units of ft/sec and a conventional positive Fourier series representation is used.

INPUTTED VARIABLE INFLOW DISTRIBUTIONS (OUTPUT FROM PROGRAM F380 OR EQUIVALENT), FPS

HARMONIC COEFFICIENTS: $LAMBDA(X(J),PSI) = R_{AMPLAN} + (VLAMB(J) + \sum(VLAMA(I,N)) \cdot \cos(n \cdot \psi) + VLAMB(J,N) \cdot \sin(n \cdot \psi)) / \Omega_{EGA-P}$

SEG. # J =	1	2	3	4	5	6	7	8	9	10	11	12	13	14	15
VLAMB 0	XX.XX	XX.XX	AA.XX	XX.XX	AX.YX	YX.XX	XX.XX								
VLAMA 1	XX.XX	XX.XX	AA.XX	XX.XX	AX.YX	YX.XX	XX.XX								
VLAMB 1	XX.XX	XX.XX	AA.XX	XX.XX	AX.YX	YX.XX	XX.XX								
VLAMA 2	XX.XX	XX.XX	AA.XX	XX.XX	AX.YX	YX.XX	XX.XX								
VLAMB 2	XX.XX	XX.XX	AA.XX	XX.XX	AX.YX	YX.XX	XX.XX								
.	XX.XX	XX.XX	AA.XX	XX.XX	AX.YX	YX.XX	XX.XX								
.	XX.XX	XX.XX	AA.XX	XX.XX	AX.YX	YX.XX	XX.XX								
VLAMA N	XX.XX	XX.XX	AA.XX	XX.XX	AX.YX	YX.XX	XX.XX								
VLAMB N	XX.XX	XX.XX	AA.XX	XX.XX	AX.YX	YX.XX	XX.XX								

AZIMUTHAL VARIATION

SEG. # J =	1	2	3	4	5	6	7	8	9	10	11	12	13	14	15
PSI															
0.	XX.XX	XX.XX	AA.XX	XX.XX	AX.YX	YX.XX	XX.XX								
XX.	XX.XX	XX.XX	AA.XX	XX.XX	AX.YX	YX.XX	XX.XX								
XX.	XX.XX	XX.XX	AA.XX	XX.XX	AX.YX	YX.XX	XX.XX								
.	XX.XX	XX.XX	AA.XX	XX.XX	AX.YX	YX.XX	XX.XX								
.	XX.XX	XX.XX	AA.XX	XX.XX	AX.YX	YX.XX	XX.XX								
.	XX.XX	XX.XX	AA.XX	XX.XX	AX.YX	YX.XX	XX.XX								
XXX.	XX.XX	XX.XX	AA.XX	XX.XX	AX.YX	YX.XX	XX.XX								

Parameters Calculated from the Input Data

Sample Pages 3 and 4 list a variety of intermediate parameter calculations which, for the most part are directly applicable only to the composite bearingless rotor. Sample Page 3 presents the matrices and vectors used to define, respectively, the elastic bending characteristics of the torque tube and the inboard (snubber) end vertical deflection of the torque tube. For each, a quadratic variation with pitch angle is assumed so that the total bending stiffness matrix, FDEFL, and inboard deflection vector, Z5I, are formed in the indicated manner wherein the total blade pitch angle at the 75 percent span, TIHO , is taken in radians. Furthermore, all the results outputted for these two quantities are nondimensional (see the superscripts section of the List of Symbols for the proper nondimensionalization). The matrix FDEFL duplicates matrix S, whose rows and columns are defined by equation (108) in the text; vector Z5I shares the same columnar dependence with matrix FDEFL. Finally, at the bottom of Sample Page 3 are evaluations of FDEFL and Z5I, using the quadratic representations, at a pitch angle equal to the inputted collective angle, $\theta_{.75R}$. It should be noted that the functionalizations of these quantities to quadratic form is accomplished by matching exactly the quantities calculated with pitch angles equal to the collective angles.

The first group of output parameters given in Sample Page 4 consists of the (nondimensional) coefficients defining the nonlinear torsional stiffness characteristics of the flexbeam; they correspond directly to the coefficients given in equation (130a). Again the standard nondimensionalization is used. The second group of output parameters on the sample page consists of the quadratic functionality coefficients for the pitch-flat and pitch-edge couplings and the angular motions of the torque tube relative to the flexbeam at the juncture for each of the selected flatwise and edgewise modes. The quadratic functionality on pitch angle duplicates that used for FDEFL and Z5I described in the above paragraph. Note that RELMW and RELMV are calculated only on the basis of an infinitely rigid torque tube and, hence, are omitted when the redundant analysis option is invoked. The third group of output parameters consists of the specialized elastic description of the inboard end of a cantilevered torque tube (see Figure 6 and equation (83)). The outputted spanwise distributions are the static flatwise deflection shape (pseudo-flatwise mode) and its two (nondimensional) spanwise derivatives. The fourth group of output parameters are the effective torsional springs K_{θ_1} , K_{θ_2} , and K_{θ_3} , defined by equations (63b), (88), and (85), respectively, and the flexbeam stiffness, GJ and TK_A^2 , respectively. The units of the springs are lb-ft/rad and those of the stiffnesses are lb-ft².

FLEX-BEAM TORSIONAL STIFFNESS CHARACTERISTICS

$$\text{THETA-JCT} = (\text{THTMX}) * \text{MX5} + (\text{THTSX}) * \text{SX5} * (\text{Y5} * \text{Z5}^2 - \text{Z5} * \text{Y5}^2) + (\text{THTMC}) * (\text{MY5} * \text{Y5} + \text{MZ5} * \text{Z5}) + (\text{THTM1}) * (\text{MY5} * \text{Y5} + \text{MZ5} * \text{Y5}^2) + (\text{THTSD}) * (\text{SZ5} * \text{Y5} - \text{SY5} * \text{Z5}) + (\text{THTS1}) * (\text{SZ5} * \text{Y5}^2 - \text{SY5} * \text{Z5}^2)$$

THTMX	THTSX	THTMC	THTM1	THTSD	THTS1
XXX.XXXXXX	XX.XXXXXX	XXX.XXXXXX	XXY.XXXXXX	XXX.XXXXXX	XXX.XXXXXX

COEFFICIENTS FOR QUADRATIC VARIATIONS OF PITCH-FLAT AND PITCH-EDGE COUPLINGS WITH PITCH ANGLE

I	AWC(I)	AW1(I)	AW2(I)	RELMW(I)
1	.XXXXX	.XXXXX	.XXXXX	.XXXXX
2	.XXXXX	.XXXXX	.XXXXX	.XXXXX
3	.XXXXX	.XXXXX	.XXXXX	.XXXXX

K	AVC(K)	AV1(K)	AV2(K)	RELMV(K)
1	.XXXXX	.XXXXX	.XXXXX	.XXXXX
2	.XXXXX	.XXXXX	.XXXXX	.XXXXX

PSEUDO-FLATWISE MODE SHAPE (DEFLECTIONS DUE TO UNIT LOAD AT INBOARD END OF CANTILEVERED TORQUE TUBE)

ZZ = X.XXXXXE-YY IN/LB BLADE TIP DEFLECTION = X.XXXXXE-YY IN/LB

N	X	GW	GWP	GWPP
1	X.XXXXX	X.XXXXX	X.XXXXX	X.XXXXX
2	Y.XXXXX	X.XXXXX	X.XXXXX	X.XXXXX
3	X.XXXXX	X.XXXXX	X.XXXXX	X.XXXXX
.	Y.XXXXX	X.XXXXX	X.XXXXX	X.XXXXX
.	X.XXXXX	X.XXXXX	X.XXXXX	X.XXXXX
.	X.XXXXX	X.XXXXX	X.XXXXX	X.XXXXX
N	X.XXXXX	X.XXXXX	X.XXXXX	X.XXXXX

TORSIONAL RETENTION SPRINGS AND EFFECTIVE FLEX-JFAM TORSIONAL STIFFNESSES

KTHETA1	KTHETA2	KTHETA3	GJ-EFF	TKA2
XXX.XXXXX	XXX.XXXXX	XXX.XXXXX	.XXX.XXXXX	XXX.XXXXX

In Sample Page 5 are shown typical modal information for the inputted flatwise and edgewise bending modes. For each such mode the (nondimensional) modal frequency, pitch-flat (or pitch-edge) coupling and inputted mode shape and spanwise derivatives are listed. In addition the listing presents the derived incremental deflection vectors which account for blade twist (see equations (7) through (10)). Within a flatwise modal information group, the DVB and DVE arrays correspond to those first order Δv spanwise functions due to built-in twist and torsional modal twist, respectively. The DWWBB, DWWBC and DWWCC arrays correspond to those second order ΔW functions due to the combinations of built-in twist with itself, built-in twist with pseudo-torsion mode (control) twist, and pseudo-torsion mode twist with itself, respectively. The various arrays, DV2BP, DV2EP, DWW2BBP, DWW2BCP, and DWW2CCP are the first spanwise derivatives of the second components (those with superscript "2") of the above discussed arrays, DVB, DVE, DWWBB, DWWBC, and DWWCC, respectively. The UWE nonlinear deflection arrays correspond to the bracketed integral function defined in equation (36). Within the edgewise modal information group, the various arrays, DWB, DWE, DVBB, DVVBC, and DVVCC etc., correspond to similarly defined spanwise functions involving twist and the edgewise modal deflection and spanwise derivative arrays.

The first group of output parameters presented in Sample Page 6 consists of the inputted torsion modal arrays together with the derived pseudo-torsion mode shape (as defined by Figure 4) and spanwise derivative. The remaining output parameter group consists of the spanwise distributions of various pertinent aeroelastic quantities. The X and XCEN arrays are the nondimensional distances of the centers of the segments from the offset and rotor axis, respectively. The units of the CHORD array are feet. The angle of attack descriptors THETA-AERO, PHI and ALPHA are, respectively the geometric aerodynamic pitch angle, the inflow angle, and the resulting section angle-of-attack, all in degrees. These angles are calculated using the inputted initial conditions on azimuth angle and on the response variable deflections and velocities. The resulting Mach number and aerodynamic coefficients are used to define the perturbational airloads used in the eigensolution. The quantity $KAPPA/U$ is the spanwise variation in aerodynamic moment damping coefficient which when multiplied by the local pitch rate approximates the potential flow unsteady pitching moment coefficient. The quantity $(YLOC/4)/C$ is the spanwise distribution of quarter chord offset from the reference axis nondimensionalized by chord. The dynamic and structural quantities in the third group of this output page includes the QUAD array which constitutes the integration weighting numbers for spanwise integration. The THETA-STR array is the pitch angle distribution of the structural principle axes and has the units of degrees and, in general, differs from the aerodynamic pitch angle distribution. The two arrays, TWIST-BLT and TWIST-TOT, are the nondimensional structural twist rate distributions of the built-in twist and the total twist

LINEAR AND NONLINEAR MODAL DEFLECTION VECTORS

FLATWISE MODE 1		MODAL FREQUENCY = X.XXXXX					PITCH-FLAT COUPLING, AW(1) = .XXXXX					
N	X	GW	GMP	GWPP	DVB	DV2BP	DWBB	DW2BBP	DWBC	DW2BCP	DWCC	DW2CCP
1	.XXXXX	.XXXXX	.XXXXX	.XXXXX	.XXXXX	.XXXXX	.XXXXX	.XXXXX	.XXXXX	.XXXXX	.XXXXX	.XXXXX
2	.XXXXX	.XXXXX	.XXXXX	.XXXXX	.XXXXX	.XXXXX	.XXXXX	.XXXXX	.XXXXX	.XXXXX	.XXXXX	.XXXXX
3	.XXXXX	.XXXXX	.XXXXX	.XXXXX	.XXXXX	.XXXXX	.XXXXX	.XXXXX	.XXXXX	.XXXXX	.XXXXX	.XXXXX
.	.XXXXX	.XXXXX	.XXXXX	.XXXXX	.XXXXX	.XXXXX	.XXXXX	.XXXXX	.XXXXX	.XXXXX	.XXXXX	.XXXXX
.	.XXXXX	.XXXXX	.XXXXX	.XXXXX	.XXXXX	.XXXXX	.XXXXX	.XXXXX	.XXXXX	.XXXXX	.XXXXX	.XXXXX
.	.XXXXX	.XXXXX	.XXXXX	.XXXXX	.XXXXX	.XXXXX	.XXXXX	.XXXXX	.XXXXX	.XXXXX	.XXXXX	.XXXXX
.	.XXXXX	.XXXXX	.XXXXX	.XXXXX	.XXXXX	.XXXXX	.XXXXX	.XXXXX	.XXXXX	.XXXXX	.XXXXX	.XXXXX
N	.XXXXX	.XXXXX	.XXXXX	.XXXXX	.XXXXX	.XXXXX	.XXXXX	.XXXXX	.XXXXX	.XXXXX	.XXXXX	.XXXXX

QUADRATIC DEFLECTION VECTORS DUE TO TORSION MODAL TWIST (DVE(1,J), DV2EP(1,J)) AND TO FLATWISE BENDING (UWE(1,M))

N	X	J = (1)		(2)		(3)		/ M = (1) (2) (3) (4)				
		DVE	DV2EP	DVE	DV2EP	DVE	DV2EP	UWE				
1	.XXXXX	.XXXXX	.XXXXX	.XXXXX	.XXXXX	.XXXXX	.XXXXX	.XXXXX	.XXXXX	.XXXXX	.XXXXX	.XXXXX
2	.XXXXX	.XXXXX	.XXXXX	.XXXXX	.XXXXX	.XXXXX	.XXXXX	.XXXXX	.XXXXX	.XXXXX	.XXXXX	.XXXXX
3	.XXXXX	.XXXXX	.XXXXX	.XXXXX	.XXXXX	.XXXXX	.XXXXX	.XXXXX	.XXXXX	.XXXXX	.XXXXX	.XXXXX
.	.XXXXX	.XXXXX	.XXXXX	.XXXXX	.XXXXX	.XXXXX	.XXXXX	.XXXXX	.XXXXX	.XXXXX	.XXXXX	.XXXXX
.	.XXXXX	.XXXXX	.XXXXX	.XXXXX	.XXXXX	.XXXXX	.XXXXX	.XXXXX	.XXXXX	.XXXXX	.XXXXX	.XXXXX
.	.XXXXX	.XXXXX	.XXXXX	.XXXXX	.XXXXX	.XXXXX	.XXXXX	.XXXXX	.XXXXX	.XXXXX	.XXXXX	.XXXXX
.	.XXXXX	.XXXXX	.XXXXX	.XXXXX	.XXXXX	.XXXXX	.XXXXX	.XXXXX	.XXXXX	.XXXXX	.XXXXX	.XXXXX
N	.XXXXX	.XXXXX	.XXXXX	.XXXXX	.XXXXX	.XXXXX	.XXXXX	.XXXXX	.XXXXX	.XXXXX	.XXXXX	.XXXXX

EDGEWISE MODE 1

EDGEWISE MODE 1		MODAL FREQUENCY = X.XXXXX					PITCH-EDGE COUPLING, AV(1) = .XXXXX					
N	X	GV	GVP	GVPP	DWB	Dw2BP	DVV6R	DVv2BBP	DVVBC	DVv2BCP	DVVCC	DVv2CCP
1	.XXXXX	.XXXXX	.XXXXX	.XXXXX	.XXXXX	.XXXXX	.XXXXX	.XXXXX	.XXXXX	.XXXXX	.XXXXX	.XXXXX
2	.XXXXX	.XXXXX	.XXXXX	.XXXXX	.XXXXX	.XXXXX	.XXXXX	.XXXXX	.XXXXX	.XXXXX	.XXXXX	.XXXXX
3	.XXXXX	.XXXXX	.XXXXX	.XXXXX	.XXXXX	.XXXXX	.XXXXX	.XXXXX	.XXXXX	.XXXXX	.XXXXX	.XXXXX
.	.XXXXX	.XXXXX	.XXXXX	.XXXXX	.XXXXX	.XXXXX	.XXXXX	.XXXXX	.XXXXX	.XXXXX	.XXXXX	.XXXXX
.	.XXXXX	.XXXXX	.XXXXX	.XXXXX	.XXXXX	.XXXXX	.XXXXX	.XXXXX	.XXXXX	.XXXXX	.XXXXX	.XXXXX
.	.XXXXX	.XXXXX	.XXXXX	.XXXXX	.XXXXX	.XXXXX	.XXXXX	.XXXXX	.XXXXX	.XXXXX	.XXXXX	.XXXXX
.	.XXXXX	.XXXXX	.XXXXX	.XXXXX	.XXXXX	.XXXXX	.XXXXX	.XXXXX	.XXXXX	.XXXXX	.XXXXX	.XXXXX
N	.XXXXX	.XXXXX	.XXXXX	.XXXXX	.XXXXX	.XXXXX	.XXXXX	.XXXXX	.XXXXX	.XXXXX	.XXXXX	.XXXXX

DEFLECTION VECTORS DUE TO ELASTIC (MODAL) TWIST, DWE(1,J), Dw2EP(1,J)

N	X	J = (1)		(2)		(3)	
		DWE	Dw2EP	DWE	Dw2EP	DWE	Dw2EP
1	.XXXXX	.XXXXX	.XXXXX	.XXXXX	.XXXXX	.XXXXX	.XXXXX
2	.XXXXX	.XXXXX	.XXXXX	.XXXXX	.XXXXX	.XXXXX	.XXXXX
3	.XXXXX	.XXXXX	.XXXXX	.XXXXX	.XXXXX	.XXXXX	.XXXXX
.	.XXXXX	.XXXXX	.XXXXX	.XXXXX	.XXXXX	.XXXXX	.XXXXX
.	.XXXXX	.XXXXX	.XXXXX	.XXXXX	.XXXXX	.XXXXX	.XXXXX
.	.XXXXX	.XXXXX	.XXXXX	.XXXXX	.XXXXX	.XXXXX	.XXXXX
.	.XXXXX	.XXXXX	.XXXXX	.XXXXX	.XXXXX	.XXXXX	.XXXXX
N	.XXXXX	.XXXXX	.XXXXX	.XXXXX	.XXXXX	.XXXXX	.XXXXX

(including elastic response and control inputs), respectively; these arrays have the units of radians. The quantities TENS \bar{B} , EIY \bar{B} , EIZ \bar{B} and MASS \bar{B} are, respectively, the blade tension, flatwise bending stiffness, edgewise bending stiffness and mass distributions all nondimensionalized in the standard sense. The (Y \bar{LONA})/C and (Y \bar{LOCG})/C arrays are, respectively, the edgewise bending neutral axis and mass center offset distributions nondimensionalized by chord.

TORSION MODES

N	X	GT(1)	GTP(1)	GT(2)	GTP(2)	GT(3)	GTP(3)
1	.XXXXX						
2	.XXXXX						
3	.XXXXX						
.	.XXXXX						
.	.XXXXX						
.	.XXXXX						
N	.XXXXX						

RADIAL DISTRIBUTIONS OF AERODYNAMIC AND DYNAMIC/STRUCTURAL QUANTITIES

N	X	XCEN	CHORD	THETA-AERO	PHI	ALPHA	MACH	CL	CD	CM	KAPPA/U	(Y10C4)/C
1	.XXXXX	.XXXXX	.XXXXX	X.XXX	.XXX	X.XXX	.XXX	.XXXXX	.XXXXX	.XXXXX	.XXXXX	.XXXXX
2	.XXXXX	.XXXXX	.XXXXX	X.XXX	.XXX	X.XXX	.XXX	.XXXXX	.XXXXX	.XXXXX	.XXXXX	.XXXXX
3	.XXXXX	.XXXXX	.XXXXX	X.XXX	.XXX	X.XXX	.XXX	.XXXXX	.XXXXX	.XXXXX	.XXXXX	.XXXXX
.	.XXXXX	.XXXXX	.XXXXX	X.XXX	.XXX	X.XXX	.XXX	.XXXXX	.XXXXX	.XXXXX	.XXXXX	.XXXXX
.	.XXXXX	.XXXXX	.XXXXX	X.XXX	.XXX	X.XXX	.XXX	.XXXXX	.XXXXX	.XXXXX	.XXXXX	.XXXXX
.	.XXXXX	.XXXXX	.XXXXX	X.XXX	.XXX	X.XXX	.XXX	.XXXXX	.XXXXX	.XXXXX	.XXXXX	.XXXXX
N	.XXXXX	.XXXXX	.XXXXX	X.XXX	.XXX	X.XXX	.XXX	.XXXXX	.XXXXX	.XXXXX	.XXXXX	.XXXXX

N	X	XCEN	QUAD	THETA-STR	TWIST-BLT	TWIST-TOT	TENSB	EI7B	EI7B	(Y10NA)/C	MASSB	(Y10C6)/C
1	.XXXXX	.XXXXX	.XXXXX	X.XXX	.XXXXX	.XXXXX	.XXXXX	.XXXXX	.XXXXX	.XXXXX	X.XXXXX	.XXXXX
2	.XXXXX	.XXXXX	.XXXXX	X.XXX	.XXXXX	.XXXXX	.XXXXX	.XXXXX	.XXXXX	.XXXXX	X.XXXXX	.XXXXX
3	.XXXXX	.XXXXX	.XXXXX	X.XXX	.XXXXX	.XXXXX	.XXXXX	.XXXXX	.XXXXX	.XXXXX	X.XXXXX	.XXXXX
.	.XXXXX	.XXXXX	.XXXXX	X.XXX	.XXXXX	.XXXXX	.XXXXX	.XXXXX	.XXXXX	.XXXXX	X.XXXXX	.XXXXX
.	.XXXXX	.XXXXX	.XXXXX	X.XXX	.XXXXX	.XXXXX	.XXXXX	.XXXXX	.XXXXX	.XXXXX	X.XXXXX	.XXXXX
.	.XXXXX	.XXXXX	.XXXXX	X.XXX	.XXXXX	.XXXXX	.XXXXX	.XXXXX	.XXXXX	.XXXXX	X.XXXXX	.XXXXX
N	.XXXXX	.XXXXX	.XXXXX	X.XXX	.XXXXX	.XXXXX	.XXXXX	.XXXXX	.XXXXX	.XXXXX	X.XXXXX	.XXXXX

Results of Solution Part I - Eigensolutions

Sample Pages 7, 8, and 9 present the pertinent details of the eigensolutions. There are three distinct eigensolutions calculated and the three results are headed, respectively, by the following titles:

1. TRUNCATED (LINEAR TERMS ONLY) VACUUM CASE
2. LINEARIZED NONLINEAR VACUUM CASE
3. LINEARIZED NONLINEAR NONVACUUM CASE

In the first case, all terms nonlinear in the response variables and terms involving aerodynamic loadings are omitted. In the second case, those nonlinear inertial and elastic terms omitted in the first eigensolution are retained and linearized about the inputted response variables (initial conditions on response variable deflections and velocities -- locations 67 through 70 and 280 through 303). Note that if these locations are inputted equal to zero this second eigensolution is automatically omitted. The last case includes the locally linearized perturbational airloads with the linearized formulation of the second eigensolution. As shown in Sample Page 7, the beginning of each eigensolution lists the A, B, and C matrices, which pre-multiply the acceleration, velocity and displacement response vectors, respectively, to define the eigenproblem. The extracted eigensolutions (coupled roots and frequencies) are then listed by root pairs. At the bottom of Sample Page 7 and the top of Sample Page 8 are presented the typical format for the case where each of the root pair is real. For each root the eigenvector or GENERALIZED MODE SHAPE is presented, normalized to the largest amplitude. The number of elements to this vector is identical with the dimension of the A, B, and C matrices, and represent, in order, the coupled relative responses of the flatwise, edgewise, and torsion modes. The arrays labeled PHYSICAL MODE SHAPE consist of the relative spanwise distributions of inplane (Y5), and out-of-plane (Z5) and pitching (THETA) components of the coupled mode shape. The Y5 and Z5 deflections are nondimensionalized by blade radius, whereas THETA is in radians.

PART I. EIGENSOLUTIONS OF VARIOUS LINEARIZATIONS OF EQUATION SET - CHARACTERISTIC ROOTS AND COUPLED MODE SHAPES

TRUNCATED (LINEAR TERMS ONLY) VACUUM CASE

A MATRIX

.XXXXE-YY	.XXXXF-YY	.XXXXF-YY	.XXXXF-YY	.XXXXF-YY	.XXXXE-YY
.XXXXF-YY	.XXXXF-YY	.XXXXE-YY	.XXXXF-YY	.XXXXE-YY	.XXXXE-YY
.XXXXF-YY	.XXXXF-YY	.XXXXF-YY	.XXXXF-YY	.XXXXE-YY	.XXXXE-YY
.XXXXE-YY	.XXXXE-YY	.XXXXF-YY	.XXXXE-YY	.XXXXE-YY	.XXXXE-YY
.XXXXE-YY	.XXXXF-YY	.XXXXF-YY	.XXXXF-YY	.XXXXF-YY	.XXXXE-YY
.XXXXF-YY	.XXXXE-YY	.XXXXF-YY	.XXXXE-YY	.XXXXE-YY	.XXXXF-YY

B MATRIX

.XXXXE-YY	.XXXXF-YY	.XXXXF-YY	.XXXXF-YY	.XXXXE-YY	.XXXXE-YY
.XXXXE-YY	.XXXXF-YY	.XXXXF-YY	.XXXXE-YY	.XXXXE-YY	.XXXXE-YY
.XXXXF-YY	.XXXXE-YY	.XXXXF-YY	.XXXXE-YY	.XXXXF-YY	.XXXXE-YY
.XXXXE-YY	.XXXXF-YY	.XXXXF-YY	.XXXXE-YY	.XXXXE-YY	.XXXXE-YY
.XXXXF-YY	.XXXXF-YY	.XXXXE-YY	.XXXXF-YY	.XXXXE-YY	.XXXXE-YY
.XXXXE-YY	.XXXXE-YY	.XXXXE-YY	.XXXXF-YY	.XXXXE-YY	.XXXXE-YY

C MATRIX

.XXXXF-YY	.XXXXE-YY	.XXXXF-YY	.XXXXE-YY	.XXXXE-YY	.XXXXE-YY
.XXXXE-YY	.XXXXE-YY	.XXXXE-YY	.XXXXF-YY	.XXXXF-YY	.XXXXE-YY
.XXXXF-YY	.XXXXE-YY	.XXXXE-YY	.XXXXF-YY	.XXXXE-YY	.XXXXE-YY
.XXXXF-YY	.XXXXE-YY	.XXXXE-YY	.XXXXF-YY	.XXXXE-YY	.XXXXE-YY
.XXXXE-YY	.XXXXF-YY	.XXXXE-YY	.XXXXF-YY	.XXXXE-YY	.XXXXE-YY
.XXXXE-YY	.XXXXE-YY	.XXXXE-YY	.XXXXF-YY	.XXXXE-YY	.XXXXE-YY

ROOTS (1, 2) = .XXXXX ; .XXXXX

GENERALIZED MODE SHAPE (1) .XXXXX .XXXXX .XXXXX .XXXXX .XXXXX .XXXXX

PHYSICAL MODE SHAPE	N	X	Y5	Z5	THE TA
1		.XXXXX	.XXXXX	.XXXXX	.XXXXX
2		.XXXXX	.XXXXX	.XXXXX	.XXXXX
3		.XXXXX	.XXXXX	.XXXXX	.XXXXX
.		.XXXXX	.XXXXX	.XXXXX	.XXXXX
.		.XXXXX	.XXXXX	.XXXXX	.XXXXX
.		.XXXXX	.XXXXX	.XXXXX	.XXXXX
.		.XXXXX	.XXXXX	.XXXXX	.XXXXX
N		.XXXXX	.XXXXX	.XXXXX	.XXXXX

At the bottom of Sample Page 8 is presented the typical format for the case where the root pair consists of complex conjugates. For this case, in addition to the real and imaginary components of the roots, the equivalent critical damping ratio, ZETA, and undamped natural frequency, WN, are given. Note that for a complex pair of roots, the eigenvector is also complex; the sign on the imaginary component corresponds to the root with the positive imaginary part. Similarly, the physical mode shape is given, which additionally contains the velocity component distribution to account for the generally nonuniform phasing along the span. The velocity components are nondimensionalized by tip speed.

```

GENERALIZED MODE SHAPE ( 2)  .XXXXX  .XXXXX  .XXXXX  .XXXXX  .XXXXX  .XXXXX
PHYSICAL MODE SHAPE      N      X      Y5      Z5      THETA
1      .XXXXX  .XXXXX  .XXXXX  .XXXXX
2      .XXXXX  .XXXXX  .XXXXX  .XXXXX
3      .XXXXX  .XXXXX  .XXXXX  .XXXXX
.      .XXXXX  .XXXXX  .XXXXX  .XXXXX
.      .XXXXX  .XXXXX  .XXXXX  .XXXXX
.      .XXXXX  .XXXXX  .XXXXX  .XXXXX
N      .XXXXX  .XXXXX  .XXXXX  .XXXXX

ROOTS ( 2, 4) = .XXXXX +-I X.XXXXX  ZETA = .XXXXX  WN = X.XXXXXX
GENERALIZED MODE SHAPE      (RE)  .XXXXX  .XXXXX  .XXXXX  .XXXXX  .XXXXX  .XXXXX
                        (IM)  .XXXXX  .XXXXX  .XXXXX  .XXXXX  .XXXXX  .XXXXX
PHYSICAL MODE SHAPE      N      X      Y5      Y5*      Z5      Z5*      THETA  THETA*
1      .XXXXX  .XXXXX  .XXXXX  .XXXXX  .XXXXX  .XXXXX  .XXXXX  .XXXXX
2      .XXXXX  .XXXXX  .XXXXX  .XXXXX  .XXXXX  .XXXXX  .XXXXX  .XXXXX
3      .XXXXX  .XXXXX  .XXXXX  .XXXXX  .XXXXX  .XXXXX  .XXXXX  .XXXXX
.      .XXXXX  .XXXXX  .XXXXX  .XXXXX  .XXXXX  .XXXXX  .XXXXX  .XXXXX
.      .XXXXX  .XXXXX  .XXXXX  .XXXXX  .XXXXX  .XXXXX  .XXXXX  .XXXXX
.      .XXXXX  .XXXXX  .XXXXX  .XXXXX  .XXXXX  .XXXXX  .XXXXX  .XXXXX
N      .XXXXX  .XXXXX  .XXXXX  .XXXXX  .XXXXX  .XXXXX  .XXXXX  .XXXXX

```

Sample Page 8

Should one of the roots in the nonvacuum eigensolution be unstable, as indicated by a positive root or real part of a complex pair, an output listing of the force phasing matrices appropriate to the instability is generated and outputted as depicted in Sample Page 9. These matrices, having the same size as the A, B, and C dynamic matrices, enable the various destabilizing forces to be identified; descriptive material for their definition and interpretation are contained in Reference 13.

A PHASING MATRIX

.XXXXE-YY	.XXXXF-YY	.XXXXE-YY	.XXXXF-YY	.XXXXE-YY	.XXXXE-YY
.XXXXE-YY	.XXXXF-YY	.XXXXE-YY	.XXXXF-YY	.XXXXE-YY	.XXXXE-YY
.XXXXE-YY	.XXXXF-YY	.XXXXE-YY	.XXXXF-YY	.XXXXE-YY	.XXXXE-YY
.XXXXE-YY	.XXXXF-YY	.XXXXE-YY	.XXXXF-YY	.XXXXE-YY	.XXXXE-YY
.XXXXE-YY	.XXXXF-YY	.XXXXE-YY	.XXXXF-YY	.XXXXE-YY	.XXXXE-YY
.XXXXE-YY	.XXXXF-YY	.XXXXE-YY	.XXXXF-YY	.XXXXE-YY	.XXXXE-YY

B PHASING MATRIX

.XXXXE-YY	.XXXXE-YY	.XXXXF-YY	.XXXXE-YY	.XXXXE-YY	.XXXXE-YY
.XXXXE-YY	.XXXXF-YY	.XXXXE-YY	.XXXXF-YY	.XXXXE-YY	.XXXXE-YY
.XXXXE-YY	.XXXXE-YY	.XXXXF-YY	.XXXXE-YY	.XXXXE-YY	.XXXXE-YY
.XXXXE-YY	.XXXXF-YY	.XXXXE-YY	.XXXXF-YY	.XXXXE-YY	.XXXXE-YY
.XXXXE-YY	.XXXXE-YY	.XXXXF-YY	.XXXXE-YY	.XXXXE-YY	.XXXXE-YY
.XXXXE-YY	.XXXXF-YY	.XXXXE-YY	.XXXXF-YY	.XXXXE-YY	.XXXXE-YY

C PHASING MATRIX

.XXXXF-YY	.XXXXE-YY	.XXXXF-YY	.XXXXE-YY	.XXXXE-YY	.XXXXE-YY
.XXXXE-YY	.XXXXF-YY	.XXXXE-YY	.XXXXF-YY	.XXXXE-YY	.XXXXE-YY
.XXXXE-YY	.XXXXE-YY	.XXXXE-YY	.XXXXE-YY	.XXXXE-YY	.XXXXE-YY
.XXXXE-YY	.XXXXF-YY	.XXXXE-YY	.XXXXE-YY	.XXXXE-YY	.XXXXE-YY
.XXXXE-YY	.XXXXE-YY	.XXXXF-YY	.XXXXE-YY	.XXXXE-YY	.XXXXE-YY
.XXXXE-YY	.XXXXF-YY	.XXXXE-YY	.XXXXE-YY	.XXXXE-YY	.XXXXE-YY

Sample Page 9

Results of Solution Part II -- Time History Solutions

Sample Page 10 presents a variety of response and load quantities defining the transient aeroelastic responses. The first row of parameters following the page title presents, for the subsequent time-history solution, a listing of the parameters defining the flight condition. These parameters consist of the various control angles (in degrees), the inflow and advance ratios, and the nondimensionalized values of the "momentum" induced velocity components. The remainder of Sample Page 10 comprises the typical azimuthal listing; this listing is outputted for every azimuth angle which is a multiple of the print azimuth increment, input item no. 23.

The first of the four groups of result quantities on this sample page lists the spanwise distributions of the pertinent aerodynamic quantities. The inflow and total section angles of attack PHI and ALPHA, respectively, are in degrees. The MACH NO., CL, CD, and CM are self-explanatory and nondimensional. The airload distributions in the Z5 and Y5 directions, SAZ5 and SAY5, respectively, have the units of lb/in., the aerodynamic pitching moment distribution, MAX5, has the units of in.-lb/in. The quantities SDZ5, SDY5, and MDX5 are "semi-dynamic" load distributions. These distributions are dimensionally similar to those above described resulting from aerodynamics, but instead arise from all the dynamic effects except the doubly time differentiated ones (see equations 41c, 41b and 44a, respectively). The quantity MEX9 is the elastic torsion moment distribution which consists of those torsion couplings arising from ΔEI , the tension-neutral axis offset and other twist related elastic effects; it too, has the units of in.-lb/in.

The second group of result quantities consists of the instantaneous generalized excitations, XI, and the generalized accelerations, velocities, and displacements (Q^{**} , Q^* , and Q , respectively) for each of the modal response variables selected, all appropriately nondimensionalized. The generalized excitations are defined to be the elements of the right hand side of equation (34).

The third group of result quantities are composed mainly of blade deflection and stress distributions. The vertical and inplane deflections are those in the Z5 and Y5 directions, respectively. All stress quantities have the units of lb/in.², whereas the torsion moment has the units of lb-in. It should be noted that, over the flexbeam-torque tube span, the flatwise and edgewise stresses outputted are those only for the flexbeam whereas the torsion moments and stresses outputted are those only for the torque tube. The last two columns are the distributions of the A and B parameters needed to define the unsteady airloads (see Reference 9). The fourth group of result quantities at the bottom of the sample page consists of miscellaneous deflection, load and stress results for the flexbeam and push-rod.

The line titled SPAR/FLEXURE PARAMETERS presents similar stresses and torsion moments for the flexbeam at the indicated spanwise location; note, however, that the outputted torsion moment is for the flexbeam immediately inboard of the juncture. Of the remaining four quantities, PUSH-ROD (RELATIVE) DEFL. (in.), TORQUE TUBE ROOT DEFL. (in.), and TORQUE TUBE ROOT SHEAR (lb.) pertain only to cantilevered torque tube configurations wherein the "wobble mode" option is invoked (input location 985). All three quantities are defined in the positive Z5 direction. The quantity PUSH-ROD LOAD (lb) is the upward (+Z5) directed load the push-rod exerts on the pitch horn/push-rod attachment point; this quantity is calculated for all blade types. For composite bearingless rotors, the push-rod load accounts for the total blade torsion moment at the root less that torsion moment resisted by the flexbeam.

PART II. TIME HISTORY SOLUTION OF COMPLETE (NONLINEAR) EQUATION SET - AEROELASTIC TRANSIENT RESPONSES

#15	B15	A25	B25	THETA 75	LAMBDA	MU	VO	VIC	VIS					
X.XXX	X.XXX	X.YXX	F.XXX	X.YXX	.XXXXX	.XXX	X.XXXXX	X.XXXXX	X.XXXXX					
PSI = X.XX DEG.		PFV = XX												
N	X CEN	PHI	ALPHA	MACH NO.	CL	CU	CM	SAZ5	SAYS	MAXE	SDZ5	SDY5	MDX5	MEY9
1	.XXXX	X.YXX	X.YXX	.XXX	Y.XXXX	.XXXX	Y.XXXX	.XXXX	.XXXX	.XXXX	.XXXX	.XXXX	.XXXX	.XXXX
2	.XXXX	X.YXX	X.YXX	.XXX	Y.XXXX	.XXXX	Y.XXXX	.XXXX	.XXXX	.XXXX	.XXXX	.XXXX	.XXXX	.XXXX
3	.XXXX	X.YXX	X.YXX	.XXX	Y.XXXX	.XXXX	Y.XXXX	.XXXX	.XXXX	.XXXX	.XXXX	.XXXX	.XXXX	.XXXX
.	.XXXX	X.YXX	X.YXX	.XXX	Y.XXXX	.XXXX	Y.XXXX	.XXXX	.XXXX	.XXXX	.XXXX	.XXXX	.XXXX	.XXXX
.	.XXXX	X.YXX	X.YXX	.XXX	Y.XXXX	.XXXX	Y.XXXX	.XXXX	.XXXX	.XXXX	.XXXX	.XXXX	.XXXX	.XXXX
.	.XXXX	X.YXX	X.YXX	.XXX	Y.XXXX	.XXXX	Y.XXXX	.XXXX	.XXXX	.XXXX	.XXXX	.XXXX	.XXXX	.XXXX
N	.XXXX	X.YXX	X.YXX	.XXX	Y.XXXX	.XXXX	Y.XXXX	.XXXX	.XXXX	.XXXX	.XXXX	.XXXX	.XXXX	.XXXX

	Cw1	Cw2	Cw3	Cw4	OV1	OV2	OV3	OT1	OT2	OT3	BETA	DELTA
XI	X.XXE-YY	X.XXL-YY	X.XXE-YY	.XXX	X.XXE-YY	X.XXE-YY	.XXX	X.XXL-YY	.XXX	.XXX	.XXX	.XXX
0**	X.XXE-YY	X.XXL-YY	X.XXE-YY	.XXX	X.XXE-YY	X.XXE-YY	.XXX	X.XXL-YY	.XXX	.XXX	.XXX	.XXX
0*	X.XXE-YY	X.XXL-YY	X.XXE-YY	.XXX	X.XXE-YY	X.XXL-YY	.XXX	X.XXL-YY	.XXX	.XXX	.XXX	.XXX
0	X.XXE-YY	X.XXL-YY	X.XXE-YY	.XXX	X.XXE-YY	X.XXE-YY	.XXX	X.XXE-YY	.XXX	.XXX	.XXX	.XXX

N	CEN	VERTICAL DEFL-IN	INPLANE DEFL-IN	TORSION DEFL-DEG	FLATWISE STRESS	EDGEWISE STRESS	TORSION STRESS	CORNER STRESS	TORSION MOMENT	A	B
1	.XXXX	.XXX	.XXX	.XXX	XXXX.	XXXX.	XXXX.	XXXX.	XXX.XX	.XXXXX	.XXXXX
2	.XXXX	.XXX	.XXX	.XXX	XXXX.	XXXX.	XXXX.	XXXX.	XXX.XX	.XXXXX	.XXXXX
3	.XXXX	.XXX	.XXX	.XXX	XXXX.	XXXX.	XXXX.	XXXX.	XXX.XX	.XXXXX	.XXXXX
.	.XXXX	.XXX	.XXX	.XXX	XXXX.	XXXX.	XXXX.	XXXX.	XXX.XX	.XXXXX	.XXXXX
.	.XXXX	.XXX	.XXX	.XXX	XXXX.	XXXX.	XXXX.	XXXX.	XXX.XX	.XXXXX	.XXXXX
.	.XXXX	.XXX	.XXX	.XXX	XXXX.	XXXX.	XXXX.	XXXX.	XXX.XX	.XXXXX	.XXXXX
N	.XXXX	.XXX	.XXX	.XXX	XXXX.	XXXX.	XXXX.	XXXX.	XXX.XX	.XXXXX	.XXXXX

SPAR/FLEXURE PARAMETERS:

2	.XXXX	XXXX.	XXX.	XXXX.	XXXX.	XXX.XX
PUSH-ROD (RELATIVE) DEFL. =	.XX IN				PUSH-ROD LOAD =	XXX.XX LB
TORQUE-TUBE ROOT DEFL. =	.XX IN				TORQUE-TUBE ROOT SHEAR =	XXX.XX LB

After the time-history solution has either converged to periodicity or run to maximum flapping trials (input location 10) various integrated loads are calculated for one final blade revolution to form the aerodynamic performance and stress results depicted in Sample Page 11. For each of eight (8) performance quantities results are presented in nondimensional coefficient form, in nondimensional form divided by solidity, and in actual dimensional form. Note that ten (10) dimensional quantities are listed and the units are lb for forces and lb-ft for moments, as appropriate. The quantity EQU. DRAG (lb) represents the combined power expended by the rotor due to rotor rotation (torque) and translation (drag) divided by flight speed.

The next line duplicates the parameters defining the flight condition and includes four (4) additional quantities which depend on the integrated performance for evaluation. At the beginning of the time-history calculation it is not known which part of the inflow ratio being used is due to ram effects and which due to momentum induced effects. Once the integrated rotor thrust is calculated, however, the induced portion of the inflow can then be calculated using the simple usual momentum formula derived for flight in an infinite continuum (Reference 14). The complementary portion of the inflow represents the ram effect from which the shaft angle-of-attack ALPHA S, in degrees, can be calculated. The quantity VEL ACT. is the actual forward flight velocity, in knots, consistent with the advance ratio used and the shaft angle of attack. For finite forward flight speeds EQU. L/D is the lift divided by the equivalent drag; for hovering cases this quantity is the figure of merit. PAR. AREA, the rotor parasite (drag) area, in square feet, is the rotor drag divided by dynamic pressure. The line titled CORRECTIONS DUE TO WIND TUNNEL WALL INTERFERENCE: consists of recalculations of those quantities which depend on the induced portion of the inflow wherein the induced inflow is calculated using the formulae derived for flight in wind tunnels or in ground effect (Reference 11). The remainder of Sample Page 11 consists of reductions of the various stresses (lb/in.²) and the push-rod load (lb.) to median and $\frac{1}{2}$ peak-to-peak values over the final rotor revolution.

AERODYNAMIC PERFORMANCE AND STRESSES

	H FORCE	Y FORCE	THRUST	ROLL. MOM.	PITCH MOM.	TORQUE	LIFT	PROP. FORCE	HORSEPOWER	EQU. DRAG
C ()	.XXXXXXXX	.XXXXXXXX	.XXXXXXXX	.XXXXXXXX	.XXXXXXXX	.XXXXXXXX	.XXXXXXXX	.XXXXXXXX		
CI)/SIG	.XXXXXXXX	.XXXXXXXX	.XXXXXXXX	.XXXXXXXX	.XXXXXXXX	.XXXXXXXX	.XXXXXXXX	.XXXXXXXX		
DIMENS.	.XX	.XX	X.XX	.XX	.XX	.XX	X.XX	.XX	.XX	X.XX

AIS	B1S	A2S	B2S	THETA 75	LAMBDA	MU	VEL ACT.	EQU. L/D	PAR. AREA	ALPHA S
X.XXX	X.XXX	X.XXX	X.XXX	X.XXX	.XXXXX	.XXX	XX.XX	.XXX	X.XXX	X.XXX

CORRECTIONS DUE TO WIND TUNNEL WALL INTERFERENCE:

ALPHA S = X.XXX DEG. LIFT = XXXX.XX LB PF = XXX.XX LB VFL ACT. = XXX.XX KT.

N	X CEA	/ MEDIAN STRESSES / FLATWISE	/ EDGWISE	/ 1/2 PTP STRESSES / FLATWISE	/ EDGWISE	/ MAX CORNER / STRESSES	/ TORSION MOMENTS / MEDIAN	/ 1/2 PTP
1	.XXXX	XXXXX.X	XXXX.X	XXXX.X	XXXX.X	XXXXX.X	.X	.XX
2	.XXXX	XXXXX.X	XXXX.X	XXXX.X	XXXX.X	XXXXX.X	.X	.XX
3	.XXXX	XXXXX.X	XXXX.X	XXXX.X	XXXX.X	XXXXX.X	.X	.XX
.	.XXXX	XXXXX.X	XXXX.X	XXXX.X	XXXX.X	XXXXX.X	.X	.XX
.	.XXXX	XXXXX.X	XXXX.X	XXXX.X	XXXX.X	XXXXX.X	.X	.XX
.	.XXXX	XXXXX.X	XXXX.X	XXXX.X	XXXX.X	XXXXX.X	.X	.XX
N	.XXXX	XXXXX.X	XXXX.X	XXXX.X	XXXX.X	XXXXX.X	.X	.XX

PUSH-ROD LOAD (MEDIAN, 1/2 PTP):

.XX .XX

Should major (trim) iterations be used (see description of input items 60 and 62 through 65 in Appendix II) output depicted on Sample Page 12 will be generated by the program. The first line consists of the zeroth, first cosine and first and second sine harmonics of first flatwise mode response, in radians, and an estimate of an effective angle-of-attack on the retreating blade side ($\psi = 270^\circ$), in degrees. The nonzero elements of the depicted (G) MATRIX give, for each row, the partial derivatives of the four trim quantities (C_L , C_{PF} , C_{PM} , C_{RM} , respectively) with respect to the four control quantities being used ($\theta_{.75}$, A_{1s} , B_{1s} , and $(\sin \alpha_g)$), or v_o , v_{1c} , v_{1s} , and $(\sin \alpha_g)$), for each respective column. The elements of this matrix are formulated using approximate linear strip theory with reversed flow effects and are calculated for either set of control quantities, as appropriate. The ERROR VECTOR consists of the differences between the four requested trim quantities and those achieved in the preceeding time-history. The two lines depicted give the error vector in dimensional (lb and lb-ft) and nondimensional forms, respectively. The CORRECTION VECTOR consists of those changes to the control quantities which should null the above described error vector. The correction vector is obtained from the premultiplication of the inverse of the G matrix with the error vector, but the corrections are scaled, if necessary, to prevent control changes of more than 2 degrees within any one iteration. The control parameters whose increments are depicted in this output page are, in respective order: $\theta_{.75}$, A_{1s} , B_{1s} , $(\sin \alpha_g)$, λ , C_T , v_o , v_{1c} , and v_{1s} ; the first three have units of degrees and the remainder are dimensionless or nondimensionalized.

TRIM ITERATION, GW10 = X.XXXE-YY GW1C = X.XXXE-YY GW1S = X.XXXE-YY GW2S = X.XXXE-YY A(270) = XX.XX

(G) MATRIX

X.XXXE-YY	X.XXXE-YY	X.XXXE-YY	X.XXXE-YY	0.000	0.000	0.000	0.000	0.000
X.XXXE-YY	X.XXXE-YY	X.XXXE-YY	X.XXXE-YY	0.000	0.000	0.000	0.000	0.000
X.XXXE-YY	X.XXXE-YY	X.XXXE-YY	X.XXXE-YY	0.000	0.000	0.000	0.000	0.000
X.XXXE-YY	X.XXXE-YY	X.XXXE-YY	X.XXXE-YY	0.000	0.000	0.000	0.000	0.000

ERROR VECTOR

X.XXXE-YY	X.XXXE-YY	X.XXXE-YY	X.XXXE-YY	0.000	0.000	0.000	0.000	0.000
X.XXXE-YY	X.XXXE-YY	X.XXXE-YY	X.XXXE-YY	0.000	0.000	0.000	0.000	0.000

CORRECTION VECTOR

X.XXXE-YY								
-----------	-----------	-----------	-----------	-----------	-----------	-----------	-----------	-----------

Once the time-history solution has converged to periodicity and all major iterations have been completed, the program optionally performs harmonic analyses of the azimuthal variations of various response quantities (see descriptions of input items 48 and 73 through 75 in Appendix II). The outputs of these harmonic analyses are depicted in Sample Pages 13 through 15. In each of these sample pages the harmonic information for each response variable is contained in the appropriate horizontal band of five rows. The harmonics are listed by columns up to a maximum of 10 harmonics. All harmonic analysis output depicted on these sample pages assume a negative harmonic content form in keeping with the (negative) harmonic form conventionally assumed for the blade pitch control and rigid flapping angles. For each harmonic of response variable five quantities are outputted; these quantities are, respectively, the cosine and sine components, the equivalent amplitude and phase angle, and lastly, the amplitude of the harmonic relative to all the other harmonic amplitudes outputted. Sample Page 13 depicts the harmonic analyses of the dimensionless modal response variables selected wherein $QW(I)$, $QV(K)$ and $QT(J)$ are, respectively, the (I) flatwise, (K) edgewise and (J) torsional uncoupled mode responses.

Sample Page 14 depicts the harmonic analyses of the total shears and moments exerted by one blade to the hub. In contrast to the steady hub loads listed in the AERODYNAMIC PERFORMANCE AND STRESSES output (Sample Page 11) which are calculated by integrating only the aerodynamic load distributions, the total hub loads which are herein harmonically analyzed are calculated by similarly integrating the combined aerodynamic and the dynamic load distributions. The longitudinal, lateral and vertical hub shears comprising the first three quantities of this sample page all have the dimensions of lb and are defined in the x_1 - (aft), y_1 - (starboard), and z_1 - (up and along axis of rotation) axis directions, respectively. The roll, pitch and yaw moments comprising the latter three quantities on this sample page have the dimensions of lb-ft and are defined positive (using the right-hand rule) about the x_1 -, y_1 -, and z_1 - axes, respectively. Note that the aerodynamic rolling moment whose output is depicted in Sample Page 11 is defined positive starboard side down and is opposite from the harmonically analyzed total rolling moment depicted in Sample Page 14. Sample Page 15 depicts the harmonic analysis of the flatwise stresses at the center of each of the spanwise segments. A similar output listing is provided for both edgewise and torsional stresses.

HARMONIC ANALYSIS OF HUB SHEARS AND MOMENTS

	A0	1	2	3	4	5	6	7	8	9	10
LONG. SHR	XX.X	XXXXX.X XXXXX.X XXXXX.X XXX.XX X.XX	XXX.X XXX.X XXX.X XXX.XX .XX	XXX.X XXX.X XXX.X XXX.XX .XX	XX.X XX.X XX.X XXX.XX .XX						
LAT. SHR	XX.X	XXXXX.X XXXXX.X XXXXX.X XXX.XX X.XX	XXX.X XXX.X XXX.X XXX.XX .XX	XXX.X XXX.X XXX.X XXX.XX .XX	XX.X XX.X XX.X XXX.XX .XX						
VERT. SHR	XX.X	XXXXX.X XXXXX.X XXXXX.X XXX.XX X.XX	XXX.X XXX.X XXX.X XXX.XX .XX	XXX.X XXX.X XXX.X XXX.XX .XX	XX.X XX.X XX.X XXX.XX .XX						
ROLL MOMT	XX.X	XXXXX.X XXXXX.X XXXXX.X XXX.XX X.XX	XXX.X XXX.X XXX.X XXX.XX .XX	XXX.X XXX.X XXX.X XXX.XX .XX	XX.X XX.X XX.X XXX.XX .XX						
PITCH MOMT	XX.X	XXXXX.X XXXXX.X XXXXX.X XXX.XX X.XX	XXX.X XXX.X XXX.X XXX.XX .XX	XXX.X XXX.X XXX.X XXX.XX .XX	XX.X XX.X XX.X XXX.XX .XX						
YAW MOMT	XX.X	XXXXX.X XXXXX.X XXXXX.X XXX.XX X.XX	XXX.X XXX.X XXX.X XXX.XX .XX	XXX.X XXX.X XXX.X XXX.XX .XX	XX.X XX.X XX.X XXX.XX .XX						

HARMONIC ANALYSIS OF FLATWISE STRESSES

N	X	CEN	AD	1	2	3	4	5	6	7	8	9	10	
1	.XXXX		XXXX.X	XXXX.X XXXX.X XXXX.X XX.X .XXX	XXXX.X XXX.X XXXX.X XX.X X.XXX	XXXX.X XXXX.X XXXX.X XX.X .XXX	XX.X XXX.X XXX.X XX.X .XXX	XXX.X XXX.X XXX.X XX.X .XXX	XXX.X XXX.X XXX.X XX.X .XXX	XX.X XX.X XX.X XX.X .XXX	XX.X XX.X XX.X XX.X .XXX	XX.X XX.X XX.X XX.X .XXX	XX.X XX.X XX.X XX.X .XXX	
2	.XXXX		XXXX.X	XXXX.X XXXX.X XXXX.X XX.X .XXX	XXXX.X XXX.X XXXX.X XX.X X.XXX	XXXX.X XXXX.X XXXX.X XX.X .XXX	XX.X XXX.X XXX.X XX.X .XXX	XXX.X XXX.X XXX.X XX.X .XXX	XXX.X XXX.X XXX.X XX.X .XXX	XX.X XX.X XX.X XX.X .XXX	XX.X XX.X XX.X XX.X .XXX	XX.X XX.X XX.X XX.X .XXX	XX.X XX.X XX.X XX.X .XXX	XX.X XX.X XX.X XX.X .XXX
3	.XXXX		XXXX.X	XXXX.X XXXX.X XXXX.X XX.X .XXX	XXXX.X XXX.X XXXX.X XX.X X.XXX	XXXX.X XXXX.X XXXX.X XX.X .XXX	XX.X XXX.X XXX.X XX.X .XXX	XXX.X XXX.X XXX.X XX.X .XXX	XXX.X XXX.X XXX.X XX.X .XXX	XX.X XX.X XX.X XX.X .XXX	XX.X XX.X XX.X XX.X .XXX	XX.X XX.X XX.X XX.X .XXX	XX.X XX.X XX.X XX.X .XXX	XX.X XX.X XX.X XX.X .XXX
4	.XXXX		XXXX.X	XXXX.X XXXX.X XXXX.X XX.X .XXX	XXXX.X XXX.X XXXX.X XX.X X.XXX	XXXX.X XXXX.X XXXX.X XX.X .XXX	XX.X XXX.X XXX.X XX.X .XXX	XXX.X XXX.X XXX.X XX.X .XXX	XXX.X XXX.X XXX.X XX.X .XXX	XX.X XX.X XX.X XX.X .XXX	XX.X XX.X XX.X XX.X .XXX	XX.X XX.X XX.X XX.X .XXX	XX.X XX.X XX.X XX.X .XXX	XX.X XX.X XX.X XX.X .XXX
5	.XXXX		XXXX.X	XXXX.X XXXX.X XXXX.X XX.X .XXX	XXXX.X XXX.X XXXX.X XX.X X.XXX	XXXX.X XXXX.X XXXX.X XX.X .XXX	XX.X XXX.X XXX.X XX.X .XXX	XXX.X XXX.X XXX.X XX.X .XXX	XXX.X XXX.X XXX.X XX.X .XXX	XX.X XX.X XX.X XX.X .XXX	XX.X XX.X XX.X XX.X .XXX	XX.X XX.X XX.X XX.X .XXX	XX.X XX.X XX.X XX.X .XXX	XX.X XX.X XX.X XX.X .XXX
6	.XXXX		XXXX.X	XXXX.X XXXX.X XXXX.X XX.X .XXX	XXXX.X XXX.X XXXX.X XX.X X.XXX	XXXX.X XXXX.X XXXX.X XX.X .XXX	XX.X XXX.X XXX.X XX.X .XXX	XXX.X XXX.X XXX.X XX.X .XXX	XXX.X XXX.X XXX.X XX.X .XXX	XX.X XX.X XX.X XX.X .XXX	XX.X XX.X XX.X XX.X .XXX	XX.X XX.X XX.X XX.X .XXX	XX.X XX.X XX.X XX.X .XXX	XX.X XX.X XX.X XX.X .XXX

145

Results of Solution Part III - Transient Spectral Stability Analysis

Transient time-history solutions are often difficult to interpret for quantitative stability information. This is due to the fact that the total responses so calculated inherently consist of several component modes simultaneously and transiently approaching (or departing from) multi-harmonic periodicity with a wide range of natural frequencies and inherent damping levels. The extraction of the component responses at discrete frequencies in order to examine their individual attenuation characteristics is the purpose of the Transient Spectral Stability Analysis (TSSA) portion of Program G400. The details of this analysis, which utilizes Fourier Transform techniques, are beyond the scope of this report but are treated in References 15.

Essentially the TSSA first performs Fourier transformations of selected time-history data strings, which have been previously generated in the time-history solution portion of the analysis (Solution Part II) and appropriately saved. The purpose of the Fourier Transform is to identify, within these time-histories, those frequencies whose amplitudes are relatively largest and which are herein denoted as "resonances". The TSSA then calculates the transient behavior of the extracted amplitudes of these resonances over the time-history time interval and estimates equivalent linear stability indices (characteristic exponent, critical damping ratio, and time to half amplitude).

Sample Pages 16 through 18 depict the output typically generated by the TSSA. The sequence of output depicted is duplicated for each of the transient response channels selected (see input locations 84 through 86, Appendix II). Sample Page 16 depicts the output generated by the Fourier Transform frequency identification portion of the TSSA. Shown at the top of the page is the transient response channel being analyzed and the frequency range wherein resonance identification is desired (input locations 87 and 88). The series of five output items to follow consist of parameters defining the numerical Fourier Transform; note that the results of the TSSA incorporate a time nondimensionalization based on rotor speed, Ω . The tabulation of the Fourier Transform follows wherein, for each frequency (harmonic of the fundamental as determined by the total nondimensional time interval), the real and imaginary parts, the square of the amplitude and the logarithm to the base 10 of the amplitude are outputted. Generally, this tabulation will consume more than the one page indicated in Sample Page 16. After this listing is completed, those frequencies and their respective square amplitudes which are found to be resonances, as defined above, are listed.

PART III. TRANSIENT SPECTRAL STABILITY ANALYSES OF SELECTED AEROELASTIC TRANSIENT RESPONSES

TRANSIENT RESPONSE CHANNEL NO. XX - FOURIER TRANSFORM AND RESONANT FREQUENCY IDENTIFICATION

DESIRED FREQUENCY RANGE = .XX TO X.XX (/REV)

NUMBER OF POINTS IN TIME SERIES = .XXX
 (ND) TIME INCREMENT = .XXXXX RAD
 LENGTH OF INTERVAL = XX.XXXXX RAD
 FUNDAMENTAL FREQUENCY = .XXXXX /REV
 HIGHEST FREQUENCY = XX.XXXXX /REV

TABULATION OF FOURIER TRANSFORM BY HARMONIC OF FUNDAMENTAL FREQUENCY

HARMONIC	FREQUENCY	COMPLX FOURIER TRANSFORM	TRANSFORM MAGNITUDE	LOG TO BASE 10 OF MAGNITUDE
0	.XXXXXX	X.XXXXXXE-YY	.000000 I	X.XXXXXXE-YY
1	.XXXXXX	X.XXXXXXF-YY	X.XXXXXE-YYI	X.XXXXXE-YY
2	.XXXXXX	X.XXXXXXE-YY	X.XXXXXE-YYI	X.XXXXXE-YY
3	.XXXXXX	X.XXXXXXE-YY	X.XXXXXE-YYI	X.XXXXXE-YY
.	.XXXXXX	X.XXXXXXE-YY	X.XXXXXE-YYI	X.XXXXXE-YY
.	.XXXXXX	X.XXXXXXE-YY	X.XXXXXE-YYI	X.XXXXXE-YY
.	.XXXXXX	X.XXXXXXE-YY	X.XXXXXE-YYI	X.XXXXXE-YY
N	.XXXXXX	X.XXXXXXE-YY	X.XXXXXE-YYI	X.XXXXXE-YY

RESONANCE FREQUENCIES FOUND BY SEARCH ROUTINE

1	X.XXXXXXF-YY	X.XXXXXXE-YY
2	X.XXXXXE-YY	X.XXXXXE-YY
3	X.XXXXXXF-YY	X.XXXXXXE-YY
4	X.XXXXXE-YY	X.XXXXXE-YY

THERE ARE LESS FUNDAMENTAL RESONANCE FREQUENCIES THAN EXPECTED, INPUT = 4 FOUND = 3

RESONANT FREQUENCIES DETERMINED TO BE FUNDAMENTALS

1	X.XXXXXXF-YY
2	X.XXXXXE-YY
3	X.XXXXXXF-YY

Sample Page 16

Aside from their several nonlinearities, the dynamic equations of motion of helicopter rotor blades implicitly contain several linear terms with period coefficients, which arise from the periodic character of the airloads in forward flight. It is not unexpected then, that the aeroelastic time-history responses generated by these equations should manifest Floquet Theory characteristics (see Reference 16). In particular, the Fourier Transform is capable of identifying "multiple resonances" which are separated by (plus or minus) multiples of the rotor frequency and which would be found to have approximately the same damping level. Hence, the resonant frequencies found by the resonance search are further screened to extract only those frequencies with distinct noninteger values and which, within the set having the same noninteger values, have the largest transform magnitudes. These extracted frequencies are herein denoted "fundamental resonances" and are the only ones examined further for stability in the TSSA.

Sample Page 17 depicts the results of frequency fine tuning and response stability estimation for each of the fundamental resonances extracted earlier in the TSSA. The results for each of these frequencies are presented in columnar fashion. The top horizontal blocks of output represent the frequency fine-tuning results. Of most practical importance are the values labeled OPTIMIZED FREQUENCY which are, in nondimensional (per rotor rev) form, the best estimates of the frequency of the fundamental resonant frequencies. These frequencies are obtained by an optimization technique, the details of which are beyond the scope of this report. The remainder of the output depicted on this sample page (for each fundamental resonance) consists of three horizontal blocks of output representing various estimates of the effective damping characteristics. These three types of blocks are best explained by first describing Sample Page 18. This sample page depicts, columnarly for each of the fundamental resonances indicated in Sample Page 17, the natural logarithm of the magnitude of resonant frequency content at each (nondimensional) time indicated. If these amplitude logarithms attenuate with time, then that frequency content (mode) is deemed stable, and conversely the slope of that attenuation with time is a measure of the effective linear damping; in the analysis this slope is obtained by a simple least-square fit. It may happen that the variation of amplitude logarithms with time is neither monotonic increasing or decreasing in which case a condition of maximum or minimum amplitude is defined. By weighting the least-square fit either uniformly or with an appropriate function accentuating the initial or terminal ends of the amplitude logarithms data string, the three latter horizontal blocks of output depicted in Sample Page 17 are generated. Within each of these blocks, the first quantity depicted is the nondimensional CHARACTERISTIC EXPONENT, which is analogous to and interpreted in the same way as the real part of the eigenvalue discussed in the output for Solution Part I. The REVS to (MAX/MIN) AMPL. is an indication of the asymptotic behavior of the component response. STANDARD DEVIATION is the root-mean-squared error achieved in the least-square curve-fit and is an indication of the regularity of the amplitude logarithm function depicted in Sample Page 18, and of the accuracy of the stability estimation. Based upon the OPTIMIZED FREQUENCY outputted at the top of the sample page, the equivalent CRITICAL DAMPING RATIO is calculated from the characteristic exponent using standard formulae. Finally, the output item labeled REVS TO HALF AMPLITUDE is the third alternate way in which the equivalent linear damping result is presented.

In Sample Page 19 is depicted the typical additional page of output generated at the beginning of every case following the first case of a multiple case sum. The two columns depict, respectively, the location numbers and data values for the newly inputted data distinguishing the present case from the previous one. This feature is intended solely as an ease of usage output to assist in data management.

TRANSIENT RESPONSE CHANNEL NO. XX - RESONANT FREQUENCY FINE TUNING AND CRITICAL DAMPING RATIO CALCULATIONS

INITIAL PERCENTAGE	XX.XX		
INITIAL NO. OF DATA PTS.	XXX		
NO. FOURIER COEF. CALCS.	XXX		
-FINAL NO. OF DATA PTS.	XXX	XXX	XXX
INITIAL FREQUENCY ESTIMATE (/REV)	.XXXXX	X.XXXXX	X.XXXXX
OPTIMIZED FREQUENCY (/REV)	.XXXXX	X.XXXXX	X.XXXXX
HARMONIC	YX	YY	XX
UNIFORMLY WEIGHTED CHARACTERISTICS			
CHARACTERISTIC EXPONENT	.XXXXX	.XXXXX	.XXXXX
REVS TO (MAX/MIN) AMPL.	X.XXXXX	X.XXXXX	X.XXXXX
STANDARD DEVIATION	.XXXXX	.XXXXX	.XXXXX
CRITICAL DAMPING RATIO	.XXXXX	.XXXXX	.XXXXX
REVS TO HALF AMPLITUDE	XX.XXXXX	XX.XXXXX	XX.XXXXX
INITIAL END WEIGHTED CHARACTERISTICS			
CHARACTERISTIC EXPONENT	.XXXXX	.XXXXX	.XXXXX
REVS TO (MAX/MIN) AMPL.	X.XXXXX	X.XXXXX	X.XXXXX
STANDARD DEVIATION	.XXXXX	.XXXXX	.XXXXX
CRITICAL DAMPING RATIO	.XXXXX	.XXXXX	.XXXXX
REVS TO HALF AMPLITUDE	XX.XXXXX	XX.XXXXX	XX.XXXXX
TERMINAL END WEIGHTED CHARACTERISTICS			
CHARACTERISTIC EXPONENT	.XXXXX	.XXXXX	.XXXXX
REVS TO (MAX/MIN) AMPL.	X.XXXXX	X.XXXXX	X.XXXXX
STANDARD DEVIATION	.XXXXX	.XXXXX	.XXXXX
CRITICAL DAMPING RATIO	.XXXXX	.XXXXX	.XXXXX
REVS TO HALF AMPLITUDE	XX.XXXXX	XX.XXXXX	XX.XXXXX

